

NRC Publications Archive Archives des publications du CNRC

UMAR theory & user manual: version 1.0

Martin-Perez, B.; Nofal, M.

For the publisher's version, please access the DOI link below. / Pour consulter la version de l'éditeur, utilisez le lien DOI ci-dessous.

Publisher's version / Version de l'éditeur:

<https://doi.org/10.4224/20378987>

Internal Report (National Research Council of Canada. Institute for Research in Construction), 2002-05-01

NRC Publications Archive Record / Notice des Archives des publications du CNRC :

<https://nrc-publications.canada.ca/eng/view/object/?id=6d7ecbac-65c7-440b-a38a-e8bd59f2e39f>

<https://publications-cnrc.canada.ca/fra/voir/objet/?id=6d7ecbac-65c7-440b-a38a-e8bd59f2e39f>

Access and use of this website and the material on it are subject to the Terms and Conditions set forth at

<https://nrc-publications.canada.ca/eng/copyright>

READ THESE TERMS AND CONDITIONS CAREFULLY BEFORE USING THIS WEBSITE.

L'accès à ce site Web et l'utilisation de son contenu sont assujettis aux conditions présentées dans le site

<https://publications-cnrc.canada.ca/fra/droits>

LISEZ CES CONDITIONS ATTENTIVEMENT AVANT D'UTILISER CE SITE WEB.

Questions? Contact the NRC Publications Archive team at

PublicationsArchive-ArchivesPublications@nrc-cnrc.gc.ca. If you wish to email the authors directly, please see the first page of the publication for their contact information.

Vous avez des questions? Nous pouvons vous aider. Pour communiquer directement avec un auteur, consultez la première page de la revue dans laquelle son article a été publié afin de trouver ses coordonnées. Si vous n'arrivez pas à les repérer, communiquez avec nous à PublicationsArchive-ArchivesPublications@nrc-cnrc.gc.ca.



National Research
Council Canada

Conseil national
de recherches Canada

NRC - CNRC

UMAR - Theory and User Manual

Martin-Pérez, B.; Nofal, M.

IR-852

www.nrc.ca/irc/ircpubs





**National Research
Council Canada**

**Conseil national
de recherches Canada**

Institute for
Research
In Construction

Institut de
recherche
en construction

NRC · CNRC

UMAR

Theory & User Manual

Version 1.0

B. Martín-Pérez and M. Nofal

Internal Report No. 852

Date of issue: May 2002

TABLE OF CONTENTS

1	INTRODUCTION.....	1
2	PROGRAM STRUCTURE.....	2
3	ELEMENT LIBRARY.....	4
3.1	SPACE TRUSS ELEMENT	4
3.2	SHEAR CONNECTOR ELEMENT.....	6
3.3	REFINED QUADRILATERAL PLANE ELEMENT (RQD4)	8
3.4	PLATE BENDING ELEMENTS	12
3.4.1	Quadrilateral bending element (QBE)	12
3.4.2	Improved discrete Kirchhoff quadrilateral (IDKQ).....	13
3.5	QUADRILATERAL FACET SHELL ELEMENT (QFSE)	23
3.6	SOLID ISOPARAMETRIC ELEMENT	26
3.6.1	Layered solid isoparametric element.....	29
4	MATERIAL LIBRARY.....	31
4.1	THEORY OF ELASTICITY	31
4.1.1	Linear elastic model	31
4.1.2	Orthotropic hypoelastic model.....	36
4.1.3	Resilient modulus models.....	42
4.2	THEORY OF PLASTICITY	44
4.2.1	Yield criteria.....	44
4.2.2	Hardening laws	47
4.2.3	Rate-independent plastic model	50
4.2.4	Isotropic visco-plastic model	51
4.3	THEORY OF CONTINUUM DAMAGE MECHANICS	54
4.3.1	Crack compliance.....	56
4.3.2	Crack evolution criteria	63
5	STRUCTURAL ANALYSIS.....	73
5.1	BOUNDARY CONDITIONS	74
5.2	SOLUTION PROCEDURE	74
5.2.1	Material non-linearity.....	74
5.3	CONVERGENCE CRITERIA	76
6	CONSTRUCTION ANALYSIS.....	78
6.1	REMOVAL ANALYSIS	78
6.2	RESTORATION ANALYSIS	78
7	TRANSIENT ANALYSIS.....	79
7.1	GOVERNING EQUATION	79
7.2	BOUNDARY CONDITIONS	79
7.3	FINITE ELEMENT FORMULATION	80
7.4	TRANSIENT ELEMENTS	82
7.5	NUMERICAL SOLUTION	82
8	TYPES OF SOLVERS.....	83
8.1	LU DECOMPOSITION METHOD.....	83
8.2	FRONTAL SOLVER.....	83

8.3 GAUSS-SEIDEL METHOD	84
8.4 DOMAIN DECOMPOSITION METHOD.....	85
8.5 BICONJUGATE GRADIENT METHOD	87
8.5.1 Convergence criteria.....	88
9 REFERENCES.....	90
APPENDIX A: USING THE PROGRAM	94
A.1 ENTERING REQUIRED INPUT	94
A.2 READING PROGRAM OUTPUT.....	105
A.3 PROBLEM REPORTING	106

TABLE OF FIGURES

Figure 2-1: Modular nature of program UMAR.	2
Figure 3-1: Space truss element.	5
Figure 3-2: Shear connector element.....	6
Figure 3-3: Load-slip relationship for the shear connector [44].	7
Figure 3-4: Elements QUAD8 and RQD4.....	9
Figure 3-5: Normal displacement u_n to side 1-2 due to $w_1 = 1$	10
Figure 3-6: Plate bending elements QBE and IDKQ.	13
Figure 3-7: Transformation of element QUAD9 into element IDKQ.	14
Figure 3-8: Co-ordinate transformation along of the side of a QUAD9 element.....	16
Figure 3-9: The facet shell element QFSE.	23
Figure 3-10: Layered shell element.....	25
Figure 3-11: Hexahedral elements of the “serendipity” family implemented in UMAR.	26
Figure 3-12: Eight-to-twenty nodes solid isoparametric element.	27
Figure 4-1: Uniaxial stress-strain curve for compressive and tensile loading.	38
Figure 4-2: (a) Crack formation in principal tension direction; (b) Tensile uniaxial stress-strain curve.....	40
Figure 4-3: Triaxial compressive strength envelope.	41
Figure 4-4: Triaxial tensile strength envelope.	42
Figure 4-5: Rheological analogue of elasto-visco-plastic model.	52
Figure 4-6: Typical section subjected to general state of stresses.....	58
Figure 4-7: Flowchart to implement micro-mechanical damage-based model [27].....	72
Figure 5-1: Algorithm implemented in UMAR for non-linear analysis.....	76
Figure 6-1: Removal forces (adapted from [38]).	78
Figure 8-1: Finite element mesh partitioned into sub-domains.	86

TABLE OF TABLES

Table 4-1: Constants defining isotropic yield surfaces implemented in UMAR.	49
Table 7-1: Correspondence between Eq. 7.1 and the governing differential equations.	79
Table 7-2: Correspondence between Eq. 7.2 and the imposed boundary conditions.	80
Table A-1: Heading information.	95
Table A-2: Control data (refer to Table A-3.).....	95
Table A-3: Input indicators for control data.	96
Table A-4: User output options.....	96
Table A-5: Nodal point data.	97
Table A-6: Material data.	97
Table A-7: Constitutive models implemented in program UMAR.	99
Table A-8: Yield criteria and hardening functions implemented in program UMAR.....	99
Table A-9: Equivalent yield stress.	99
Table A-10: Layering systems data.....	100
Table A-11: Cross-section data (refer to Table A-12.).....	100
Table A-12: Input indicators for cross sections data.	101
Table A-13: Element data.....	101
Table A-14: Line commands for different element types.....	102
Table A-15: Deformation boundary conditions data (if stress analysis required.).....	102
Table A-16: Analysis data for field problems (if thermal or/and hygroscopic or/and chloride analysis required.).....	102
Table A-17: Numerical data.	103
Table A-18: Load data for each time step if stress, removal or restoration analysis required.	103
Table A-19: Input indicators for load data.	103
Table A-20: Consistent nodal loads.	104

1 Introduction

Program UMAR, which stands for Unified Method of Analysis for Rehabilitation, is a general-purpose finite element program for rehabilitation analysis and design of various structural and building components. UMAR solves for the static response of linear and non-linear two- and three-dimensional structural systems under the action of mechanical loads. The computer program can include time-dependent phenomena such as creep, shrinkage and cyclic loading. UMAR also offers transient analysis capabilities for parabolic initial-value problems in fluid mechanics, and it can couple this type of analysis with that due to mechanical loads. Some features which are available in the program include:

- Multi-field/physics analysis capabilities to couple heat-mass transfer problems with stress problems;
- Element options to model addition or removal of elements (material) in the physical system to simulate construction/rehabilitation processes;
- Six basic elements for structural analysis: a space truss element, a shear connector element, a quadrilateral membrane element, a quadrilateral plate-bending element, a quadrilateral shell element, and a layered-solid element. All the quadrilateral elements can be layered in the out-of-plane direction. The membrane and solid elements can also be used for transient analysis;
- Prescribed nodal displacements and/or surface traction options for structural analysis;
- Prescribed nodal values and/or surface flux options for transient analysis;
- Prescribed arbitrary load-time functions (both mechanical and environmental);
- Comprehensive library of material models: isotropic linear-elastic, orthotropic linear-elastic, transversely-isotropic linear-elastic, orthotropic hypo-elastic, elasto-(plastic)-damage, and a family of multi-yield elasto(-visco)-plastic;
- Several symmetric and non-symmetric matrix equation solvers: LU decomposition solvers for banded and full matrices, a sky-line solver for banded matrices, a domain decomposition solver, a symmetric frontal solver, and a Gauss-Seidel iterative solver;
- ASCII input file, where data is organised into recognisable blocks.

Program UMAR is written in Fortran 90, and the executable is available for PC computing platforms by compiling and linking the code with the Compaq Visual Fortran 6.1a compiler.

2 Program structure

UMAR is a general purpose finite element program with a modular structure. A series of options can be specified by the user in order to select different components that constitute the system of a particular field of application and the manner in which it is solved. The modular nature of UMAR gives the program tremendous flexibility, and facilitates the addition to the program of mathematical models not included in the current UMAR library. Its basic modular nature ensures that all the steps in a finite element analysis are transparent, so that the user can modify the element matrix formation and introduce new element types and/or solution procedures.

The two main application fields of UMAR are:

- structural mechanics (static analysis, removal analysis, and restoration analysis), and
- scalar field analyses (all physical processes described by a diffusive-type equation).

These two basic application fields may be used independently, but they are both based on the same finite element model database. Program UMAR has been structured into the following libraries (see Figure 2-1):

- element library (two-dimensional and three-dimensional elements),
- material library (elasticity, plasticity, continuum damage mechanics),
- loading library (uniform load, concentrated load, removal load, hygrothermal load),
- analysis library (structural analysis, removal analysis, restoration analysis, transient analysis),
- solver library (direct and iterative methods), and
- math and utilities libraries (collection of routines that perform many of the basic tasks required by a finite element program).

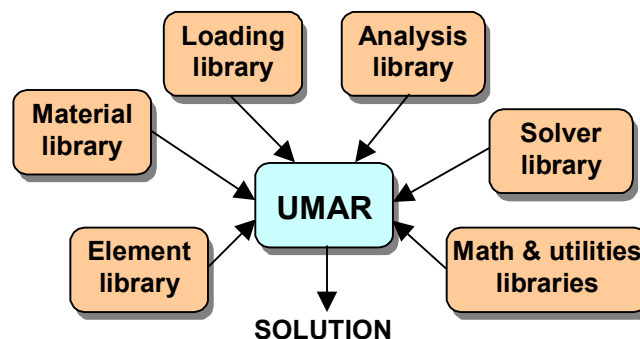


Figure 2-1: Modular nature of program UMAR.

Program UMAR is written in Fortran 90 and conforms to the Standard. The actual structure of the program is based on an object-oriented concept intended to reduce the overall program

complexity and enable ease of implementation. The objects are generated by means of the TYPE feature of Fortran 90 (which can be found in file `types.f90`). Further, several objects of similar functionality are grouped into modules by means of the MODULE feature of Fortran 90. The library software and any programs written using the library are very portable. This makes the use of the library attractive in many different research applications.

3 Element library

Equation Section (Next) There are six basic elements implemented in program UMAR:

- a two-node truss element;
- a two-node shear connector element;
- a quadratic, four-node, quadrilateral plane element;
- a four-node quadrilateral plate-bending element;
- a four-node shell element; and
- a layered solid isoparametric element.

All elements in UMAR are integrated numerically, which allows for independent material response at each integration point and irregular element shapes. The above elements are implemented in the module <formulate_structural_elements_library>, which can be found in the file `formulate_structural_elements.f90`. A discussion of the formulation of each element follows.

3.1 Space truss element

A truss element is a bar which can resist only axial forces (compressive or tensile) and can deform only in the axial direction. The truss element implemented in UMAR has two end nodes, each with three degrees of freedom u , v , and w in the x , y , and z directions, respectively, as illustrated in Figure 3-1. The displacement field between the nodes is assumed to be linear, i.e.,

$$u(x) = q_1 + (q_2 - q_1) \frac{x}{l} \quad (3.1)$$

Equation 3.1 is expressed in matrix form as:

$$\{u\}_{1 \times 1} = [N]_{1 \times 2} \{q\}_{2 \times 1} \quad (3.2)$$

where

$$[N] = \left[\left(1 - \frac{x}{l} \right) \quad \frac{x}{l} \right]; \quad \{q\} = \begin{Bmatrix} q_1 \\ q_2 \end{Bmatrix} \quad (3.3)$$

where q_1 and q_2 are the nodal degrees of freedom in the local co-ordinate system and l is the element length. The strain along the length of the element is given by:

$$\epsilon_x = \frac{\partial u}{\partial x} = \frac{q_2 - q_1}{l} \quad \text{or} \quad \{\epsilon_x\}_{1 \times 1} = [B]_{1 \times 2} \{q\}_{2 \times 1} \quad (3.4)$$

where

$$[B] = \begin{bmatrix} -\frac{1}{l} & \frac{1}{l} \end{bmatrix} \quad (3.5)$$

The element stiffness matrix in the local co-ordinate system is obtained from:

$$[k]_{2 \times 2} = \int \int \int_{V^{(e)}} [B]^T [D] [B] dV = A \int_{x=0}^l \begin{Bmatrix} -\frac{1}{l} \\ \frac{1}{l} \end{Bmatrix} E \begin{Bmatrix} -\frac{1}{l} & \frac{1}{l} \end{Bmatrix} dx = \frac{AE}{l} \begin{bmatrix} 1 & -1 \\ -1 & 1 \end{bmatrix} \quad (3.6)$$

where A is the cross-section area of the truss bar and E is the Young's modulus of the material.

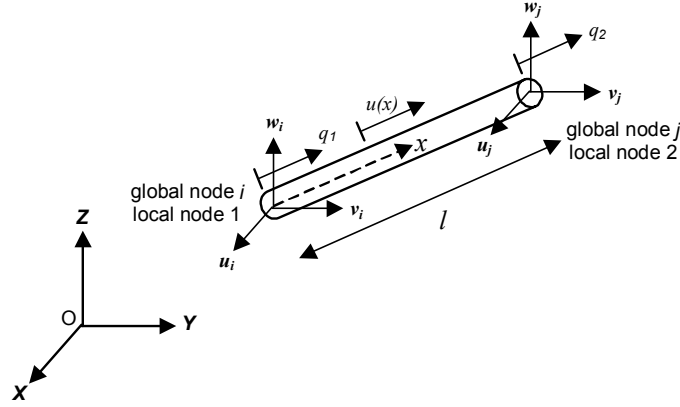


Figure 3-1: Space truss element.

The local displacements q_1 and q_2 are resolved into the global components u , v , and w through a transformation matrix, i.e.,

$$\{q\} = [T] \{Q\} \quad (3.7)$$

where the transformation matrix $[T]$ and the vector of global nodal displacements $\{Q\}$ are given by:

$$[T] = \begin{bmatrix} l_{ij} & m_{ij} & n_{ij} & 0 & 0 & 0 \\ 0 & 0 & 0 & l_{ij} & m_{ij} & n_{ij} \end{bmatrix} \quad (3.8)$$

$$\{Q\}^T = \{u_i \quad v_i \quad w_i \quad u_j \quad v_j \quad w_j\} \quad (3.9)$$

and l_{ij} , m_{ij} , and n_{ij} respectively denote the direction cosines of the angles between the line ij and the global x -, y - and z -axis. The direction cosines are calculated from:

$$l_{ij} = \frac{x_j - x_i}{l}, \quad m_{ij} = \frac{y_j - y_i}{l}, \quad n_{ij} = \frac{z_j - z_i}{l} \quad (3.10)$$

where (x_i, y_i, z_i) and (x_j, y_j, z_j) are the global co-ordinates of nodes i and j , respectively. Thus, the element stiffness matrix in the global co-ordinate system is obtained from:

$$[k^*]_{6 \times 6} = [T]_{6 \times 2}^T [k]_{2 \times 2} [T]_{2 \times 6} \quad (3.11)$$

The total nodal load vector in the local co-ordinate system is given by:

$$\{f\} = \underbrace{AE\alpha T \begin{Bmatrix} -1 \\ 1 \end{Bmatrix}}_{\text{due to initial thermal strains}} + \underbrace{\frac{\phi Al}{2} \begin{Bmatrix} 1 \\ 1 \end{Bmatrix}}_{\text{due to constant body force } \phi} \quad (3.12)$$

Likewise, the load vector is referred to the global co-ordinate system by:

$$\{f^*\} = [T]^T \{f\} \quad (3.13)$$

where $[T]$ is given by Eq. 3.8.

3.2 Shear connector element

This element, developed by Nofal [27], can be used to model the relative deformation or slip at the interface of two different materials or structural elements under mechanical load. The load-slip characteristics of this element are defined by the empirical load-slip relationship proposed by [43]:

$$F = a(1 - e^{-b\lambda}) \quad (3.14)$$

where F is the shear force acting on the shear connector, λ is the slip or relative deformation between its ends, a and b are empirical constants, and e is the base of natural logarithm.

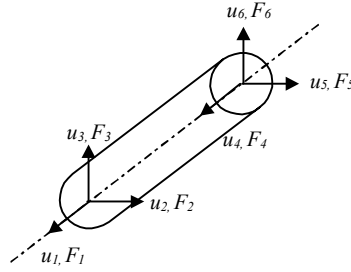


Figure 3-2: Shear connector element.

To write the stiffness matrix of this element, consider the two-node bar element with six displacement degrees of freedom of Figure 3-2. Because shear connectors are relatively short and they transfer the load primarily by shear, it is assumed that their flexural and torsional stiffness are equal to zero. From basic finite element procedures, the nodal forces $\{F\}$ of this element can be related to the nodal displacements $\{u\}$ as:

$$\begin{Bmatrix} F_1 \\ F_2 \\ F_3 \\ F_4 \\ F_5 \\ F_6 \end{Bmatrix} = \begin{bmatrix} k_1 & 0 & 0 & -k_1 & 0 & 0 \\ 0 & k_2 & 0 & 0 & -k_2 & 0 \\ 0 & 0 & k_3 & 0 & 0 & -k_3 \\ -k_1 & 0 & 0 & k_1 & 0 & 0 \\ 0 & -k_2 & 0 & 0 & k_2 & 0 \\ 0 & 0 & -k_3 & 0 & 0 & k_3 \end{bmatrix} \begin{Bmatrix} u_1 \\ u_2 \\ u_3 \\ u_4 \\ u_5 \\ u_6 \end{Bmatrix} \quad (3.15)$$

where $k_1 = EA/L$, E is the Young's modulus, and A and L are the cross-sectional area and length of the element, respectively. Constants k_2 and k_3 are the shear stiffness coefficients of the bar. They can be determined from the experimental load-slip curve proposed by [44] and illustrated in Figure 3-3.

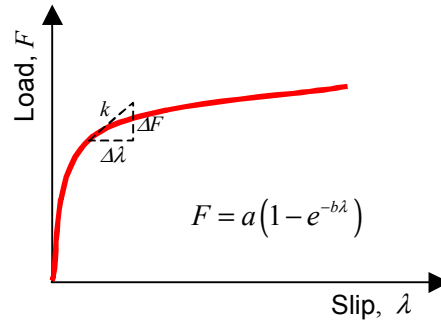


Figure 3-3: Load-slip relationship for the shear connector [44].

The increment of shear force ΔF shown in Figure 3-3 can be related to the increment of slip $\Delta\lambda$ as:

$$\Delta F = k\Delta\lambda \quad (3.16)$$

where k is the slope of the load-slip curve and is given by:

$$k = \frac{dF}{d\lambda} \quad (3.17)$$

By differentiating Eq. 3.14,

$$k = abe^{-b\lambda} \quad (3.18)$$

and substituting in Eq. 3.16, the following relationship results:

$$\Delta F = abe^{-b\lambda} \Delta\lambda \quad (3.19)$$

For the element in Figure 3-2, the slip in the y and z directions can be written respectively as:

$$\begin{aligned} \lambda_y &= u_2 - u_5 \\ \lambda_z &= u_3 - u_6 \end{aligned} \quad (3.20)$$

or in incremental form:

$$\begin{aligned}\Delta\lambda_y &= \Delta u_2 - \Delta u_5 \\ \Delta\lambda_z &= \Delta u_3 - \Delta u_6\end{aligned}\tag{3.21}$$

where Δu_i is the increment of displacement due to an increment of shear force ΔF_i .

Note that in some cases the location of shear connectors may not coincide with the nodal points in the finite element mesh. In these cases, the actual connector is substituted by two equivalent connectors which are positioned at the nearest nodal points. The cross-sectional area of the substitute connectors is found by linearly interpolating the area of the actual connector. This procedure is akin to the determination of equivalent nodal forces in the customary finite element procedures.

In the non-linear incremental/iterative analysis procedure used in UMAR, increments of slip are summed up to obtain the total slip at any load level. Then, the shear force corresponding to the total slip is determined from Eq. 3.14, and the shear stiffness of the bar for the next iteration is calculated using Eq. 3.18. The axial stiffness of the bar is found the same way as for an ordinary truss element (see Section 3.1).

3.3 Refined quadrilateral plane element (RQD4)

This four-node quadrilateral element is geometrically isotropic, and its stiffness can be derived from the stiffness matrix of QUAD8, the eight-node isoparametric element. Element RQD4 has three degrees of freedom per node as illustrated in Figure 3-4, and its displacement functions can be derived from the displacement functions of QUAD8, also shown in Figure 3-4. Typical nodal displacements u_i and v_i in the x and y directions, respectively, are the same as in QUAD8, while w_i is a typical nodal-rotation normal to the plane of the element. This element was developed by Razaqpur and Nofal [32] using the classical beam displacement function.

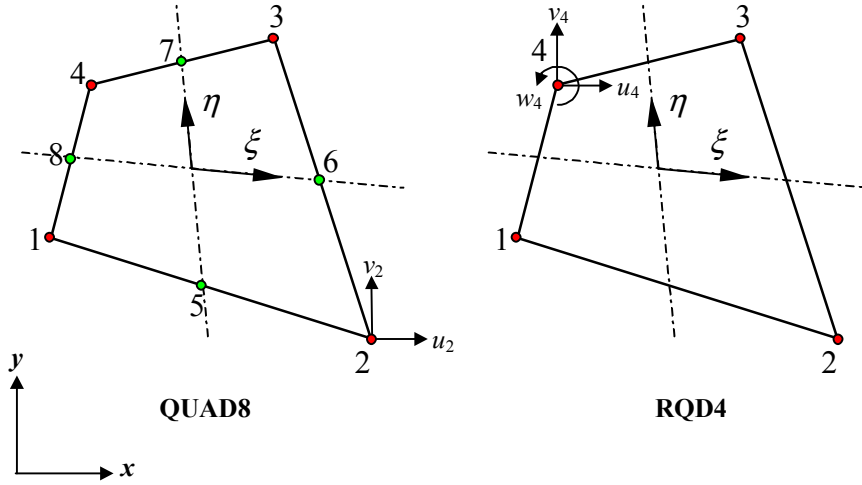


Figure 3-4: Elements QUAD8 and RQD4.

Using the kinematics relationship described below, the degrees of freedom in QUAD8 are related to the degrees of freedom in the new element. Consider side 1-2 of RQD4, and introduce a unit rotation $w_1 = 1$ at node 1 as in Figure 3-5. The displacement normal to side 1-2, u_n , due to this rotation can be expressed as a cubic polynomial similar to the lateral displacement function for an ordinary beam, i.e.,

$$u_n = -\frac{s(l-s)^2}{l^2} \quad (3.22)$$

where s is a local co-ordinate running from node 1 to 2, and l is the length of side 1-2. For $s = \frac{l}{2}$,

$$(u_n)_{s=\frac{l}{2}} = -\frac{l}{8} \quad (3.23)$$

Similarly, for $w_2 = 1$:

$$(u_n)_{s=\frac{l}{2}} = \frac{l}{8} \quad (3.24)$$

Therefore, for end rotations w_1 and w_2 , the normal displacement u_n is given by:

$$u_n = l \frac{(w_2 - w_1)}{8} \quad (3.25)$$

Decomposing u_n in Eq. 3.25 into its components in the x and y directions results in:

$$\begin{aligned}
 u_{n_s} &= l \frac{(w_2 - w_1)}{8} \sin \theta \\
 u_{n_y} &= l \frac{(w_2 - w_1)}{8} \cos \theta
 \end{aligned}
 \tag{3.26}$$

From Figure 3-5, $\sin \theta = (y_2 - y_1)/l$ and $\cos \theta = (x_2 - x_1)/l$, where x_i, y_i are the co-ordinates of node i ($i = 1, 2$). By substituting these quantities in Eq. 3.26, the total displacement components at the middle of side 1-2 are:

$$\begin{aligned}
 u_5 &= \frac{(u_2 + u_1)}{2} - \frac{(y_1 - y_2)(w_2 - w_1)}{8} \\
 v_5 &= \frac{(v_2 + v_1)}{2} - \frac{(x_1 - x_2)(w_2 - w_1)}{8}
 \end{aligned}
 \tag{3.27}$$

Equation 3.27 can be written in matrix form as:

$$\begin{Bmatrix} u_5 \\ v_5 \end{Bmatrix} = \begin{bmatrix} \frac{1}{2} & 0 & a & \frac{1}{2} & 0 & -a \\ 0 & \frac{1}{2} & -b & 0 & \frac{1}{2} & b \end{bmatrix} \begin{Bmatrix} u_1 \\ v_1 \\ w_1 \\ u_2 \\ v_2 \\ w_2 \end{Bmatrix}
 \tag{3.28}$$

where $a = (y_1 - y_2)/8$ and $b = (x_1 - x_2)/8$.

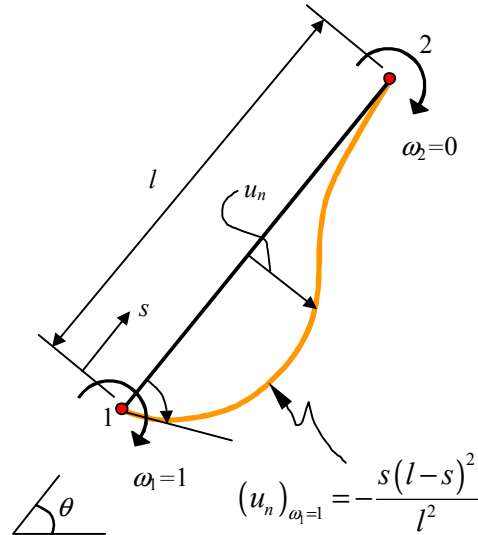


Figure 3-5: Normal displacement u_n to side 1-2 due to $w_1 = 1$.

By writing similar equations for the other mid-side nodes, the nodal displacements in QUAD8, $\{d\}^{\text{QUAD8}}$, are related to the corresponding displacements in RQD4, $\{d\}^{\text{RQD4}}$, as:

$$\{d\}_{16 \times 1}^{\text{QUAD8}} = [T]_{16 \times 12} \{d\}_{12 \times 1}^{\text{RQD4}} \quad (3.29)$$

where $[T]$ is a 16 x 12 transformation matrix. In expanded form, Eq. 3.29 is given by:

$$\begin{Bmatrix} u_1 \\ v_1 \\ u_2 \\ v_2 \\ u_3 \\ v_3 \\ u_4 \\ v_4 \\ u_5 \\ v_5 \\ u_6 \\ v_6 \\ u_7 \\ v_7 \\ u_8 \\ v_8 \end{Bmatrix} = \begin{bmatrix} 1 & 0 & 0 & 0 & 0 & 0 & 0 & 0 & 0 & 0 & 0 & 0 \\ 0 & 1 & 0 & 0 & 0 & 0 & 0 & 0 & 0 & 0 & 0 & 0 \\ 0 & 0 & 0 & 1 & 0 & 0 & 0 & 0 & 0 & 0 & 0 & 0 \\ 0 & 0 & 0 & 0 & 1 & 0 & 0 & 0 & 0 & 0 & 0 & 0 \\ 0 & 0 & 0 & 0 & 0 & 0 & 1 & 0 & 0 & 0 & 0 & 0 \\ 0 & 0 & 0 & 0 & 0 & 0 & 0 & 1 & 0 & 0 & 0 & 0 \\ 0 & 0 & 0 & 0 & 0 & 0 & 0 & 0 & 0 & 1 & 0 & 0 \\ 0 & 0 & 0 & 0 & 0 & 0 & 0 & 0 & 0 & 0 & 1 & 0 \\ \frac{1}{2} & 0 & b_1 & \frac{1}{2} & 0 & -b_1 & 0 & 0 & 0 & 0 & 0 & 0 \\ 0 & \frac{1}{2} & a_1 & 0 & \frac{1}{2} & -a_1 & 0 & 0 & 0 & 0 & 0 & 0 \\ 0 & 0 & 0 & \frac{1}{2} & 0 & b_2 & \frac{1}{2} & 0 & -b_2 & 0 & 0 & 0 \\ 0 & 0 & 0 & 0 & \frac{1}{2} & a_2 & 0 & \frac{1}{2} & -a_2 & 0 & 0 & 0 \\ 0 & 0 & 0 & 0 & 0 & 0 & \frac{1}{2} & 0 & b_3 & \frac{1}{2} & 0 & -b_3 \\ 0 & 0 & 0 & 0 & 0 & 0 & 0 & \frac{1}{2} & a_3 & 0 & \frac{1}{2} & -a_3 \\ \frac{1}{2} & 0 & -b_4 & 0 & 0 & 0 & 0 & 0 & 0 & \frac{1}{2} & 0 & b_4 \\ 0 & \frac{1}{2} & -a_4 & 0 & 0 & 0 & 0 & 0 & 0 & 0 & \frac{1}{2} & a_4 \end{bmatrix} \begin{Bmatrix} u_1 \\ v_1 \\ w_1 \\ u_2 \\ v_2 \\ w_2 \\ u_3 \\ v_3 \\ w_3 \\ u_4 \\ v_4 \\ w_4 \end{Bmatrix} \quad (3.30)$$

where $a_i = (x_i - x_{i+1})/8$ and $b_i = (y_i - y_{i+1})/8$ for $i=1,2,3$; and $a_4 = (x_1 - x_4)/8$ and $b_4 = (y_1 - y_4)/8$.

Using the principle of virtual work, the stiffness $[k^*]$ and nodal load vector $\{f^*\}$ of RQD4 can be related to the corresponding matrices $[k]$ and $\{f\}$ of QUAD8 as:

$$[k^*] = [T]^T [k] [T] \quad (3.31)$$

and

$$\{f^*\}_{12 \times 1} = [T]_{12 \times 16}^T \{f\}_{16 \times 1} \quad (3.32)$$

The last two equations show that once the transformation matrix $[T]$ has been established, the remaining steps of the analysis are relatively straightforward. Although Eqs. 3.31 and 3.32 yield

the desired stiffness and load matrices, it is possible to introduce further simplifications and to reduce the amount of calculations. The stiffness matrix, $[k]$, is given by:

$$[k] = \int [B]^T [D] [B] dV \quad (3.33)$$

where, as usual, $[B]$ is the strain-displacement matrix, $[D]$ is the material matrix, and V is the element volume. According to Eq. 3.31, $[k^*]$ can be written as:

$$[k^*] = [T]^T \left(\int [B]^T [D] [B] dV \right) [T] \quad (3.34)$$

Rewriting the above equation results in:

$$[k^*] = \int [T]^T [B]^T [D] [B] [T] dV \quad (3.35)$$

By letting

$$[B^*]_{3 \times 12} = [B]_{3 \times 16} [T]_{16 \times 12} \quad (3.36)$$

then,

$$[k^*] = \int [B^*]^T [D] [B^*] dV \quad (3.37)$$

Therefore, if matrix $[B]$ of QUAD8 is transformed according to Eq. 3.36, then the stiffness matrix of RQD4 can be derived from Eq. 3.37. By doing so, computation time is reduced, because Eq. 3.36 involves fewer multiplications. Several performance tests of element RQD4 can be found in [27] and [32].

3.4 Plate bending elements

Plate bending elements implemented in UMAR include the quadrilateral bending element (QBE) and the improved discrete Kirchhoff quadrilateral (IDKQ).

3.4.1 Quadrilateral bending element (QBE)

This element is the quadrilateral version of the rectangular bending element developed by [47]. It was formulated by [11], and its performance has been reported to be satisfactory for moderate deviations from the rectangular shape. The general features of this element are briefly discussed below; complete details can be found in [11].

Element QBE, which is illustrated in Figure 3-6, is a four-node quadrilateral element with three degrees of freedom per node: the lateral displacement w , and the normal rotations $\partial w / \partial x$ and $\partial w / \partial y$. The displacement function in terms of the natural co-ordinates ξ and η is given by:

$$w = [p] \{\bar{A}\} \quad (3.38)$$

where

$$[p] = [1 \quad \xi \quad \eta \quad \xi^2 \quad \xi\eta \quad \eta^2 \quad \xi^3 \quad \xi^2\eta \quad \xi\eta^2 \quad \eta^3 \quad \xi^3\eta \quad \xi\eta^3] \quad (3.39)$$

and $\{\bar{A}\}$ is a vector that contains the polynomial coefficients. In this element, as in element RQD4, the geometry of the element is interpolated using the following relationships:

$$\begin{aligned} x &= \sum_{i=1}^4 \frac{1}{4} (1 + \xi \xi_i) (1 + \eta \eta_i) x_i \\ y &= \sum_{i=1}^4 \frac{1}{4} (1 + \xi \xi_i) (1 + \eta \eta_i) y_i \end{aligned} \quad (3.40)$$

where x, y are the Cartesian co-ordinates of a general point, and ξ, η are the natural co-ordinates of the same point. Variables x_i, y_i, ξ_i and η_i are, respectively, the Cartesian and natural co-ordinates of node i . Note that the summation is carried out over the four nodes of the element.

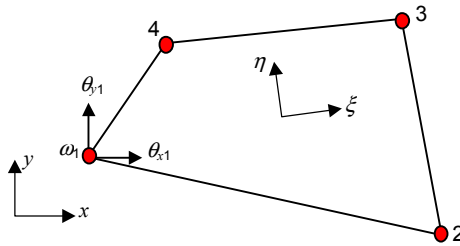


Figure 3-6: Plate bending elements QBE and IDKQ.

3.4.2 Improved discrete Kirchhoff quadrilateral (IDKQ)

This type of element, like element QBE, is also a four-node quadrilateral element with three degrees of freedom at each node (see Figure 3-6). Element IDKQ is developed based on the Mindlin plate theory where the nodal rotations are defined independently of the transverse displacements [41]. The element shape functions are derived as the least square polynomial version of the customary Lagrange functions. Kirchhoff's hypothesis is only applied to the Lagrange element at the rotational degrees of freedom θ_x and θ_y . This element is designed to analyse thin plates where the transverse shear energy may be considered negligible compared to the bending one. The essential step in its formulation is the enforcement of the so-called Kirchhoff constraints ($\gamma_{yz} = \gamma_{zx} = 0$) at certain discrete points in such a manner that all shear-strain modes are totally suppressed. Feasible discrete points are the element nodes where the displacement modes are represented by the discrete values of the nodal displacements.

The starting point in the formulation of the IDKQ is the Mindlin isoparametric finite element QUAD9 that accounts for shear deformations and requires only $C^{(0)}$ -continuity. By imposing the Kirchhoff constraints on all shear strain modes, the 27 degrees of freedom (9 nodes x 3 dof per

node) of the QUAD9 may be transformed into 12 equivalent degrees of freedom (4 nodes x 3 dof per node) in the IDKQ element.

Similarly to the displacement transformation of RQD4, the aim of the transformation illustrated in Figure 3-7 is to derive the transformation matrix $[T]$ that maps the degrees of freedom of element QUAD9 into the equivalent degrees of freedom of element IDKQ, i.e.,

$$\{d\}_{18 \times 1}^{QUAD9} = [T]_{18 \times 12} \{d\}_{12 \times 1}^{IDKQ} \quad (3.41)$$

The nodal loads transformation may be also expressed by means of the transformation matrix $[T]$:

$$[T]_{12 \times 18}^T \{f\}_{18 \times 1}^{QUAD9} = \{f\}_{12 \times 1}^{IDKQ} \quad (3.42)$$

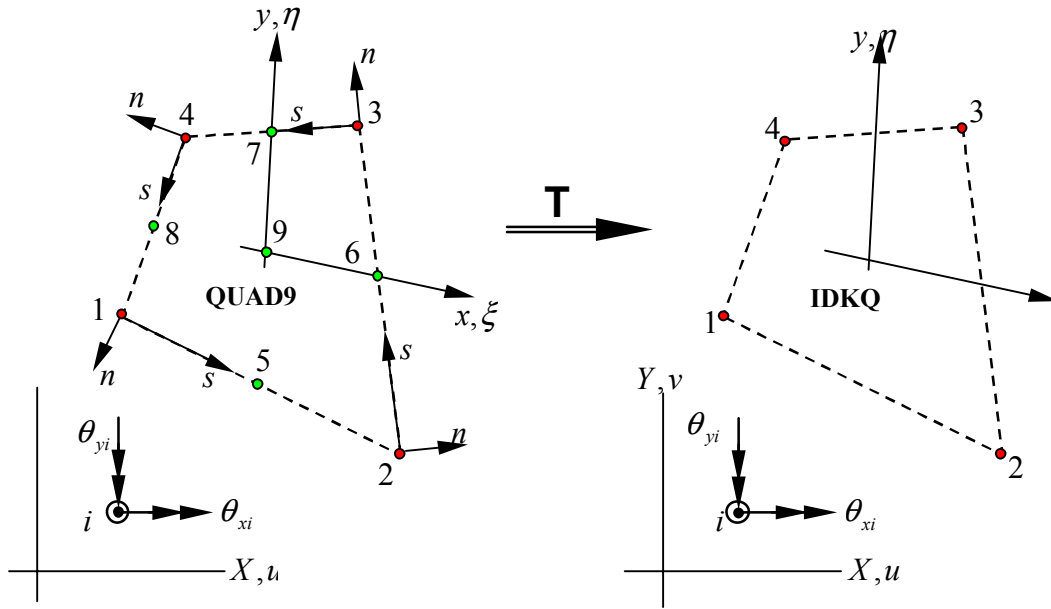


Figure 3-7: Transformation of element QUAD9 into element IDKQ.

The transformation matrix $[T]$ in Eqs. 3.41 and 3.42 is determined by relating the mid-side and central nodes degrees of freedom of QUAD9 to the corner nodes degrees of freedom. This relation is established by imposing the Kirchhoff constraints so that $\gamma_z = 0$ is exactly represented over the element. It should be noted that the element strains and the strain energy in QUAD9 depend only on rotations θ_x and θ_y , which are independent of the out-of-plane displacements w . Consequently, only the eighteen rotational degrees of freedom $\theta_{xi} \neq w_{,xi}$ and $\theta_{yi} \neq w_{,yi}$ at nodes 1 through 9 of the QUAD9 must be expressed in terms of the twelve degrees

of freedom w_i , $w_{,xi} = \theta_{xi}$ and $w_{,yi} = \theta_{yi}$ ($i = 1, \dots, 4$) at the corners of the IDKQ element. This transformation is achieved by imposing the Kirchhoff constraints at the nodal points corresponding to the element sides and centrelines as follows:

Transverse shear strains γ_{yz} and γ_{zx} vanish at the corner nodes

$$\theta_{xi} = w_{,xi} \quad \theta_{yi} = w_{,yi} \quad \text{at nodes } i = 1, 2, 3, 4, 9 \quad (3.43)$$

Transverse shear strains γ_{sz} (expressed in edge tangent co-ordinate s) vanish at the mid-side nodes

$$\theta_{sk} = w_{,sk} \quad \text{at nodes } k = 5, 6, 7, 8 \quad (3.44)$$

Normal slopes $w_{,n} = \theta_n$ of the cubic displacement function along the element sides are assumed to vary linearly

$$\theta_{nk} = \frac{1}{2}(\theta_{ni} + \theta_{nj}) \quad \text{at nodes } k = 5, 6, 7, 8 \quad \text{for } \begin{matrix} i = 1, 2, 3, 4 \\ j = 2, 3, 4, 1 \end{matrix} \quad (3.45)$$

In order to determine the transformation matrix $[T]$, the foregoing Kirchhoff constraints are applied along the element sides and centrelines making use of the corresponding co-ordinate transformations and a redefinition of the out-of-plane displacement field w , which must be assumed cubic in the edge tangent co-ordinate s along the element sides in order to be able to satisfy the Kirchhoff constraints as stated in Eqs. 3.43, 3.44 and 3.45, i.e.,

$$w_{\zeta} |_{side(ij)} = \frac{1}{4} \begin{bmatrix} 2 - 3\zeta + \zeta^3 & 2 + 3\zeta - \zeta^3 \end{bmatrix} \begin{bmatrix} w_i \\ w_j \end{bmatrix} + \frac{l_{ij}}{8} (\zeta^2 - 1) [\zeta - 1 \quad \zeta + 1] \begin{bmatrix} \theta_{si} \\ \theta_{sj} \end{bmatrix} \quad (3.46)$$

$i = 1, 2, 3, 4 \quad j = 2, 3, 4, 1$

where ζ and l_{ij} are respectively the natural co-ordinate and the length of the element side ij , and θ_{si} and θ_{sj} are the nodal tangential rotations along the element side ij at the end nodes i and j , respectively. The expression in Eq. 3.46 is obtained from a standard cubic Lagrangian function in natural co-ordinates $-1 \leq \zeta \leq +1$ so that $\zeta = 0$ at the mid-side nodes. In order to express the rotations $\theta_s = w_{,s}$, the derivatives of w_{ζ} in Eq. 3.46 must be related to the physical co-ordinate s by means of the co-ordinate transformation illustrated in Figure 3-8.

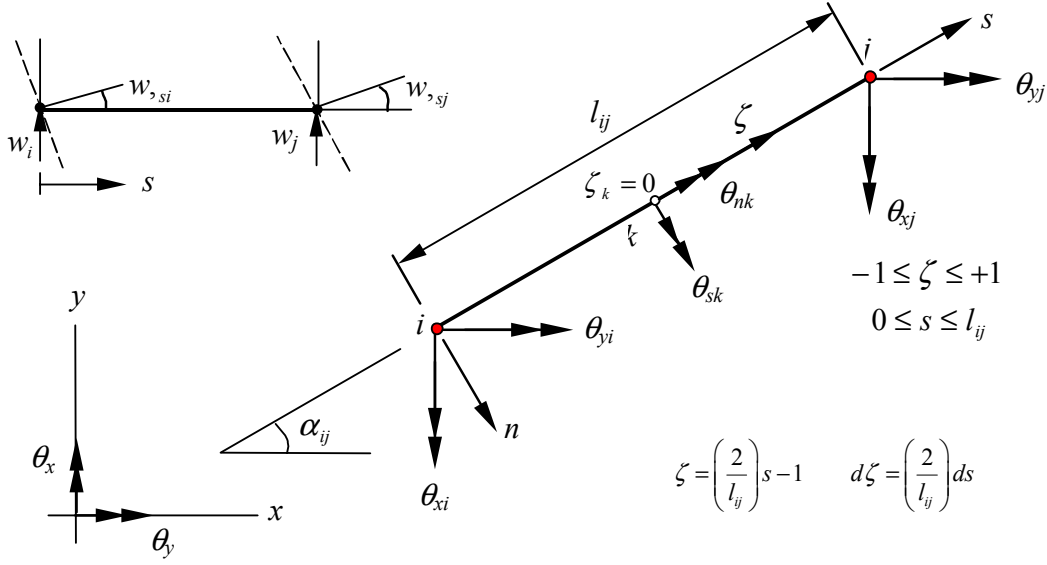


Figure 3-8: Co-ordinate transformation along of the side of a QUAD9 element.

The rotations $\theta_{sk} = w_{,sk}$ ($k = 5, 6, 7, 8$) at the mid-nodes of the QUAD9 element are thus obtained by differentiating Eq. 3.46 with respect to s , i.e.,

$$\theta_{sk} = -\frac{3}{2l_{ij}}w_i - \frac{1}{4}\theta_{si} + \frac{3}{2l_{ij}}w_j - \frac{1}{4}\theta_{sj} \quad (3.47)$$

or in matrix form:

$$\begin{bmatrix} \theta_{sk} \\ \theta_{nk} \end{bmatrix} = \begin{bmatrix} -\frac{3}{2l_{ij}} & -\frac{1}{4} & 0 & \frac{3}{2l_{ij}} & -\frac{1}{4} & 0 \\ 0 & 0 & \frac{1}{2} & 0 & 0 & \frac{1}{2} \end{bmatrix} \begin{bmatrix} w_i \\ \theta_{si} \\ \theta_{ni} \\ w_j \\ \theta_{sj} \\ \theta_{nj} \end{bmatrix} \quad (3.48)$$

where $i = 1, 2, 3, 4$, $j = 2, 3, 4, 1$, and $k = 5, 6, 7, 8$. Two other equations similar to Eq. 3.47 can be expressed for the centrelines of the QUAD9 element:

$$\theta_{x9} = -\frac{3}{2l_{68}}w_8 - \frac{1}{4}\theta_{x8} + \frac{3}{2l_{68}}w_6 - \frac{1}{4}\theta_{x6} \quad (3.49)$$

$$\theta_{y9} = -\frac{3}{2l_{57}}w_7 - \frac{1}{4}\theta_{y7} + \frac{3}{2l_{57}}w_5 - \frac{1}{4}\theta_{y5} \quad (3.51)$$

The set of six equations expressed in Eqs. 3.48, 3.49 and 3.51 provides the relationships needed to transform the rotational degrees of freedom θ_{xk} and θ_{yk} ($k = 5, \dots, 9$) of the QUAD9 element into the out-of-plane displacements w_i and rotational degrees of freedom $w_{,xi} = \theta_{xi}$ and $w_{,yi} = \theta_{yi}$ ($i = 1, \dots, 4$) at the corners of the IDKQ element.

Equation 3.48 needs to be expressed in terms of the element Cartesian co-ordinates x and y . The transformation between side co-ordinates s, n and Cartesian co-ordinates x, y is achieved by means of the Jacobian transformation matrices of each element side:

$$[J]_{ij} = \begin{bmatrix} x_{,s} & y_{,s} \\ x_{,r} & y_{,r} \end{bmatrix}_{ij} = \begin{bmatrix} \cos \alpha_{ij} & \sin \alpha_{ij} \\ \sin \alpha_{ij} & -\cos \alpha_{ij} \end{bmatrix} \quad (3.52)$$

where $i = 1, 2, 3, 4$, $j = 2, 3, 4, 1$, and $[J]_{ij} = [J]_{ij}^{-1}$. Thus,

$$\begin{bmatrix} \theta_{sk} \\ \theta_{nk} \end{bmatrix} = [J]_{ij} \begin{bmatrix} \theta_{xk} \\ \theta_{yk} \end{bmatrix} \quad (3.53)$$

and Eq. 3.48 is expressed in Cartesian co-ordinates as:

$$\begin{bmatrix} \theta_{xk} \\ \theta_{yk} \end{bmatrix} = [J]_{ij} \begin{bmatrix} -\frac{3}{2l_{ij}} & -\frac{1}{4} & 0 & \frac{3}{2l_{ij}} & -\frac{1}{4} & 0 \\ 0 & 0 & \frac{1}{2} & 0 & 0 & \frac{1}{2} \end{bmatrix} \begin{bmatrix} w_i \\ [J]_{ij} \theta_{si} \\ [J]_{ij} \theta_{ni} \\ w_j \\ [J]_{ij} \theta_{xj} \\ [J]_{ij} \theta_{nj} \end{bmatrix} \quad (3.55)$$

The transformation matrix $[T]_{18 \times 12}$ of Eq. 3.41 is thus given by:

$$\begin{Bmatrix} \theta_{x1} \\ \theta_{y1} \\ \theta_{x2} \\ \theta_{y2} \\ \theta_{x3} \\ \theta_{y3} \\ \theta_{x4} \\ \theta_{y4} \\ \theta_{x5} \\ \theta_{y5} \\ \theta_{x6} \\ \theta_{y6} \\ \theta_{x7} \\ \theta_{y7} \\ \theta_{x8} \\ \theta_{y8} \\ \theta_{x9} \\ \theta_{y9} \end{Bmatrix} = \begin{bmatrix} 0 & 0 & -1 & 0 & 0 & 0 & 0 & 0 & 0 & 0 & 0 & 0 \\ 0 & -1 & 0 & 0 & 0 & 0 & 0 & 0 & 0 & 0 & 0 & 0 \\ 0 & 0 & 0 & 0 & 0 & 0 & -1 & 0 & 0 & 0 & 0 & 0 \\ 0 & 0 & 0 & 0 & -1 & 0 & 0 & 0 & 0 & 0 & 0 & 0 \\ 0 & 0 & 0 & 0 & 0 & 0 & 0 & 0 & -1 & 0 & 0 & 0 \\ 0 & 0 & 0 & 0 & 0 & 0 & 0 & -1 & 0 & 0 & 0 & 0 \\ 0 & 0 & 0 & 0 & 0 & 0 & 0 & 0 & 0 & 0 & 0 & -1 \\ 0 & 0 & 0 & 0 & 0 & 0 & 0 & 0 & 0 & 0 & -1 & 0 \\ T_{9,1} & T_{9,2} & T_{9,3} & T_{9,4} & T_{9,5} & T_{9,6} & 0 & 0 & 0 & 0 & 0 & 0 \\ T_{10,1} & T_{10,2} & T_{10,3} & T_{10,4} & T_{10,5} & T_{10,6} & 0 & 0 & 0 & 0 & 0 & 0 \\ 0 & 0 & 0 & T_{11,4} & T_{11,5} & T_{11,6} & T_{11,7} & T_{11,8} & T_{11,9} & 0 & 0 & 0 \\ 0 & 0 & 0 & T_{12,4} & T_{12,5} & T_{12,6} & T_{12,7} & T_{12,8} & T_{12,9} & 0 & 0 & 0 \\ 0 & 0 & 0 & 0 & 0 & 0 & T_{13,7} & T_{13,8} & T_{13,9} & T_{13,10} & T_{13,11} & T_{13,12} \\ 0 & 0 & 0 & 0 & 0 & 0 & T_{14,7} & T_{14,8} & T_{14,9} & T_{14,10} & T_{14,11} & T_{14,12} \\ T_{15,1} & T_{15,2} & T_{15,3} & 0 & 0 & 0 & 0 & 0 & 0 & T_{15,10} & T_{15,11} & T_{15,12} \\ T_{16,1} & T_{16,2} & T_{16,3} & 0 & 0 & 0 & 0 & 0 & 0 & T_{16,10} & T_{16,11} & T_{16,12} \\ T_{17,1} & T_{17,2} & T_{17,3} & T_{17,4} & T_{17,5} & T_{17,6} & T_{17,7} & T_{17,8} & T_{17,9} & T_{17,10} & T_{17,11} & T_{17,12} \\ T_{18,1} & T_{18,2} & T_{18,3} & T_{18,4} & T_{18,5} & T_{18,6} & T_{18,7} & T_{18,8} & T_{18,9} & T_{18,10} & T_{18,11} & T_{18,12} \end{bmatrix} \begin{Bmatrix} u_1 \\ v_1 \\ \theta_1 \\ u_2 \\ v_2 \\ \theta_2 \\ u_3 \\ v_3 \\ \theta_3 \\ u_4 \\ v_4 \\ \theta_4 \end{Bmatrix} \quad (3.56)$$

where

$$\begin{aligned} T(9,1) &= 1.50 * a(1) / c(1) \\ T(9,2) &= -0.75 * (b(1) * a(1)) / c(1) \\ T(9,3) &= -0.25 * (2.0 * b(1)^2 - a(1)^2) / c(1) \\ T(9,4) &= -1.50 * a(1) / c(1) \\ T(9,5) &= -0.75 * (b(1) * a(1)) / c(1) \\ T(9,6) &= -0.25 * (2.0 * b(1)^2 - a(1)^2) / c(1) \end{aligned} \quad (3.57)$$

$$\begin{aligned} T(10,1) &= 1.50 * b(1) / c(1) \\ T(10,2) &= 0.25 * (2.0 * a(1)^2 - b(1)^2) / c(1) \\ T(10,3) &= 0.75 * (b(1) * a(1)) / c(1) \\ T(10,4) &= -1.50 * b(1) / c(1) \\ T(10,5) &= 0.25 * (2.0 * a(1)^2 - b(1)^2) / c(1) \\ T(10,6) &= 0.75 * (a(1) * b(1)) / c(1) \end{aligned} \quad (3.58)$$

$$\begin{aligned}
T(11,4) &= 1.50 * a(2) / c(2) \\
T(11,5) &= -0.75 * (b(2) * a(2)) / c(2) \\
T(11,6) &= -0.25 * (2.0 * b(2)^2 - a(2)^2) / c(2) \\
T(11,7) &= -1.50 * a(2) / c(2) \\
T(11,8) &= -0.75 * (a(2) * b(2)) / c(2) \\
T(11,9) &= -0.25 * (2.0 * b(2)^2 - a(2)^2) / c(2)
\end{aligned} \tag{3.59}$$

$$\begin{aligned}
T(12,4) &= 1.50 * b(2) / c(2) \\
T(12,5) &= 0.25 * (2.0 * a(2)^2 - b(2)^2) / c(2) \\
T(12,6) &= 0.75 * (b(2) * a(2)) / c(2) \\
T(12,7) &= -1.50 * b(2) / c(2) \\
T(12,8) &= 0.25 * (2.0 * a(2)^2 - b(2)^2) / c(2) \\
T(12,9) &= 0.75 * (a(2) * b(2)) / c(2)
\end{aligned} \tag{3.60}$$

$$\begin{aligned}
T(13,7) &= 1.50 * a(3) / c(3) \\
T(13,8) &= -0.75 * (a(3) * b(3)) / c(3) \\
T(13,9) &= -0.25 * (2.0 * b(3)^2 - a(3)^2) / c(3) \\
T(13,10) &= -1.50 * a(3) / c(3) \\
T(13,11) &= -0.75 * (a(3) * b(3)) / c(3) \\
T(13,12) &= -0.25 * (2.0 * b(3)^2 - a(3)^2) / c(3)
\end{aligned} \tag{3.61}$$

$$\begin{aligned}
T(14,7) &= 1.50 * b(3) / c(3) \\
T(14,8) &= 0.25 * (2.0 * a(3)^2 - b(3)^2) / c(3) \\
T(14,9) &= 0.75 * (a(3) * b(3)) / c(3) \\
T(14,10) &= -1.50 * b(3) / c(3) \\
T(14,11) &= 0.25 * (2.0 * a(3)^2 - b(3)^2) / c(3) \\
T(14,12) &= 0.75 * (a(3) * b(3)) / c(3)
\end{aligned} \tag{3.62}$$

$$\begin{aligned}
T(15,1) &= 1.50 * a(4) / c(4) \\
T(15,2) &= -0.75 * (a(4) * b(4)) / c(4) \\
T(15,3) &= -0.25 * (2.0 * b(4)^2 - a(4)^2) / c(4) \\
T(15,10) &= 1.50 * a(4) / c(4) \\
T(15,11) &= -0.75 * (a(4) * b(4)) / c(4) \\
T(15,12) &= -0.25 * (2.0 * b(4)^2 - a(4)^2) / c(4)
\end{aligned} \tag{3.63}$$

$$\begin{aligned}
T(16,1) &= -1.50 * b(4) / c(4) \\
T(16,2) &= 0.25 * (2.0 * a(4)^2 - b(4)^2) / c(4) \\
T(16,3) &= 0.75 * (a(4) * b(4)) / c(4) \\
T(16,10) &= 1.50 * b(4) / c(4) \\
T(16,11) &= 0.25 * (2.0 * a(4)^2 - b(4)^2) / c(4) \\
T(16,12) &= 0.75 * (a(4) * b(4)) / c(4)
\end{aligned} \tag{3.64}$$

$$\begin{aligned}
T(17,1) &= -12.0 * \Delta * d(1) \\
T(17,2) &= \Delta * d(1) * \left(2.0 * b(1) - 2.0 * b(4) + \sum_{i=1}^4 b(i) \right) \\
T(17,3) &= -\Delta * d(1) * \left(2.0 * a(1) - 2.0 * a(4) + \sum_{i=1}^4 a(i) \right) \\
T(17,4) &= -12.0 * \Delta * d(3) \\
T(17,5) &= -\Delta * d(3) * \left(2.0 * b(1) - 2.0 * b(2) + \sum_{i=1}^4 b(i) \right) \\
T(17,6) &= \Delta * d(3) * \left(2.0 * a(1) - 2.0 * a(2) + \sum_{i=1}^4 a(i) \right) \\
T(17,7) &= 12.0 * \Delta * d(1) \\
T(17,8) &= \Delta * d(1) * \left(2.0 * b(2) - 2.0 * b(3) - \sum_{i=1}^4 b(i) \right) \\
T(17,9) &= -\Delta * d(1) * \left(2.0 * a(2) - 2.0 * a(3) - \sum_{i=1}^4 a(i) \right) \\
T(17,10) &= 12.0 * \Delta * d(3) \\
T(17,11) &= -\Delta * d(3) * \left(2.0 * b(4) - 2.0 * b(3) - \sum_{i=1}^4 b(i) \right) \\
T(17,12) &= \Delta * d(3) * \left(2.0 * a(4) - 2.0 * a(3) - \sum_{i=1}^4 a(i) \right)
\end{aligned} \tag{3.65}$$

$$\begin{aligned}
T(18,1) &= 12.0 * \Delta * d(2) \\
T(18,2) &= -\Delta * d(2) * \left(2.0 * b(1) - 2.0 * b(4) + \sum_{i=1}^4 b(i) \right) \\
T(18,3) &= \Delta * d(2) * \left(2.0 * a(1) - 2.0 * a(4) + \sum_{i=1}^4 a(i) \right) \\
T(18,4) &= 12.0 * \Delta * d(4) \\
T(18,5) &= \Delta * d(4) * \left(2.0 * b(1) - 2.0 * b(2) + \sum_{i=1}^4 b(i) \right) \\
T(18,6) &= -\Delta * d(4) * \left(2.0 * a(1) - 2.0 * a(2) + \sum_{i=1}^4 a(i) \right) \\
T(18,7) &= -12.0 * \Delta * d(2) \\
T(18,8) &= -\Delta * d(2) * \left(2.0 * b(2) - 2.0 * b(3) - \sum_{i=1}^4 b(i) \right) \\
T(18,9) &= \Delta * d(2) * \left(2.0 * a(2) - 2.0 * a(3) - \sum_{i=1}^4 a(i) \right) \\
T(18,10) &= -12.0 * \Delta * d(4) \\
T(18,11) &= \Delta * d(4) * \left(2.0 * b(4) - 2.0 * b(3) - \sum_{i=1}^4 b(i) \right) \\
T(18,12) &= -\Delta * d(4) * \left(2.0 * a(4) - 2.0 * a(3) - \sum_{i=1}^4 a(i) \right)
\end{aligned} \tag{3.66}$$

with

$$\begin{aligned}
a(i) &= x(i) - x(j); \quad i = 1, 2, 3, 4 \\
b(i) &= y(i) - y(j); \quad j = 2, 3, 4, 1 \\
c(i) &= \sum_{i=1}^4 (a(i)^2) - \sum_{i=1}^4 (b(i)^2) \\
d(1) &= 2[b(1) + b(4)] - \sum_{i=1}^4 b(i); \quad d(2) = 2[a(1) + a(4)] - \sum_{i=1}^4 a(i) \\
d(3) &= 2[b(1) + b(2)] - \sum_{i=1}^4 b(i); \quad d(4) = 2[a(1) + a(2)] - \sum_{i=1}^4 a(i) \\
\Delta &= 0.125 / \{ [a(3) - a(1)][b(4) - b(2)] - [a(4) - a(2)][b(3) - b(1)] \}
\end{aligned} \tag{3.67}$$

The stiffness transformation can be easily derived by substituting Eqs. 3.41 and 3.42 into the stiffness relationship for element QUAD9:

$$[K]^{QUAD9} \underbrace{[T] \{d\}}_{\{d\}^{QUAD9}} = \{f\}^{QUAD9} \Rightarrow [K]^{IDKQ} = [T]^T [K]^{QUAD9} [T] \tag{3.68}$$

As it can be observed, Eq. 3.68 does not change the element properties or its orientation in the global co-ordinate system. Rather, it represents a static condensation of the central and mid-node

degrees of freedom of the element QUAD9 in terms of the degrees of freedom at the corner nodes of the IDKQ element.

Further simplifications similar to that already shown for the RQD4 element are possible in order to reduce the amount of calculations required in the numerical integration process. These are achieved by rewriting $[K]^{IDKQ}$ as follows:

$$[K]^{IDKQ} = [T]^T \left(\int [B]_{QUAD9}^T [D] [B]_{QUAD9} dV \right) [T] \quad (3.69)$$

or

$$[K]^{IDKQ} = \int [T]^T [B]_{QUAD9}^T [D] [B]_{QUAD9} [T] dV = \int [B]_{IDKQ}^T [D] [B]_{IDKQ} dV \quad (3.70)$$

where

$$[B]_{3 \times 12}^{IDKQ} = [B]_{3 \times 18}^{QUAD9} [T]_{18 \times 12} \quad (3.71)$$

Finally, the stiffness matrix of the IDKQ element may be expressed as:

$$[K]_{12 \times 12}^{IDKQ} = \int_{-1}^{+1} \int_{-1}^{+1} [B]_{IDKQ}^T [D]_b [B]_{IDKQ} |J| d\xi d\eta \quad (3.72)$$

in which $[B]_{IDKQ}$ is the curvature-transformation matrix of the IDKQ element, $[D]_b$ is the bending elasticity matrix, and $|J|$ is the determinant of the Jacobian matrix of the co-ordinate transformation. As it can be observed, $[T]_{18 \times 12}$ is not a square matrix, and it cannot be inverted. For this reason, the transformation of degrees of freedom by means of the matrix $[T]$ can be only done from element QUAD9 to element IDKQ.

The fact that the transformation matrix $[T]_{18 \times 12}$ relates only to the rotational degrees of freedom makes it difficult to formulate the work equivalent nodal loads corresponding to distributed load. The cubic out-of-plane displacements w in Eq. 3.46 apply only on the border and centre lines of the element. Therefore, it is not simple to formulate the work equivalent load vector for distributed loads. However, a lumped nodal load vector f_l^{IDKQ} can be employed as an approximation for the normal distributed load $q_z^T = [q_{zi} \ 0 \ 0]$. For quadrilateral elements, bilinear shape functions can be used to represent the equivalent lumped nodal loads of the distributed load. For a rectangular element, the lumped nodal loads are:

$$\{f_l^{IDKQ}\} = q_z \begin{pmatrix} \frac{A_e}{4} & 0 & 0 & \frac{A_e}{4} & 0 & 0 & \frac{A_e}{4} & 0 & 0 & \frac{A_e}{4} & 0 & 0 \end{pmatrix} \quad (3.73)$$

where A_e is the area of the element. Since w is represented by a cubic interpolation as shown in Eq. 3.46, a cubic polynomial expansion \bar{N}_c may be more consistent with the derivation of the equivalent nodal loads f_c^{IDKQ} :

$$\{f_c^{IDKQ}\} = \int_{A_e} \bar{N}_c^T q_z dA_e \quad (3.74)$$

where

$$\bar{N}_c^T = [1 \quad \xi \quad \eta \quad \xi^2 \quad \xi\eta \quad \eta^2 \quad \xi^3 \quad \xi^2\eta \quad \xi\eta^2 \quad \eta^3 \quad \xi^3\eta \quad \xi\eta^3] \{a\} \quad (3.75)$$

is a complete two-dimensional expansion from the Pascal Triangle, completed by the two bi-cubic extra terms $\xi^3\eta$ and $\xi\eta^3$ corresponding to the twelve generalised co-ordinates $\{a\}$ that must be exchanged with the twelve degrees of freedom $\{d^{IDKQ}\}$. Such exchange corresponds to the derivation of the shape function for w in the Kirchhoff Plate Bending Theory. For a general quadrilateral shape of the element, numerical integration must be employed to obtain either f_l^{IDKQ} or f_c^{IDKQ} . Numerical experiments on element IDKQ show that the lumped nodal load vector f_l^{IDKQ} is a very good approximation for practical applications [41].

3.5 Quadrilateral facet shell element (QFSE)

The quadrilateral facet shell element QFSE, illustrated in Figure 3-9, is obtained by coupling the in-plane element RQUAD4 with the plate bending elements of Section 3.4 [27], [28]. The element has four nodes with six degrees of freedom per node: three displacements (u , v , w) and three rotations (θ_x , θ_y , ω_z). Because of material non-linearity, this element is an anisotropic shell in which the membrane and bending actions are assumed to be coupled.

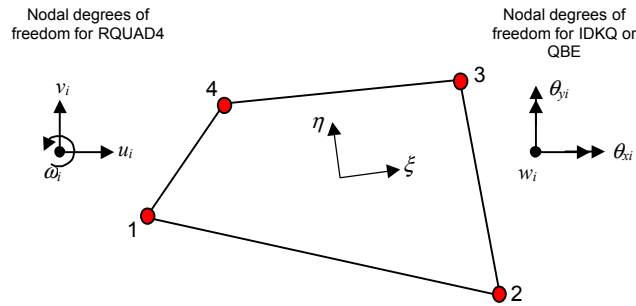


Figure 3-9: The facet shell element QFSE.

The strain $\{\mathcal{E}\}$ at any point within the element is obtained from:

$$\{\mathcal{E}\} = \{\mathcal{E}_o\} - z\{\mathcal{X}\} \quad (3.76)$$

where $\{\varepsilon_o\}$ is the vector of in-plane strains of the projection of a given point on the reference plane, $\{\chi\}$ is the vector of curvatures due to bending, and z is the local z -co-ordinate through the thickness of the element of the point under consideration (see Figure 3-10). The z -axis is considered normal to the middle plane, and its origin coincides with the middle plane of the element. From basic theory:

$$\{\varepsilon\} = [B_m] \{d_m\} \quad (3.77)$$

$$\{\chi\} = [B_b] \{d_b\} \quad (3.78)$$

where subscripts m and b denote respectively membrane and bending actions. Equation 3.76 can be re-written as:

$$\{\varepsilon\} = \left[[B_m] - z[B_b] \right] \begin{Bmatrix} d_m \\ d_b \end{Bmatrix} = [B] \{d\} \quad (3.79)$$

By substituting $[B]$ from Eq. 3.79 into the element stiffness equation, matrix $[k]$ results in:

$$[k] = \int \begin{bmatrix} [B_m]^T [D] [B_m] & -z[B_m]^T [D] [B_b] \\ -z[B_b]^T [D] [B_m] & z^2 [B_b]^T [D] [B_b] \end{bmatrix} dV = \begin{bmatrix} [k]_{mm} & [k]_{mb} \\ [k]_{bm} & [k]_{bb} \end{bmatrix} \quad (3.80)$$

The diagonal terms in Eq. 3.80 are the respective stiffness matrices of element RQUAD4 and the plate bending element. The off-diagonal terms are the coupling matrices, which are non-zero if the material properties are not symmetric with respect to the middle surface of the shell. This situation can occur when yielding and/or cracking takes place in some fibres above or below the middle surface and not in others. In program UMAR, plate and shell elements are divided into layers of different materials, as illustrated in Figure 3-10. Each layer is assumed to be in a state of plane stress. Within the thickness of each layer, the stresses and material properties are assumed to be constant.

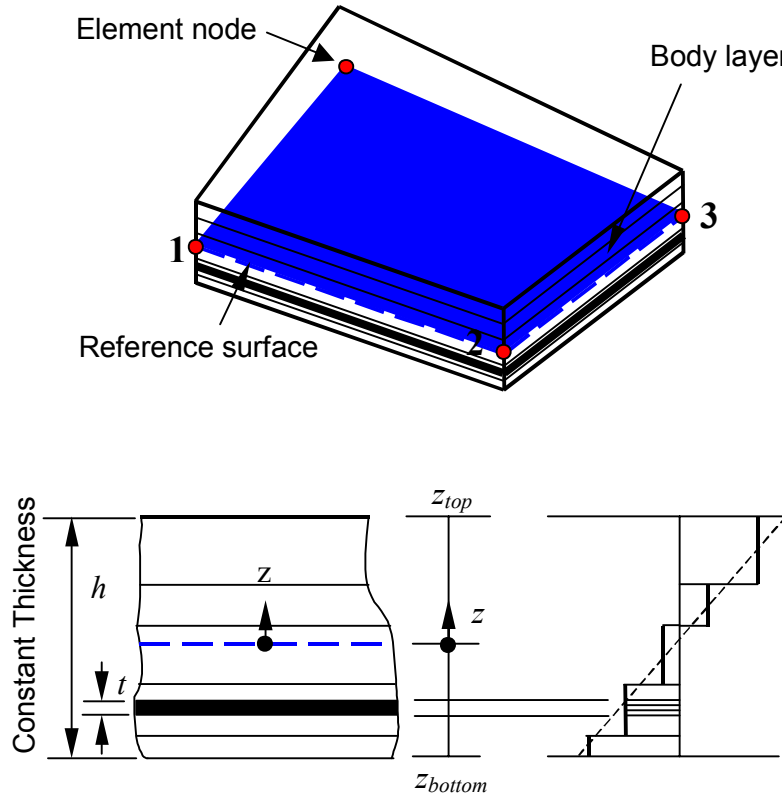


Figure 3-10: Layered shell element.

In evaluating the sub-matrices that comprise the stiffness matrix $[k]$ in Eq. 3.80, the volume integral is split into a summation over the number of layers through the thickness and an area integral over the surface of the element. For example,

$$[k]_{mm} = \int [B_m]^T [D] [B_m] dV = \iint [B_m]^T \left(\int_z [D] dz \right) [B_m] dxdy \quad (3.81)$$

The line integral along the thickness of the shell of Eq. 3.81, denoted by $[D]_{mm}$, is calculated in the following fashion:

$$[D]_{mm} = \int_z [D] dz = \sum_{i=1}^n (z_{i+1} - z_i) [D]_i \quad (3.82)$$

where z_{i+1} and z_i are the z co-ordinates of the top and bottom surfaces of layer i , and n is the total number of layers in a given element. The constitutive matrix $[D]_i$ for each layer will depend upon the material forming that layer. The remaining sub-matrices in Eq. 3.80 are evaluated in a similar way, the line integral for the remaining terms resulting in:

$$[D]_{mb} = \int_z [D] dz = -\frac{1}{2} \sum_{i=1}^n (z_{i+1}^2 - z_i^2) [D]_i \quad (3.83)$$

$$[D]_{bb} = \int_z z^2 [D] dz = \frac{1}{3} \sum_{i=1}^n (z_{i+1}^3 - z_i^3) [D]_i \quad (3.84)$$

The equivalent nodal forces $\{F\}_{\bar{\sigma}}$ and $\{F\}_{\bar{\varepsilon}}$ due to initial stresses and strains are similarly calculated, i.e.,

$$\{F\}_{\bar{\varepsilon}} = \iint \left\{ \begin{bmatrix} B_m \end{bmatrix}^T \{ \sigma_{\bar{\varepsilon}} \}_m \right. \left. \begin{bmatrix} B_b \end{bmatrix}^T \{ \sigma_{\bar{\varepsilon}} \}_b \right\} dx dy \quad (3.85)$$

$$\{F\}_{\bar{\sigma}} = \iint \left\{ \begin{bmatrix} B_m \end{bmatrix}^T \{ \sigma_{\bar{\sigma}} \}_m \right. \left. \begin{bmatrix} B_b \end{bmatrix}^T \{ \sigma_{\bar{\sigma}} \}_b \right\} dx dy \quad (3.86)$$

where

$$\{ \sigma_{\bar{\varepsilon}} \}_m = \int [D] \{ \bar{\varepsilon} \} dz = \sum_{i=1}^n (z_{i+1} - z_i) [D]_i \{ \bar{\varepsilon} \}_i \quad (3.87)$$

$$\{ \sigma_{\bar{\varepsilon}} \}_b = - \int z [D] \{ \bar{\varepsilon} \} dz = -\frac{1}{2} \sum_{i=1}^n (z_{i+1}^2 - z_i^2) [D]_i \{ \bar{\varepsilon} \}_i \quad (3.88)$$

$$\{ \sigma_{\bar{\sigma}} \}_m = \int \{ \bar{\sigma} \} dz = \sum_{i=1}^n (z_{i+1} - z_i) \{ \bar{\sigma} \}_i \quad (3.89)$$

$$\{ \sigma_{\bar{\sigma}} \}_b = - \int z \{ \bar{\sigma} \} dz = -\frac{1}{2} \sum_{i=1}^n (z_{i+1}^2 - z_i^2) \{ \bar{\sigma} \}_i \quad (3.90)$$

3.6 Solid isoparametric element

Program UMAR has two hexahedral isoparametric elements of the “serendipity” family (i.e., containing boundary nodes only): a linear brick element (8 nodes) and a quadratic brick element (20 nodes), see Figure 3-11.

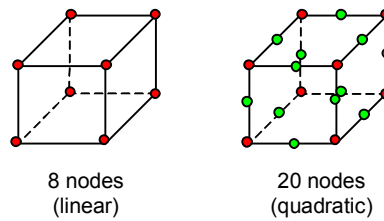


Figure 3-11: Hexahedral elements of the “serendipity” family implemented in UMAR.

The element geometry and field quantity ϕ of a solid isoparametric element are given by:

$$x = \sum N_i x_i \quad y = \sum N_i y_i \quad z = \sum N_i z_i \quad \phi = \sum N_i \phi_i \quad (3.91)$$

where i ranges over the number of nodes in the element. The shape functions N_i are functions of the isoparametric coordinates ξ , η , and ζ , and the faces of the element lie at $\xi = \pm 1$, $\eta = \pm 1$, and $\zeta = \pm 1$, respectively (see Figure 3-12). The node numbering convention used in Figure 3-12 is that of corner nodes being numbered first, followed by mid-side nodes for the second-order element (20-node brick element). The shape functions for the 8-node brick element can be summarized in:

$$N_i = \frac{1}{8}(1 + \xi\xi_i)(1 + \eta\eta_i)(1 + \zeta\zeta_i) \quad (3.92)$$

where ξ_i , η_i , and ζ_i denote the natural co-ordinates of the i^{th} node. The shape functions of the 20-node brick can be grouped as follows:

$$\text{For the corner nodes } i=1,2,\dots,8: \quad N_i = \frac{1}{8}(1 + \xi\xi_i)(1 + \eta\eta_i)(1 + \zeta\zeta_i)(\xi\xi_i + \eta\eta_i + \zeta\zeta_i - 2) \quad (3.93)$$

$$\text{For the midside nodes } i=9,11,13,15: \quad N_i = \frac{1}{4}(1 - \xi^2)(1 + \eta\eta_i)(1 + \zeta\zeta_i) \quad (3.94)$$

$$\text{For the midside nodes } i=10,12,14,16: \quad N_i = \frac{1}{4}(1 + \xi\xi_i)(1 - \eta^2)(1 + \zeta\zeta_i) \quad (3.95)$$

$$\text{For the midside nodes } i=17,18,19,20: \quad N_i = \frac{1}{4}(1 + \xi\xi_i)(1 + \eta\eta_i)(1 - \zeta^2) \quad (3.96)$$

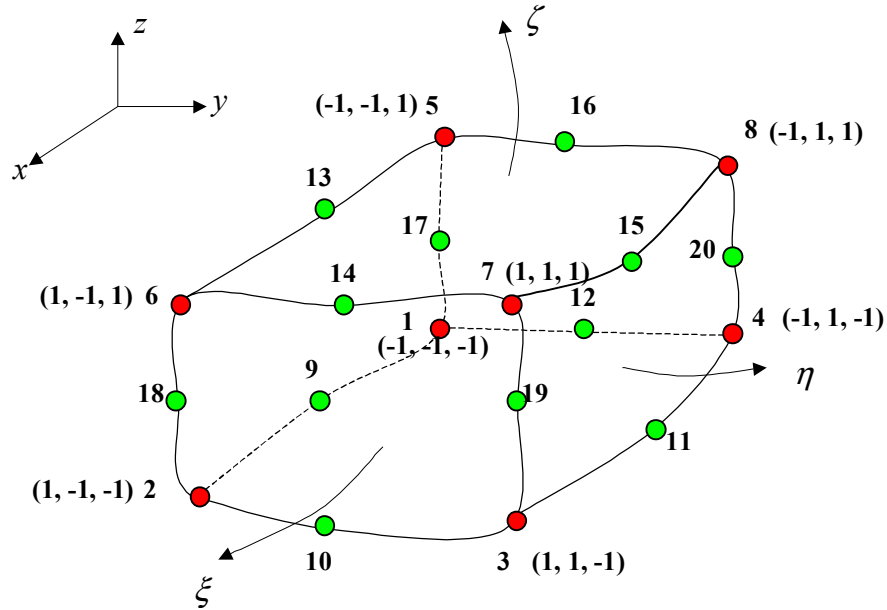


Figure 3-12: Eight-to-twenty nodes solid isoparametric element.

In structural mechanics, the nodal degrees of freedom are given by the displacements u , v , and w , which are respectively parallel to the x , y , and z directions. The strain-displacement relation is $\{\varepsilon\} = [B]\{d\}$, where $\{d\} = [u_1 \ v_1 \ w_1 \ u_2 \ \cdots \ w_n]^T$, n being the number of nodes, and $[B]$ is the product of $[M]_1$, $[M]_2$, and $[M]_3$ as given by Eqs. 3.97, 3.98, and 3.99.

$$\begin{Bmatrix} \varepsilon_x \\ \varepsilon_y \\ \varepsilon_z \\ \gamma_{yz} \\ \gamma_{zx} \\ \gamma_{xy} \end{Bmatrix} = \underbrace{\begin{bmatrix} 1 & 0 & 0 & 0 & 0 & 0 & 0 & 0 & 0 \\ 0 & 0 & 0 & 0 & 1 & 0 & 0 & 0 & 0 \\ 0 & 0 & 0 & 0 & 0 & 0 & 0 & 0 & 1 \\ 0 & 0 & 0 & 0 & 0 & 1 & 0 & 1 & 0 \\ 0 & 0 & 1 & 0 & 0 & 0 & 1 & 0 & 0 \\ 0 & 1 & 0 & 1 & 0 & 0 & 0 & 0 & 0 \end{bmatrix}}_{[M]_1} \begin{Bmatrix} u_{,x} \\ u_{,y} \\ u_{,z} \\ v_{,x} \\ v_{,y} \\ v_{,z} \\ w_{,x} \\ w_{,y} \\ w_{,z} \end{Bmatrix} \quad (3.97)$$

$$\begin{Bmatrix} u_{,x} \\ u_{,y} \\ u_{,z} \\ v_{,x} \\ v_{,y} \\ v_{,z} \\ w_{,x} \\ w_{,y} \\ w_{,z} \end{Bmatrix} = \underbrace{\begin{bmatrix} \Gamma_{11} & \Gamma_{12} & \Gamma_{13} & 0 & 0 & 0 & 0 & 0 & 0 \\ \Gamma_{21} & \Gamma_{22} & \Gamma_{23} & 0 & 0 & 0 & 0 & 0 & 0 \\ \Gamma_{31} & \Gamma_{32} & \Gamma_{33} & 0 & 0 & 0 & 0 & 0 & 0 \\ 0 & 0 & 0 & \Gamma_{11} & \Gamma_{12} & \Gamma_{13} & 0 & 0 & 0 \\ 0 & 0 & 0 & \Gamma_{21} & \Gamma_{22} & \Gamma_{23} & 0 & 0 & 0 \\ 0 & 0 & 0 & \Gamma_{31} & \Gamma_{32} & \Gamma_{33} & 0 & 0 & 0 \\ 0 & 0 & 0 & 0 & 0 & 0 & \Gamma_{11} & \Gamma_{12} & \Gamma_{13} \\ 0 & 0 & 0 & 0 & 0 & 0 & \Gamma_{21} & \Gamma_{22} & \Gamma_{23} \\ 0 & 0 & 0 & 0 & 0 & 0 & \Gamma_{31} & \Gamma_{32} & \Gamma_{33} \end{bmatrix}}_{[M]_2} \begin{Bmatrix} u_{,\xi} \\ u_{,\eta} \\ u_{,\zeta} \\ v_{,\xi} \\ v_{,\eta} \\ v_{,\zeta} \\ w_{,\xi} \\ w_{,\eta} \\ w_{,\zeta} \end{Bmatrix} \quad (3.98)$$

$$\begin{Bmatrix} u_{,\xi} \\ u_{,\eta} \\ u_{,\zeta} \\ v_{,\xi} \\ v_{,\eta} \\ v_{,\zeta} \\ w_{,\xi} \\ w_{,\eta} \\ w_{,\zeta} \end{Bmatrix} = \underbrace{\begin{bmatrix} N_{1,\xi} & 0 & 0 & N_{2,\xi} & \cdots & 0 \\ N_{1,\eta} & 0 & 0 & N_{2,\eta} & \cdots & 0 \\ N_{1,\zeta} & 0 & 0 & N_{2,\zeta} & \cdots & 0 \\ 0 & N_{1,\xi} & 0 & 0 & \cdots & 0 \\ 0 & N_{1,\eta} & 0 & 0 & \cdots & 0 \\ 0 & N_{1,\zeta} & 0 & 0 & \cdots & 0 \\ 0 & 0 & N_{1,\xi} & 0 & \cdots & N_{n,\xi} \\ 0 & 0 & N_{1,\eta} & 0 & \cdots & N_{n,\eta} \\ 0 & 0 & N_{1,\zeta} & 0 & \cdots & N_{n,\zeta} \end{bmatrix}}_{[M]_3} \begin{Bmatrix} u_1 \\ v_1 \\ w_1 \\ u_2 \\ \vdots \\ w_n \end{Bmatrix} \quad (3.99)$$

Matrix $[I]$ is the inverse of the Jacobian matrix $[J]$, which is given by:

$$[J] = \begin{bmatrix} x_{,\xi} & y_{,\xi} & z_{,\xi} \\ x_{,\eta} & y_{,\eta} & z_{,\eta} \\ x_{,\zeta} & y_{,\zeta} & z_{,\zeta} \end{bmatrix} = \sum \begin{bmatrix} N_{i,\xi} x_i & N_{i,\xi} y_i & N_{i,\xi} z_i \\ N_{i,\eta} x_i & N_{i,\eta} y_i & N_{i,\eta} z_i \\ N_{i,\zeta} x_i & N_{i,\zeta} y_i & N_{i,\zeta} z_i \end{bmatrix} \quad (3.100)$$

For the three-dimensional element, the structural element stiffness is given by:

$$[k]_{dof \times dof} = \int_{-1}^1 \int_{-1}^1 \int_{-1}^1 [B]^T [D] [B] J d\xi d\eta d\zeta \quad (3.101)$$

$\begin{matrix} dof \times 6 & 6 \times 6 & 6 \times dof \end{matrix}$

where $[D]$ is the material property matrix and J is the determinant of the Jacobian matrix. The latter parameter expresses the ratio of volume $dx dy dz$ to $d\xi d\eta d\zeta$. Contributions to the element load vector include the terms

$$\int_{-1}^1 \int_{-1}^1 \int_{-1}^1 \left([B]^T [D] \{\epsilon_0\} - [B]^T \{\sigma_0\} + [N]^T \{F\} \right) J d\xi d\eta d\zeta \quad (3.102)$$

$\begin{matrix} n \times 6 & 6 \times 6 & 6 \times 1 & n \times 6 & 6 \times 1 & n \times 3 & 3 \times 1 \end{matrix}$

where $\{\epsilon_0\}$ and $\{\sigma_0\}$ represent the initial strain and stress fields, respectively, and $\{F\}$ is the vector of body forces. Equations 3.101 and 3.102 are numerically integrated by Gauss quadrature in program UMAR.

For a scalar field problem in three dimensions, with n the number of nodes per element, the element characteristic matrix becomes:

$$[K]_{n \times n} = \int_{-1}^1 \int_{-1}^1 \int_{-1}^1 [B]^T [D] [B] J d\xi d\eta d\zeta \quad (3.103)$$

$\begin{matrix} n \times 3 & 3 \times 3 & 3 \times n \end{matrix}$

where $[D]$ is the principal axes diffusivity/permeability tensor,

$$[D] = \begin{bmatrix} D_x & 0 & 0 \\ 0 & D_y & 0 \\ 0 & 0 & D_z \end{bmatrix} \quad (3.104)$$

and matrix $[B]$ is given by:

$$[B]^T = \begin{bmatrix} \frac{\partial [N]^T}{\partial x} & \frac{\partial [N]^T}{\partial y} & \frac{\partial [N]^T}{\partial z} \end{bmatrix} \quad (3.105)$$

3.6.1 Layered solid isoparametric element

The three-dimensional element can be used for the analysis of laminated composite solids by specifying several layers of different materials in different orientations. The material layers can be stacked in any of the three isoparametric directions, parallel to opposite faces of the parent isoparametric element. Layering directions 1, 2, and 3 correspond respectively to isoparametric directions ξ , η , and ζ . The layered solid element uses the same shape functions as the homogeneous one, but integration along the layering direction takes into account the variation of material properties.

The element matrices and vectors are obtained by numerical integration using Gauss quadrature. Whereas Gauss quadrature in the plane of the lamina is carried out in the same manner as a two-dimensional isoparametric element, the order of integration along the layering direction is given by the number of layers specified in that direction. Program UMAR can calculate the weights of any number of Gauss points given their co-ordinates. Thus, there is not a maximum on the number of layers that can be specified in the program. Yet, it is desirable the minimum number of layers be at least the order of integration used in the plane of the lamina. After having specified the number of layers and the layering direction, program UMAR calculates the co-ordinate of the centre plane of each layer where Gauss points are to be positioned and element matrices and vectors are to be evaluated.

4 Material library

To address the behaviour of different types of materials, UMAR provides a broad library of linear and non-linear, isotropic and anisotropic constitutive models. These material models are described in the following sub-sections.

4.1 Theory of elasticity

A stressed body is said to behave elastically if its strains are recovered when the stresses are removed, i.e., there is a one-to-one correspondence between stresses and strains, irrespective of the history of loading. All elastic models that are implemented in UMAR can be found in the module <elasticity_library> in the file elasticity.f90.

4.1.1 Linear elastic model

A body is said to be linearly elastic if each stress component can be expressed as a linear combination of all the strain components, i.e.,

$$\{\sigma\} = [D]\{\varepsilon\} \quad (4.1)$$

where $\{\sigma\}$ and $\{\varepsilon\}$ respectively denote the stress and strain vectors, and $[D]$ is a symmetric square matrix that contains the elastic properties of the material. Program UMAR can handle both isotropic problems, in which the material elastic parameters are independent of orientation, and anisotropic problems, in which the elastic constants vary according to the orientation.

Isotropic linear-elastic models

Isotropic materials are those whose material properties are independent of orientation. These materials are described by two independent elastic constants: Young's modulus (also called modulus of elasticity) E and Poisson's ratio ν . The stress-strain relations for an isotropic, linearly elastic material implemented in UMAR are given by:

$$\text{Uniaxial stress: } \sigma_x = E\varepsilon_x \quad (4.2)$$

$$\text{Plane stress } (\sigma_z = \tau_{yz} = \tau_{zx} = 0): \quad \begin{Bmatrix} \sigma_x \\ \sigma_y \\ \tau_{xy} \end{Bmatrix} = \frac{E}{1-\nu^2} \begin{bmatrix} 1 & \nu & 0 \\ \nu & 1 & 0 \\ 0 & 0 & \frac{1-\nu}{2} \end{bmatrix} \begin{Bmatrix} \varepsilon_x \\ \varepsilon_y \\ \gamma_{xy} \end{Bmatrix} \quad (4.3)$$

$$\text{Axisymmetry } (\tau_{r\theta} = \tau_{\theta z} = \gamma_{r\theta} = \gamma_{\theta z} = 0):$$

$$\begin{Bmatrix} \sigma_r \\ \sigma_\theta \\ \sigma_z \\ \tau_{rz} \end{Bmatrix} = \frac{E}{(1+\nu)(1-2\nu)} \begin{bmatrix} 1-\nu & \nu & \nu & 0 \\ \nu & 1-\nu & \nu & 0 \\ \nu & \nu & 1-\nu & 0 \\ 0 & 0 & 0 & \frac{1-2\nu}{2} \end{bmatrix} \begin{Bmatrix} \varepsilon_r \\ \varepsilon_\theta \\ \varepsilon_z \\ \gamma_{rz} \end{Bmatrix} \quad (4.4)$$

$$\text{Curved shell: } \begin{Bmatrix} \sigma_x \\ \sigma_y \\ \tau_{yz} \\ \tau_{zx} \\ \tau_{xy} \end{Bmatrix} = \frac{E}{1-\nu^2} \begin{bmatrix} 1 & \nu & 0 & 0 & 0 \\ \nu & 1 & 0 & 0 & 0 \\ 0 & 0 & \frac{1-\nu}{2} & 0 & 0 \\ 0 & 0 & 0 & \frac{1-\nu}{2} & 0 \\ 0 & 0 & 0 & 0 & \frac{1-\nu}{2} \end{bmatrix} \begin{Bmatrix} \varepsilon_x \\ \varepsilon_y \\ \gamma_{yz} \\ \gamma_{zx} \\ \gamma_{xy} \end{Bmatrix} \quad (4.5)$$

$$\text{3-D: } \begin{Bmatrix} \sigma_x \\ \sigma_y \\ \sigma_z \\ \tau_{yz} \\ \tau_{zx} \\ \tau_{xy} \end{Bmatrix} = \frac{E}{(1+\nu)(1-2\nu)} \begin{bmatrix} 1-\nu & \nu & \nu & 0 & 0 & 0 \\ \nu & 1-\nu & \nu & 0 & 0 & 0 \\ \nu & \nu & 1-\nu & 0 & 0 & 0 \\ 0 & 0 & 0 & \frac{1-2\nu}{2} & 0 & 0 \\ 0 & 0 & 0 & 0 & \frac{1-2\nu}{2} & 0 \\ 0 & 0 & 0 & 0 & 0 & \frac{1-2\nu}{2} \end{bmatrix} \begin{Bmatrix} \varepsilon_x \\ \varepsilon_y \\ \varepsilon_z \\ \gamma_{yz} \\ \gamma_{zx} \\ \gamma_{xy} \end{Bmatrix} \quad (4.6)$$

The above relations can be found in subroutine <isotropic_D_matrix> in the module <mechanics_library> (file mechanics.f90.)

Orthotropic linear-elastic models

An orthotropic material is an anisotropic material that has different elastic properties in the three-principal directions (directions of elastic symmetry). Such material is characterised by nine independent elastic constants: three Young's moduli (E_x , E_y , E_z), three Poisson's ratios (ν_{xy} , ν_{yz} , ν_{zx}), and three shear moduli (G_{xy} , G_{yz} , G_{zx}).

The compliance matrix $[C]$ of an orthotropic material takes the form:

$$\begin{Bmatrix} \varepsilon_x \\ \varepsilon_y \\ \varepsilon_z \\ \gamma_{yz} \\ \gamma_{zx} \\ \gamma_{xy} \end{Bmatrix} = \begin{bmatrix} \frac{1}{E_x} & -\frac{\nu_{yx}}{E_y} & -\frac{\nu_{zx}}{E_z} & 0 & 0 & 0 \\ -\frac{\nu_{xy}}{E_x} & \frac{1}{E_y} & -\frac{\nu_{zy}}{E_z} & 0 & 0 & 0 \\ -\frac{\nu_{xz}}{E_x} & -\frac{\nu_{yz}}{E_y} & \frac{1}{E_z} & 0 & 0 & 0 \\ 0 & 0 & 0 & \frac{1}{G_{yz}} & 0 & 0 \\ 0 & 0 & 0 & 0 & \frac{1}{G_{zx}} & 0 \\ 0 & 0 & 0 & 0 & 0 & \frac{1}{G_{xy}} \end{bmatrix} \begin{Bmatrix} \sigma_x \\ \sigma_y \\ \sigma_z \\ \tau_{yz} \\ \tau_{zx} \\ \tau_{xy} \end{Bmatrix} \quad (4.7)$$

In general, ν_{ij} is not equal to ν_{ji} ; however, they are related by $\nu_{ij}/E_i = \nu_{ji}/E_j$ for $i \neq j$. Thus, matrix $[C]$ can be written as:

$$[C] = \begin{bmatrix} \frac{1}{E_x} & -\frac{\nu_{xy}}{E_x} & -\frac{\nu_{xz}}{E_x} & 0 & 0 & 0 \\ -\frac{\nu_{xy}}{E_x} & \frac{1}{E_y} & -\frac{\nu_{yz}}{E_y} & 0 & 0 & 0 \\ -\frac{\nu_{xz}}{E_x} & -\frac{\nu_{yz}}{E_y} & \frac{1}{E_z} & 0 & 0 & 0 \\ 0 & 0 & 0 & \frac{1}{G_{yz}} & 0 & 0 \\ 0 & 0 & 0 & 0 & \frac{1}{G_{zx}} & 0 \\ 0 & 0 & 0 & 0 & 0 & \frac{1}{G_{xy}} \end{bmatrix} \quad (4.8)$$

The stiffness matrix $[D]$ for orthotropic materials is found from the inverse of the compliance matrix, i.e., $[D] = [C]^{-1}$. The stress-strain relations for orthotropic, linearly elastic materials implemented in UMAR are given by:

$$\text{Uniaxial stress: } \sigma_x = E_x \varepsilon_x \quad (4.9)$$

$$\text{Plane stress } (\sigma_z = \tau_{yz} = \tau_{zx} = 0): \begin{Bmatrix} \sigma_x \\ \sigma_y \\ \tau_{xy} \end{Bmatrix} = \begin{bmatrix} \frac{E_x^2}{E_x - \nu_{xy}^2 E_y} & \frac{\nu_{xy} E_x E_y}{E_x - \nu_{xy}^2 E_y} & 0 \\ \frac{\nu_{xy} E_x E_y}{E_x - \nu_{xy}^2 E_y} & \frac{E_x E_y}{E_x - \nu_{xy}^2 E_y} & 0 \\ 0 & 0 & G_{xy} \end{bmatrix} \begin{Bmatrix} \varepsilon_x \\ \varepsilon_y \\ \gamma_{xy} \end{Bmatrix} \quad (4.10)$$

Axisymmetry ($\tau_{r\theta} = \tau_{\theta z} = \gamma_{r\theta} = \gamma_{\theta z} = 0$):

$$\begin{Bmatrix} \sigma_r \\ \sigma_\theta \\ \sigma_z \\ \tau_{rz} \end{Bmatrix} = \begin{bmatrix} \frac{(E_\theta - \nu_{\theta z}^2 E_z) E_r^2}{\Delta} & \frac{(E_\theta \nu_{r\theta} + \nu_{\theta z} \nu_{rz} E_z) E_r E_\theta}{\Delta} & \frac{(\nu_{rz} + \nu_{r\theta} \nu_{\theta z}) E_r E_\theta E_z}{\Delta} & 0 \\ \frac{(E_\theta \nu_{r\theta} + \nu_{\theta z} \nu_{rz} E_z) E_r E_\theta}{\Delta} & \frac{(E_r - \nu_{rz}^2 E_z) E_\theta^2}{\Delta} & \frac{(E_r \nu_{\theta z} + \nu_{r\theta} \nu_{rz} E_\theta) E_\theta E_z}{\Delta} & 0 \\ \frac{(\nu_{rz} + \nu_{r\theta} \nu_{\theta z}) E_r E_\theta E_z}{\Delta} & \frac{(E_r \nu_{\theta z} + \nu_{r\theta} \nu_{rz} E_\theta) E_\theta E_z}{\Delta} & \frac{(E_r - \nu_{rz}^2 E_z) E_\theta E_z}{\Delta} & 0 \\ 0 & 0 & 0 & G_{rz} \end{bmatrix} \begin{Bmatrix} \varepsilon_r \\ \varepsilon_\theta \\ \varepsilon_z \\ \gamma_{rz} \end{Bmatrix} \quad (4.11)$$

$$\text{with } \Delta = E_r (E_\theta - E_z \nu_{\theta z}^2) - E_\theta [E_\theta \nu_{r\theta}^2 + E_z \nu_{rz} (\nu_{rz} + 2\nu_{\theta z} \nu_{r\theta})]$$

$$\text{Curved shell: } \begin{Bmatrix} \sigma_x \\ \sigma_y \\ \tau_{yz} \\ \tau_{zx} \\ \tau_{xy} \end{Bmatrix} = \begin{bmatrix} \frac{E_x^2}{E_x - \nu_{xy}^2 E_y} & \frac{\nu_{xy} E_x E_y}{E_x - \nu_{xy}^2 E_y} & 0 & 0 & 0 \\ \frac{\nu_{xy} E_x E_y}{E_x - \nu_{xy}^2 E_y} & \frac{E_x E_y}{E_x - \nu_{xy}^2 E_y} & 0 & 0 & 0 \\ 0 & 0 & G_{yz} & 0 & 0 \\ 0 & 0 & 0 & G_{zx} & 0 \\ 0 & 0 & 0 & 0 & G_{xy} \end{bmatrix} \begin{Bmatrix} \varepsilon_x \\ \varepsilon_y \\ \gamma_{yz} \\ \gamma_{zx} \\ \gamma_{xy} \end{Bmatrix} \quad (4.12)$$

3-D:

$$\begin{Bmatrix} \sigma_x \\ \sigma_y \\ \sigma_z \\ \tau_{yz} \\ \tau_{zx} \\ \tau_{xy} \end{Bmatrix} = \begin{bmatrix} \frac{(E_y - \nu_{yz}^2 E_z) E_x^2}{\Delta} & \frac{(\nu_{xy} E_y + \nu_{yz} \nu_{xz} E_z) E_x E_y}{\Delta} & \frac{(\nu_{xz} + \nu_{xy} \nu_{yz}) E_x E_y E_z}{\Delta} & 0 & 0 & 0 \\ \frac{(\nu_{xy} E_y + \nu_{yz} \nu_{xz} E_z) E_x E_y}{\Delta} & \frac{(E_x - \nu_{xz}^2 E_z) E_y^2}{\Delta} & \frac{(\nu_{yz} E_x + \nu_{xy} \nu_{xz} E_y) E_y E_z}{\Delta} & 0 & 0 & 0 \\ \frac{(\nu_{xz} + \nu_{xy} \nu_{yz}) E_x E_y E_z}{\Delta} & \frac{(\nu_{yz} E_x + \nu_{xy} \nu_{xz} E_y) E_y E_z}{\Delta} & \frac{(E_x - \nu_{xy}^2 E_y) E_y E_z}{\Delta} & 0 & 0 & 0 \\ 0 & 0 & 0 & G_{yz} & 0 & 0 \\ 0 & 0 & 0 & 0 & G_{zx} & 0 \\ 0 & 0 & 0 & 0 & 0 & G_{xy} \end{bmatrix} \begin{Bmatrix} \varepsilon_x \\ \varepsilon_y \\ \varepsilon_z \\ \gamma_{yz} \\ \gamma_{zx} \\ \gamma_{xy} \end{Bmatrix} \quad (4.13)$$

with $\Delta = E_x (E_y - E_z \nu_{yz}^2) - E_y [E_y \nu_{xy}^2 + E_z \nu_{xz} (\nu_{xz} + 2 \nu_{yz} \nu_{xy})]$

The above relations can be found in subroutine <orthotropic_D_matrix> in the module <mechanics_library> (file mechanics.f90.)

Transversely isotropic linear-elastic models

This is a special case of orthotropic materials, since the elastic properties are the same in one plane (e.g. the x - y plane) but change in the direction normal to that plane (e.g. the z -axis). A transversely isotropic material is described by five independent elastic constants: two Young's moduli (E_p , E_z), two Poisson's ratios (ν_p , ν_{zp}) and one shear modulus (G_{zp}), where subscript p denotes the plane of symmetry. The compliance matrix $[C]$ for transversely isotropic materials takes the form:

$$\begin{Bmatrix} \varepsilon_x \\ \varepsilon_y \\ \varepsilon_z \\ \gamma_{yz} \\ \gamma_{zx} \\ \gamma_{xy} \end{Bmatrix} = \begin{bmatrix} \frac{1}{E_p} & -\frac{\nu_p}{E_p} & -\frac{\nu_{zp}}{E_z} & 0 & 0 & 0 \\ -\frac{\nu_p}{E_p} & \frac{1}{E_p} & -\frac{\nu_{zp}}{E_z} & 0 & 0 & 0 \\ -\frac{\nu_{pz}}{E_p} & -\frac{\nu_{pz}}{E_p} & \frac{1}{E_z} & 0 & 0 & 0 \\ 0 & 0 & 0 & \frac{1}{G_{zp}} & 0 & 0 \\ 0 & 0 & 0 & 0 & \frac{1}{G_{zp}} & 0 \\ 0 & 0 & 0 & 0 & 0 & \frac{1+\nu_p}{2E_p} \end{bmatrix} \begin{Bmatrix} \sigma_x \\ \sigma_y \\ \sigma_z \\ \tau_{yz} \\ \tau_{zx} \\ \tau_{xy} \end{Bmatrix} \quad (4.14)$$

where $\nu_{pz}/E_p = \nu_{zp}/E_z$. The stress-strain relations for a transversely isotropic, linearly elastic material implemented in UMAR are given by:

$$\text{Uniaxial stress: } \sigma_x = E_p \varepsilon_x \quad (4.15)$$

$$\text{Plane stress } (\sigma_z = \tau_{yz} = \tau_{zx} = 0): \begin{Bmatrix} \sigma_x \\ \sigma_y \\ \tau_{xy} \end{Bmatrix} = \frac{E_p}{1-\nu_p^2} \begin{bmatrix} 1 & \nu_p & 0 \\ \nu_p & 1 & 0 \\ 0 & 0 & \frac{1-\nu_p}{2} \end{bmatrix} \begin{Bmatrix} \varepsilon_x \\ \varepsilon_y \\ \gamma_{xy} \end{Bmatrix} \quad (4.16)$$

Axisymmetry ($\tau_{r\theta} = \tau_{\theta z} = \gamma_{r\theta} = \gamma_{\theta z} = 0$):

$$\begin{Bmatrix} \sigma_r \\ \sigma_\theta \\ \sigma_z \\ \tau_{rz} \end{Bmatrix} = \begin{bmatrix} \frac{E_p(E_p - \nu_{pz}^2 E_z)}{\Delta} & \frac{E_p(\nu_p E_p + \nu_{pz}^2 E_z)}{\Delta} & \frac{E_p E_z \nu_{pz}(1+\nu_p)}{\Delta} & 0 \\ \frac{E_p(\nu_p E_p + \nu_{pz}^2 E_z)}{\Delta} & \frac{E_p(E_p - \nu_{pz}^2 E_z)}{\Delta} & \frac{E_p E_z \nu_{pz}(1+\nu_p)}{\Delta} & 0 \\ \frac{E_p E_z \nu_{pz}(1+\nu_p)}{\Delta} & \frac{E_p E_z \nu_{pz}(1+\nu_p)}{\Delta} & \frac{E_p E_z (1-\nu_p^2)}{\Delta} & 0 \\ 0 & 0 & 0 & G_{zp} \end{bmatrix} \begin{Bmatrix} \varepsilon_r \\ \varepsilon_\theta \\ \varepsilon_z \\ \gamma_{rz} \end{Bmatrix} \quad (4.17)$$

$$\text{with } \Delta = (1+\nu_p) \left[E_p (1-\nu_p) - 2E_z \nu_{pz}^2 \right]$$

$$\text{Curved shell: } \begin{Bmatrix} \sigma_x \\ \sigma_y \\ \tau_{yz} \\ \tau_{zx} \\ \tau_{xy} \end{Bmatrix} = \begin{bmatrix} \frac{E_p}{1-\nu_p^2} & \frac{E_p \nu_p}{1-\nu_p^2} & 0 & 0 & 0 \\ \frac{E_p \nu_p}{1-\nu_p^2} & \frac{E_p}{1-\nu_p^2} & 0 & 0 & 0 \\ 0 & 0 & G_{zp} & 0 & 0 \\ 0 & 0 & 0 & G_{zp} & 0 \\ 0 & 0 & 0 & 0 & \frac{E_p}{2(1+\nu_p)} \end{bmatrix} \begin{Bmatrix} \varepsilon_x \\ \varepsilon_y \\ \gamma_{yz} \\ \gamma_{zx} \\ \gamma_{xy} \end{Bmatrix} \quad (4.18)$$

3-D:

$$\begin{Bmatrix} \sigma_x \\ \sigma_y \\ \sigma_z \\ \tau_{yz} \\ \tau_{zx} \\ \tau_{xy} \end{Bmatrix} = \begin{bmatrix} \frac{E_p(E_p - \nu_{pz}^2 E_z)}{\Delta} & \frac{E_p(\nu_{pz} E_p + \nu_{pz}^2 E_z)}{\Delta} & \frac{E_p E_z \nu_{pz}(1 + \nu_p)}{\Delta} & 0 & 0 & 0 \\ \frac{E_p(\nu_{pz} E_p + \nu_{pz}^2 E_z)}{\Delta} & \frac{E_p(E_p - \nu_{pz}^2 E_z)}{\Delta} & \frac{E_p E_z \nu_{pz}(1 + \nu_p)}{\Delta} & 0 & 0 & 0 \\ \frac{E_p E_z \nu_{pz}(1 + \nu_p)}{\Delta} & \frac{E_p E_z \nu_{pz}(1 + \nu_p)}{\Delta} & \frac{E_p E_z (1 - \nu_p^2)}{\Delta} & 0 & 0 & 0 \\ 0 & 0 & 0 & G_{zp} & 0 & 0 \\ 0 & 0 & 0 & 0 & G_{zp} & 0 \\ 0 & 0 & 0 & 0 & 0 & \frac{E_p}{2(1 + \nu_p)} \end{bmatrix} \begin{Bmatrix} \varepsilon_x \\ \varepsilon_y \\ \varepsilon_z \\ \gamma_{yz} \\ \gamma_{zx} \\ \gamma_{xy} \end{Bmatrix} \quad (4.19)$$

$$\text{with } \Delta = (1 + \nu_p) [E_p (1 - \nu_p) - 2E_z \nu_{pz}^2]$$

The above relations can be found in subroutine <transversely_isotropic_D_matrix> in the module <mechanics_library> (file mechanics.f90.)

4.1.2 Orthotropic hypoelastic model

A material is said to be hypoelastic if the stress rate is a linear elastic function of the rate of deformation, i.e.,

$$\{d\sigma\} = [D]\{d\varepsilon\} \quad (4.20)$$

where $\{d\sigma\}$ and $\{d\varepsilon\}$ are respectively the vectors of incremental stresses and strains, and $[D]$ is the constitutive matrix. Equation 4.20 implies that the material is assumed to behave linear elastically at each load increment. Assuming orthotropy, the constitutive matrix $[D]$ is written as [6]:

$$[D] = \frac{1}{\phi} \begin{bmatrix} E_1(1 - \mu_{23}^2) & \sqrt{E_1 E_2}(\mu_{31}\mu_{23} + \mu_{12}) & \sqrt{E_1 E_3}(\mu_{12}\mu_{23} + \mu_{31}) & 0 & 0 & 0 \\ \sqrt{E_1 E_2}(\mu_{31}\mu_{23} + \mu_{12}) & E_2(1 - \mu_{31}^2) & \sqrt{E_2 E_3}(\mu_{12}\mu_{31} + \mu_{23}) & 0 & 0 & 0 \\ \sqrt{E_1 E_3}(\mu_{12}\mu_{23} + \mu_{31}) & \sqrt{E_2 E_3}(\mu_{12}\mu_{31} + \mu_{23}) & E_3(1 - \mu_{12}^2) & 0 & 0 & 0 \\ 0 & 0 & 0 & \phi G_{23} & 0 & 0 \\ 0 & 0 & 0 & 0 & \phi G_{31} & 0 \\ 0 & 0 & 0 & 0 & 0 & \phi G_{12} \end{bmatrix} \quad (4.21)$$

with

$$\begin{aligned} \mu_{12}^2 &= \nu_{12}\nu_{21} & \mu_{23}^2 &= \nu_{23}\nu_{32} & \mu_{31}^2 &= \nu_{31}\nu_{13} \\ \phi &= 1 - \mu_{12}^2 - \mu_{23}^2 - \mu_{31}^2 - 2\mu_{12}\mu_{23}\mu_{31} \end{aligned} \quad (4.22)$$

In Eqs. 4.21 and 4.22 subscripts 1, 2, and 3 refer to the axes of orthotropy, E_i is the orthotropic modulus of elasticity in the i^{th} direction, ν_{ij} is the Poisson's ratio, and G_{ij} is the shear modulus. It is assumed here that the material directions 1, 2, and 3 coincide with the principal stress directions. The sign convention used here is tension positive.

It is desirable that no particular direction be favoured with respect to the shear stiffness of the material. By imposing the requirement that the shear modulus be invariant under any axes transformation, G_{ij} becomes:

$$G_{ij} = \frac{1}{4\phi} \left[E_i + E_j - 2\mu_{ij}\sqrt{E_i E_j} - \left(\sqrt{E_i}\mu_{jk} + \sqrt{E_j}\mu_{ki} \right)^2 \right] \quad (4.23)$$

If working on a co-ordinate system other than the one given by the material orthotropy, the constitutive matrix $[D]$ given in Eq. 4.21 needs to be transformed into the new co-ordinate system, i.e.,

$$[D]' = [T_\varepsilon]^T [D] [T_\varepsilon] \quad (4.24)$$

where $[T_\varepsilon]$ is the matrix that transforms strains between axes [4],

$$\{d\varepsilon\} = [T_\varepsilon] \{d\varepsilon'\}; \quad [T_\varepsilon] = \begin{bmatrix} l_1^2 & m_1^2 & n_1^2 & m_1 n_1 & n_1 l_1 & l_1 m_1 \\ l_2^2 & m_2^2 & n_2^2 & m_2 n_2 & n_2 l_2 & l_2 m_2 \\ l_3^2 & m_3^2 & n_3^2 & m_3 n_3 & n_3 l_3 & l_3 m_3 \\ 2l_2 l_3 & 2m_2 m_3 & 2n_2 n_3 & m_2 n_3 + m_3 n_2 & n_2 l_3 + n_3 l_2 & l_2 m_3 + l_3 m_2 \\ 2l_3 l_1 & 2m_3 m_1 & 2n_3 n_1 & m_3 n_1 + m_1 n_3 & n_3 l_1 + n_1 l_3 & l_3 m_1 + l_1 m_3 \\ 2l_1 l_2 & 2m_1 m_2 & 2n_1 n_2 & m_1 n_2 + m_2 n_1 & n_1 l_2 + n_2 l_1 & l_1 m_2 + l_2 m_1 \end{bmatrix} \quad (4.25)$$

l_i, m_i, n_i , for $i=1,2,3$, are the direction cosines between the two co-ordinate axes, and strains $\{d\varepsilon\}$ and $\{d\varepsilon'\}$ are ordered as in Eq. 4.19.

Equivalent uniaxial strain

Using the concept of equivalent uniaxial strain developed by Darwin and Pecknold [5], the multiaxial state of stress in any material can be treated as three uniaxial stress states. This concept permits the use of experimental data from uniaxial tests to develop the constitutive matrix for a combined stress case, by separating the Poisson effect from the cumulative strain in any given direction.

The equivalent uniaxial strain ε_{iu} in the i^{th} direction for a non-linear material is defined as:

$$\varepsilon_{iu} = \sum_{\text{all increments}} \frac{\Delta\sigma_i}{E_i} \quad (4.26)$$

where $\Delta\sigma_i$ is the increment in stress during the load step, and E_i represents the tangent modulus in the i^{th} direction at the start of the load increment. The above expression is applicable for the entire stress history (both the pre- and the post-peak regions). Here, the equivalent uniaxial strains ε_{iu} are associated with the principal stress axes. The incremental elastic moduli of Eq. 4.21 are then obtained from:

$$E_i = \frac{d\sigma_i}{d\varepsilon_{iu}} \quad (4.27)$$

Equivalent compressive uniaxial stress-strain curve

The curve used in UMAR for compression loading is illustrated in Figure 4-1. Part I of the curve is represented by the equation proposed by Saenz [33]:

$$\sigma_i = \frac{E_o \varepsilon_{iu}}{1 + \left(\frac{E_o}{E_s} - 2 \right) \frac{\varepsilon_{iu}}{\varepsilon_{ic}} + \left(\frac{\varepsilon_{iu}}{\varepsilon_{ic}} \right)^2} \quad (4.28)$$

where E_s is the secant modulus of elasticity at peak stress (i.e., $E_s = \sigma_{ic} / \varepsilon_{ic}$, σ_{ic} being the compressive strength in the i^{th} direction), E_o is the initial tangent modulus, and ε_{ic} is the compressive strain at peak stress in the i^{th} direction. Part II of the compressive curve traces the Smith-Young model [37] according to:

$$\sigma_i = \sigma_{ic} \left(\frac{\varepsilon_{iu}}{\varepsilon_{ic}} \right) \exp \left(1 - \frac{\varepsilon_{iu}}{\varepsilon_{ic}} \right) \quad (4.29)$$

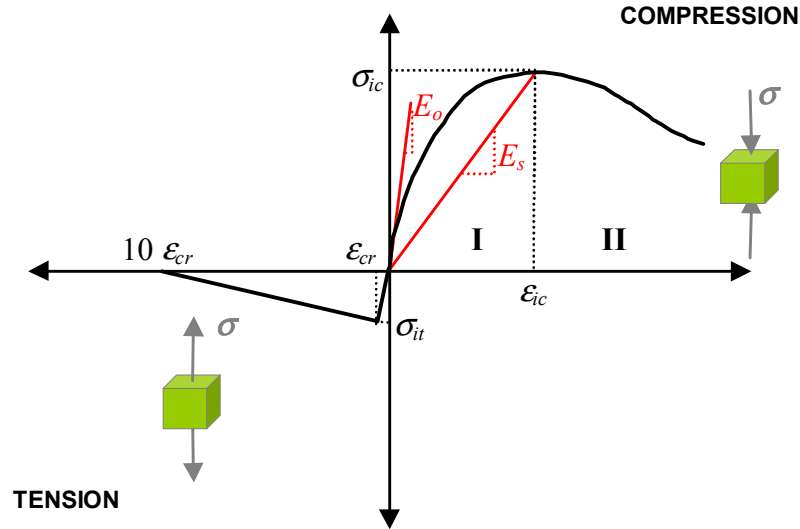


Figure 4-1: Uniaxial stress-strain curve for compressive and tensile loading.

Values of σ_{ic} are determined from the ultimate-strength surface envelopes to be discussed later in the text. To finalise the shape of the equivalent compressive uniaxial stress-strain curve, the value of the equivalent uniaxial strain at which peak compressive stress is attained, ε_{ic} , needs to be defined. Darwin and Pecknold [5] proposed the following relationships based on experimental data on Portland cement concrete specimens:

$$|\sigma_{ic}| \geq |\sigma_c|: \quad \varepsilon_{ic} = \varepsilon_{cu} \left[3 \frac{\sigma_{ic}}{\sigma_c} - 2 \right] \quad (4.30)$$

$$|\sigma_{ic}| < |\sigma_c|: \quad \varepsilon_{ic} = \varepsilon_{cu} \left[-1.6 \left(\frac{\sigma_{ic}}{\sigma_c} \right)^3 + 2.25 \left(\frac{\sigma_{ic}}{\sigma_c} \right)^2 + 0.35 \frac{\sigma_{ic}}{\sigma_c} \right] \quad (4.31)$$

where σ_c is the material compressive strength and ε_{cu} is the compressive strain at peak stress for the real uniaxial compression curve. The values of ε_{ic} are constrained to ensure that the ratio E_o/E_s in Eq. 4.28 is always greater than or equal to 2. This prevents the shape of the stress-strain curve from becoming concave upward.

By differentiating Eqs. 4.28 and 4.29 with respect to ε_{iu} , the incremental elastic moduli needed for the constitutive matrix $[D]$ in Eq. 4.21 are obtained from:

$$\text{Part I: } E_i = E_o \frac{1 - \left(\frac{\varepsilon_{iu}}{\varepsilon_{ic}} \right)^2}{\left[1 + \left(\frac{E_o}{E_s} - 2 \right) \left(\frac{\varepsilon_{iu}}{\varepsilon_{ic}} \right) + \left(\frac{\varepsilon_{iu}}{\varepsilon_{ic}} \right)^2 \right]^2} \quad (4.32)$$

$$\text{Part II: } E_i = \frac{\sigma_{ic}}{\varepsilon_{ic}} \exp \left(1 - \frac{\varepsilon_{iu}}{\varepsilon_{ic}} \right) \left[1 - \frac{\varepsilon_{iu}}{\varepsilon_{ic}} \right] \quad (4.33)$$

Equivalent tensile uniaxial stress-strain curve

The material is modelled in tension as a linear elastic material up to cracking. When the tensile stress along one principal direction exceeds the tensile strength of the material σ_t , cracking is assumed to initiate perpendicular to that particular direction (see Figure 4-2(a)). Cracking is modelled by reducing the value of E to zero along the original principal stress direction. If, for example, $\sigma_1 \geq \sigma_t$, then the constitutive matrix $[D]$ reduces to:

$$[D] = \frac{1}{\phi} \begin{bmatrix} 0 & 0 & 0 & 0 & 0 & 0 \\ 0 & E_2(1-\mu_{31}^2) & \mu_{23}\sqrt{E_2E_3} & 0 & 0 & 0 \\ 0 & \mu_{23}\sqrt{E_2E_3} & E_3 & 0 & 0 & 0 \\ 0 & 0 & 0 & \phi\beta G_{23} & 0 & 0 \\ 0 & 0 & 0 & 0 & \phi\beta G_{31} & 0 \\ 0 & 0 & 0 & 0 & 0 & \phi\beta G_{12} \end{bmatrix} \quad (4.34)$$

where $\phi = 1 - \mu_{23}^2 - \mu_{31}^2$ and β is a shear retention factor ($\beta < 1$). Equation 4.34 results from setting E_1 to zero. The factor β is used to account for the shear transferred along the crack due to aggregate interlock.

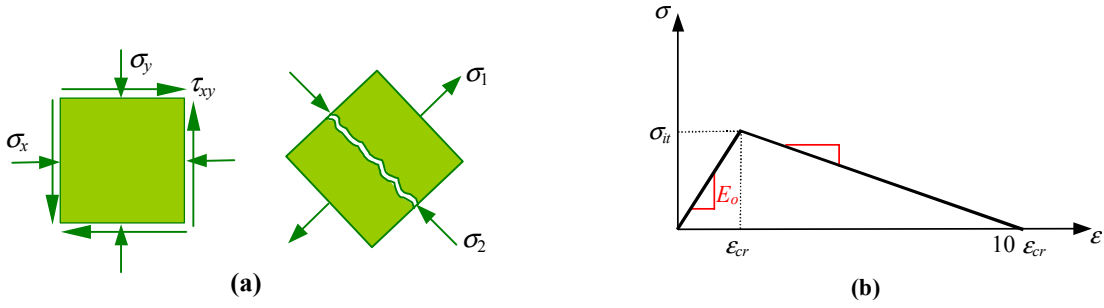


Figure 4-2: (a) Crack formation in principal tension direction; (b) Tensile uniaxial stress-strain curve.

After initiation of cracking, the tensile stress-strain curve follows a linear strain-softening branch intended to represent the post-cracking tensile stresses carried by the material (Figure 4-1 and Figure 4-2(b)). Actually, the post-cracking residual capacity, commonly known as tension stiffening in reinforced concrete, stems from the transfer of tensile stresses from the reinforcement to the concrete in between cracks (i.e., bond). After the formation of cracks at a given point, the cracked material can still carry some tension, but it is assumed to have zero stiffness normal to the direction of the crack (see the step line in Figure 4-2(b)). This effect is smeared over a finite area, which is given by the tributary area of a Gauss integration point in UMAR.

Poisson's ratios

In order to determine the values of Poisson's ratio appearing in Eq. 4.22, Elwi and Murray [6] developed a least-squares fit of a cubic polynomial from uniaxial compression data tests in concrete specimens, i.e.,

$$\nu_i = \nu_o \left[1.0 + 1.3763 \frac{\epsilon_{iu}}{\epsilon_{ic}} - 5.3600 \left(\frac{\epsilon_{iu}}{\epsilon_{ic}} \right)^2 + 8.586 \left(\frac{\epsilon_{iu}}{\epsilon_{ic}} \right)^3 \right] \leq 0.5 \quad (4.35)$$

where ν_o is the initial value of ν . Equation 4.35 assumes that an axially symmetric Poisson's ratio can be applied to each equivalent uniaxial strain, resulting in three independent Poisson's ratios. Equation 4.22 can now be written as:

$$\mu_{12}^2 = \nu_1 \nu_2 \quad \mu_{23}^2 = \nu_2 \nu_3 \quad \mu_{31}^2 = \nu_3 \nu_1 \quad (4.36)$$

Material ultimate-strength surfaces

The material ultimate-strength surfaces are surfaces in stress space that define the ultimate compressive and tensile strengths, σ_{ic} and σ_{it} , respectively, for any ratio of principal stresses. The

ultimate strength envelope developed by Kupfer and Gerstle [21] to model the behaviour of concrete under biaxial stresses has been extended here to consider a three-dimensional stress field. The triaxial compressive and tensile strength envelopes are illustrated in Figure 4-3 and Figure 4-4, respectively.

If the ratios of principal stresses are defined as:

$$\alpha_{12} = \frac{\sigma_1}{\sigma_2} \quad \alpha_{23} = \frac{\sigma_2}{\sigma_3} \quad \alpha_{13} = \frac{\sigma_1}{\sigma_3} \quad (4.37)$$

where $\sigma_1 \geq \sigma_2 \geq \sigma_3$ are the principal stresses, the increase in compressive strength due to either biaxial or triaxial compression is given by [21]:

$$\text{Biaxial compression: } \sigma_{jc} = \sigma_c \frac{1 + 3.65\alpha_{ij}}{(1 + \alpha_{ij})^2}, \quad \sigma_{ic} = \alpha_{ij}\sigma_{jc} \quad (4.38)$$

$$\text{Triaxial compression: } \sigma_{kc} = \sigma_c \frac{1 + 3.65\alpha_{ik}}{(1 + \alpha_{ik})^2} \cdot \frac{1 + 3.65\alpha_{jk}}{(1 + \alpha_{jk})^2}, \quad \sigma_{ic} = \alpha_{ik}\sigma_{kc}, \quad \sigma_{jc} = \alpha_{jk}\sigma_{kc} \quad (4.39)$$

where subscripts i, j , and k can take any value from 1 to 3, provided that $i \neq j \neq k$. Equations 4.38 and 4.39 describe the surface illustrated in Figure 4-3. Once the ratios of principal stresses are determined, the value of σ_{ic} as given by Eqs. 4.38 and 4.39 is used to define the shape of the equivalent compressive uniaxial stress-strain curve (Eqs. 4.28 and 4.29).

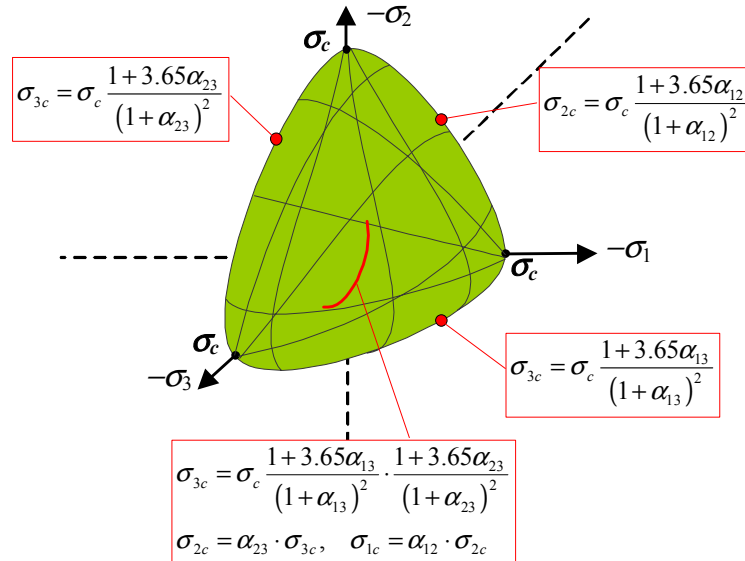


Figure 4-3: Triaxial compressive strength envelope.

Regarding the tensile strength envelope (see Figure 4-4), the tensile strength of the material along one principal direction does not change with the introduction of a tensile stress in another

principal direction (i.e., $\sigma_{ii} = \sigma_i$ for triaxial tension), but it does linearly decrease with increased compressive stress according to [21]:

$$\sigma_{it} = \sigma_t \left(1 - 0.8 \frac{\sigma_j}{\sigma_c} \right) \quad \text{with} \quad \sigma_i \geq 0, \sigma_j < 0 \quad (4.40)$$

The compressive strength is also decreased with the presence of tensile stresses according to:

$$\sigma_{jc} = \sigma_c \frac{1 + 3.28\alpha_{ij}}{(1 + \alpha_{ij})^2} \quad \text{with} \quad \sigma_i \geq 0, \sigma_j < 0 \quad (4.41)$$

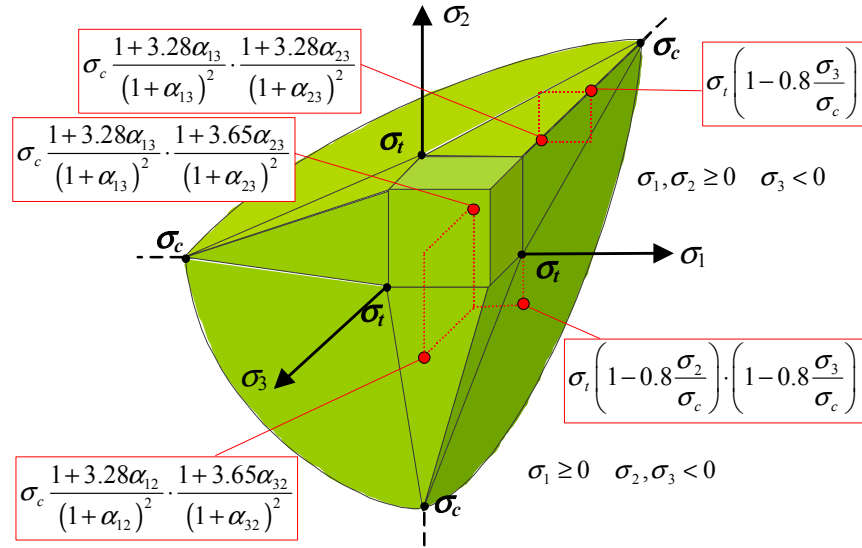


Figure 4-4: Triaxial tensile strength envelope.

The foregoing procedure can be found in the subroutine <hypo_elasticity> (file elasticity.f90).

4.1.3 Resilient modulus models

The mechanical behaviour of supporting materials in pavement structures (i.e., base, sub-base and subgrade) is generally characterised by means of the resilient modulus M_r . Resilient modulus models characterise the stress-strain properties of soils through a stress-dependent elastic modulus and a constant Poisson ratio. The following resilient modulus models are implemented in UMAR. These can be found in the subroutine <resilient_modulus_models> (file elasticity.f90).

Granular materials

k - θ Model

$$M_r = k_1 \theta^{K_2} \quad (4.42)$$

where θ is the bulk stress (i.e., $\theta = I_1 = \sigma_1 + \sigma_2 + \sigma_3$) and k_1 and k_2 are two material constants obtained from regression analysis of repeated load triaxial tests on granular materials. The model represented by Eq. 4.42 is the most commonly used to reflect the mechanical behaviour of granular materials [10]. It is a simple model; however, it neglects the effect of shear stress on the resilient response of these materials.

Uzan Model

$$M_r = k_1 \theta^{k_2} \sigma_d^{k_3} \quad (4.43)$$

where σ_d is the deviator stress (i.e., $\sqrt{3J_2}$, J_2 being the second invariant of the deviatoric stress), and k_1 , k_2 , and k_3 are material constants obtained from regression analysis of repeated load triaxial tests on granular materials. Equation 4.43 was proposed by Uzan [40] as an improvement to the k - θ model by including the shear stress effects (through the term σ_d .)

UT-Austin Model [30]

$$M_r = k_1 \sigma_d^{k_2} \sigma_3^{k_3} \quad (4.44)$$

where σ_3 is the minor principal stress (confining stress in triaxial tests) and k_1 , k_2 , and k_3 are material constants obtained from regression analysis of repeated load triaxial tests on granular materials.

IRC's Model

$$M_r = k_1 \theta^{k_2} \sigma_d^{k_3} w^{k_4} \gamma_d^{k_5} \quad (4.45)$$

where w is the moisture content (%), and k_1 to k_5 are model parameters obtained from multiple regression analyses of repeated load triaxial tests performed on granular materials. The bulk θ and deviator σ_d stresses in Eq. 4.45 are given in kPa, whereas the resilient modulus M_r is given in MPa.

Cohesive materials

Bilinear Approximation

$$M_r = \begin{cases} k_1 + k_3 (k_2 - \sigma_d) & \text{for } \sigma_d < k_2 \\ k_1 + k_4 (\sigma_d - k_2) & \text{for } \sigma_d \geq k_2 \end{cases} \quad (4.46)$$

where k_1 , k_2 , k_3 , and k_4 are material constants.

Khogali's Model

$$\ln M_r = B_0 + B_1 \ln \Psi + B_2 \ln \gamma_d + B_3 \ln T + B_4 \ln \left(\frac{J_2}{\tau_{oct}} \right); \quad \tau_{oct} = \sqrt{\frac{2}{3} J_2} \quad (4.47)$$

where Ψ is the soil matric suction (kPa), γ_d is the soil dry density (kg/m³), T is the average soil temperature (°C), J_2 is the second invariant of the deviatoric stress (kPa), and τ_{oct} is the octahedral shear stress (kPa). Constants B_0 to B_4 are dependent on the soil type. Note that M_r as given by Eq. 4.47 is given in kPa. The model given by Eq. 4.47 was proposed by Khogali [18] to characterise the resilient deformation characteristics of cohesive subgrade soils.

4.2 Theory of plasticity

The theory of plasticity provides a theoretical description of the relationship between strain ε and stress σ for materials which exhibit plastic behaviour, i.e., they undergo irreversible straining once a certain level of stress has been reached (yield criterion). Two plastic models are implemented in UMAR, namely: classic plasticity (where inelastic straining is time independent) and visco-plasticity (where inelastic straining is rate sensitive). Both of them are based on the so-called incremental theory of plasticity, in which the total irreversible strain is obtained as the sum of the increments. In order to formulate both models, three requirements have to be met:

- a yield function, which signals if the material is yielding plastically or not;
- a hardening function, which indicates the manner in which the yield function changes (if at all) with plastic straining; and,
- a flow rule, which determines the direction of plastic straining.

All plastic models that are implemented in UMAR can be found in the module <plasticity_library> in the file plasticity.f90.

4.2.1 Yield criteria

By defining a yield function F as a function of stress σ_{ij} and quantities σ_{ij}^b and κ associated with the hardening rule, yielding occurs when:

$$F(\sigma_{ij}, \sigma_{ij}^b, \kappa) = 0 \quad (4.48)$$

If $F < 0$ then the material is in the elastic range; however, if $F = 0$, it is yielding. The result of $F > 0$ is not physically possible for rate-independent plasticity, as it indicates a state of stress that does not satisfy the constitutive law. Similarly, the results $dF < 0$ and $dF = 0$ (consistency condition) respectively imply elastic unloading and continued yielding. The result $dF > 0$ is not possible in the plastic regime [4].

Isotropic failure surfaces

Isotropic failure surfaces implemented in UMAR that are independent of the mean stress are Tresca and Von-Mises. Generalisation of these two also implemented in program UMAR are respectively the Mohr-Coulomb and Drucker-Prager yield criteria, created by adding the angle of internal friction ϕ , which develops hydrostatic pressure-dependent behaviour.

Tresca yield criterion

The Tresca yield criterion assumes that plastic deformation occurs when the maximum shear stress attains a critical value. If the principal stresses are σ_1 , σ_2 , and σ_3 , where $\sigma_1 \geq \sigma_2 \geq \sigma_3$, then the onset of plastic straining occurs when:

$$\sigma_1 - \sigma_3 \geq \sigma_y(h) \quad (4.49)$$

where σ_y is a material parameter and h is the hardening parameter. The threshold value σ_y is usually the yield stress determined from one-dimensional tension tests. This yield criterion is represented in the principal stress space as an infinitely long regular hexagonal cylinder equally inclined to the three principal axes.

Von-Mises yield criterion

By using the Von-Mises yield criterion, plastic flow occurs when:

$$\sqrt{3J_2} \geq \sigma_y \quad (4.50)$$

where J_2 is explicitly given by:

$$J_2 = \frac{1}{2} s_{ij} s_{ij} = \frac{1}{2} [s_x^2 + s_y^2 + s_z^2] + \tau_{xy}^2 + \tau_{yz}^2 + \tau_{xz}^2 \quad (4.51)$$

where s_{ij} is the deviatoric stress defined as $s_{ij} = \sigma_{ij} - \frac{1}{3} \delta_{ij} \sigma_{kk}$. Equation 4.50 represents a circular cylinder of radius $\sqrt{2/3} \sigma_y$ inclined at equal angles to the three principal axes.

The quantity on the left-hand side of Eq. 4.50 is referred to as the effective or equivalent stress $\bar{\sigma}$. According to the Von-Mises criterion, if the effective stress $\bar{\sigma}$ equals or exceeds the uniaxial yield stress σ_y , then plastic flow is assumed to occur.

Mohr-Coulomb yield criterion

Mohr-Coulomb yield criterion is based on the maximum shear stress of the material, i.e.,

$$\tau = c - \sigma_n \tan \phi \quad (4.52)$$

where τ is the shearing stress, σ_n is the normal stress, c is the cohesion, and ϕ is the angle of friction. Both c and ϕ are material constants. If principal stresses are denoted as $\sigma_1 \geq \sigma_2 \geq \sigma_3$, the Mohr-Coulomb criterion can be written as:

$$(\sigma_1 - \sigma_3) = 2c \cos \phi - (\sigma_1 + \sigma_3) \sin \phi \quad (4.53)$$

In principal stress space, Eq. 4.53 represents a conical yield surface whose normal section at any point is an irregular hexagon. Expressing Eq. 4.53 in terms of stress invariants results in:

$$F(I_1, J_2, \theta) = \frac{1}{3} I_1 \sin \phi + \sqrt{J_2} \sin \left(\theta + \frac{\pi}{3} \right) + \frac{\sqrt{J_2}}{3} \cos \left(\theta + \frac{\pi}{3} \right) \sin \phi - c \cos \phi = 0 \quad (4.54)$$

where I_1 is the first invariant of the stress tensor (i.e., $I_1 = \sigma_x + \sigma_y + \sigma_z = \sigma_1 + \sigma_2 + \sigma_3$) and J_2 is the second invariant of the deviatoric stress tensor (given by Eq. 4.51). The parameter θ is defined by the second and third invariants of the deviatoric stress tensor as:

$$\cos 3\theta = \frac{3\sqrt{3}}{2} \frac{J_3}{\sqrt{J_2^3}} \quad (4.55)$$

where $0 \leq \theta \leq \pi/3$ and

$$J_3 = \frac{1}{27} (2I_1^3 + 9I_1 I_2 + 27I_3) \quad (4.56)$$

with $I_2 = \sigma_x \sigma_y + \sigma_y \sigma_z + \sigma_x \sigma_z - \tau_{xy}^2 - \tau_{xz}^2 - \tau_{yz}^2$ and $I_3 = \det(\sigma)$.

Drucker-Prager yield criterion

The Drucker-Prager yield criterion is given by:

$$F(I_1, J_2) = \alpha I_1 + \sqrt{J_2} - k = 0 \quad (4.57)$$

where α and k are defined by the cohesion c and the angle of internal friction ϕ . The yield surface represented by Eq. 4.57 has the form of a circular cone. In order to make the Drucker-Prager circle coincide with the outer apices of the Mohr-Coulomb hexagon at any section, α and k are given as:

$$\alpha = \frac{2 \sin \phi}{\sqrt{3} (3 - \sin \phi)}, \quad k = \frac{6c \cos \phi}{\sqrt{3} (3 - \sin \phi)} \quad (4.58)$$

Coincidence with the inner apices of the Mohr-Coulomb hexagon is provided by:

$$\alpha = \frac{2 \sin \phi}{\sqrt{3} (3 + \sin \phi)}, \quad k = \frac{6c \cos \phi}{\sqrt{3} (3 + \sin \phi)} \quad (4.59)$$

4.2.2 Hardening laws

When a material is subjected to plastic flow, its microstructure is altered resulting in a change of the properties observable at the macro-scale level. Due to this micro-structural changes in the material, the domain at which the material behaves elastically changes its size, its position, or both. This phenomenon is captured in plastic models by means of a hardening function, which describes the manner in which the yield function of the material is modified due to plastic straining. Hardening functions implemented in program UMAR are described in the following.

Isotropic hardening

In isotropic hardening, the progressive development of the yield surface is characterised by a single parameter: the hardening variable κ . Using the work hardening hypothesis, the hardening parameter κ is defined as:

$$d\kappa = \sigma_{ij} d\epsilon_{ij}^p \quad (4.60)$$

The yield criterion can then be rewritten as:

$$F(\sigma_{ij}) - \sigma_Y(\kappa) = 0 \quad (4.61)$$

where σ_Y is the current yield stress. The simplest case of isotropic hardening is a linear function:

$$\sigma_Y = \sigma_o + H d\bar{\epsilon}_p \quad (4.62)$$

in which σ_o is the initial yield stress. Parameter H in Eq. 4.62 is the plastic modulus, defined as $d\bar{\sigma}/d\bar{\epsilon}_p$, where $d\bar{\sigma}$ and $d\bar{\epsilon}_p$ are respectively the effective stress and effective plastic strain. If $H > 0$, true hardening occurs (i.e., the yield stress increases). If $H = 0$, perfect plasticity takes place (i.e., there is not hardening at all). And if $H < 0$, softening of the material takes place (i.e., there is a decrease in the yield stress.) For uniaxial yielding, the plastic modulus becomes:

$$H = \frac{E_T}{1 - \frac{E_T}{E}} \quad (4.63)$$

where E is the elastic modulus and E_T is the elasto-plastic tangent modulus, i.e., $E_T = d\sigma/d\epsilon$ for $\sigma > \sigma_o$.

Linear kinematic hardening

In kinematic hardening, the yield surface does not expand or contract, but it moves as a rigid body within the stress space. This type of hardening is generally used to model behaviour of materials under cyclic and transient loads.

Kinematic hardening leads to a shift of the origin of the initial yield surface. The shifted yield surface is thus described by:

$$F(\sigma_{ij} - \sigma_{ij}^b) - \sigma_o = 0 \quad (4.64)$$

where σ_{ij}^b is the back-stress that represents the centre of the shifted elastic domain. Tensor σ_{ij}^b is assumed to be zero in the initial state. There are two linear kinematic hardening models implemented in UMAR:

Melan-Prager hardening rule [25]

$$\dot{\sigma}_{ij}^b = c \dot{\epsilon}_{ij}^p \quad (4.65)$$

according to which the rate of the back-stress is proportional to the plastic strain rate. The proportionality factor c in Eq. 4.65 is a constant directly related to the plastic modulus. Negative values of c leads to softening. A model with purely kinematic softening does not make physical sense, but a model with mixed isotropic and kinematic softening can be useful for materials in which tensile loading induces a degradation of both tensile and compressive strength, with the degradation in tension being faster than in compression.

Prager-Ziegler hardening rule

$$\dot{\sigma}_{ij}^b = \dot{\mu} (\sigma_{ij} - \sigma_{ij}^b) \quad (4.66)$$

which means that the yield surface moves in the direction of the vector connecting the centre of the actual yield surface to the stress point. The multiplier $\dot{\mu}$ is obtained from:

$$\dot{\mu} = c \frac{\{a\}^T \{d\sigma\}}{\{a\}^T \{\sigma - \sigma^b\}} \quad (4.67)$$

where parameter c has the same meaning as in the Melan-Prager hardening rule and $\{a\}$ is the flow vector, which is computed from:

$$\{a\}^T = \frac{\partial F}{\partial \sigma_{ij}} = \left[\frac{\partial F}{\partial \sigma_x} \quad \frac{\partial F}{\partial \sigma_y} \quad \frac{\partial F}{\partial \sigma_z} \quad \frac{\partial F}{\partial \tau_{yz}} \quad \frac{\partial F}{\partial \tau_{zx}} \quad \frac{\partial F}{\partial \tau_{xy}} \right] \quad (4.68)$$

The flow vector $\{a\}$ in Eq. 4.68 depends on the yield criterion chosen. If vector $\{a\}$ is written as:

$$\{a\} = C_1 \{a_1\} + C_2 \{a_2\} + C_3 \{a_3\} \quad (4.69)$$

where

$$\begin{aligned}
\{a_1\}^T &= \frac{\partial I_1}{\partial \sigma_{ij}} = \{1 \quad 1 \quad 1 \quad 0 \quad 0 \quad 0\} \\
\{a_2\}^T &= \frac{\partial (J_2')^{1/2}}{\partial \sigma_{ij}} = \frac{1}{2\sqrt{J_2'}} \{s_x \quad s_y \quad s_z \quad 2\tau_{yz} \quad 2\tau_{zx} \quad 2\tau_{xy}\} \\
\{a_3\}^T &= \frac{\partial I_3}{\partial \sigma_{ij}} \\
&= \left\{ \left(s_y s_z - \tau_{yz}^2 + \frac{J_2'}{3} \right) \quad \left(s_x s_z - \tau_{xz}^2 + \frac{J_2'}{3} \right) \quad \left(s_x s_y - \tau_{xy}^2 + \frac{J_2'}{3} \right) \right. \\
&\quad \left. 2(\tau_{xz} \tau_{xy} - s_x \tau_{yz}) \quad 2(\tau_{xy} \tau_{yz} - s_y \tau_{xz}) \quad 2(\tau_{yz} \tau_{xz} - s_z \tau_{xy}) \right\}
\end{aligned} \tag{4.70}$$

and

$$\begin{aligned}
C_1 &= \frac{\partial F}{\partial I_1} \\
C_2 &= \frac{\partial F}{\partial (J_2')^{1/2}} - \frac{\tan 3\theta}{\sqrt{J_2'}} \frac{\partial F}{\partial \theta} \\
C_3 &= \frac{-\sqrt{3}}{2 \cos 3\theta} - \frac{1}{(J_2')^{3/2}} \frac{\partial F}{\partial \theta}
\end{aligned} \tag{4.71}$$

then the different yield criteria are defined by constants C_i . Table 4-1 lists constants C_i for the isotropic yield surfaces used in UMAR.

Table 4-1: Constants defining isotropic yield surfaces implemented in UMAR.

Yield criterion	C_1	C_2	C_3
Tresca	0	$2 \cos \theta (1 + \tan \theta \tan 3\theta)$	$\frac{\sqrt{3}}{J_2'} \frac{\sin \theta}{\cos 3\theta}$
Von-Mises	0	$\sqrt{3}$	0
Mohr-Coulomb	$\frac{1}{3} \sin \phi$	$\cos \theta \left[(1 + \tan \theta \tan 3\theta) + \sin \phi (\tan 3\theta - \tan \theta) / \sqrt{3} \right]$	$\frac{\sqrt{3} \sin \theta + \cos \theta \sin \phi}{2J_2' \cos 3\theta}$
Drucker-Prager	α	1.0	0

Non-linear kinematic hardening

Realistic modelling of engineering materials often requires non-linear hardening laws. For isotropic hardening, non-linearity can be easily incorporated through the function $\sigma_Y(\kappa)$, but for kinematic hardening this is not so straightforward. Non-linear kinematic hardening is

implemented in program UMAR by means of the Armstrong-Frederick rule, for which the evolution of the back-stress is governed by:

$$\dot{\sigma}_{ij}^b = c\dot{\epsilon}_{ij}^p - \gamma\sqrt{\frac{2}{3}}\|\dot{\epsilon}_{ij}^p\|\sigma_{ij}^b \quad (4.72)$$

where c and γ are material constants.

Mixed hardening

The hardening behaviour of most materials seems to be a combination of both isotropic and kinematic type of hardening, sometimes even accompanied by a change of shape of the yield surface. Mixed hardening results in a modification of the yield surface by simultaneous translation and expansion (or contraction). The yield surface is therefore rewritten as:

$$F(\sigma_{ij} - \sigma_{ij}^b) - \sigma_Y(\kappa) = 0 \quad (4.73)$$

which covers Eqs. 4.61 and 4.64 as special cases.

4.2.3 Rate-independent plastic model

In the classical theory of plasticity, it is assumed that the total strain increment $d\epsilon_{ij}$ is given by:

$$d\epsilon_{ij} = d\epsilon_{ij}^e + d\epsilon_{ij}^p \quad (4.74)$$

where $d\epsilon_{ij}^e$ and $d\epsilon_{ij}^p$ are the elastic and plastic strain increment tensors, respectively. The elastic strain increment can be obtained from the following tensor equation:

$$d\epsilon_{ij}^e = C_{ijkl}d\sigma_{kl} \quad (4.75)$$

where C_{ijkl} is the compliance of elastic moduli. The plastic strain increment is obtained from the flow rule:

$$d\epsilon_{ij}^p = d\lambda \frac{\partial Q}{\partial \sigma_{ij}} \quad (4.76)$$

where Q is a plastic potential, which has units of stress and is a function of the stresses $Q(\sigma_{ij}, \sigma_{ij}^b, \kappa)$, and $d\lambda$ is a constant called the ‘plastic multiplier’. The flow rule is called “associated” if $Q = F$, where F is the yield function, and it is called “non-associated” otherwise. Associated flow rules are commonly used for ductile metals, but non-associated rules are better suited to soil and granular materials [4], [42]. Associated flow rules imply that the plastic strain increment is normal to the yield surface, known as the normality condition.

During plastic flow, the stress state must remain on the yield surface, satisfying the consistency condition. For a yield function of the type $F(\sigma_{ij}, \sigma_{ij}^b, \kappa) = 0$, the consistency condition is given by:

$$dF = 0 = \left\{ \frac{\partial F}{\partial \sigma} \right\}^T \{d\sigma\} + \left\{ \frac{\partial F}{\partial \sigma^b} \right\}^T \{d\sigma^b\} + \frac{\partial F}{\partial \kappa} d\kappa \quad (4.77)$$

The terms $\{d\sigma_{ij}^b\}$ and $d\kappa$ are respectively obtained by assuming a kinematic hardening law (e.g., Eq. 4.65) and using Eq. 4.60. The complete elasto-plastic incremental stress-strain relation is given by:

$$\{d\sigma\} = [D] \{d\varepsilon^e\} = [D] \{d\varepsilon - d\varepsilon^p\} \quad (4.78)$$

where $[D]$ is the elastic material matrix. By substituting Eqs. 4.60, 4.65, 4.76, and 4.78 into Eq. 4.77, the plastic multiplier $d\lambda$ is obtained in explicit form as [4]:

$$d\lambda = \frac{\left\{ \frac{\partial F}{\partial \sigma} \right\}^T [D]}{\left\{ \frac{\partial F}{\partial \sigma} \right\}^T [D] \left\{ \frac{\partial Q}{\partial \sigma} \right\} - c \left\{ \frac{\partial F}{\partial \sigma^b} \right\}^T \left\{ \frac{\partial Q}{\partial \sigma} \right\} - \frac{\partial F}{\partial \kappa} \{\sigma\}^T \left\{ \frac{\partial Q}{\partial \sigma} \right\}} \{d\varepsilon\} \quad (4.79)$$

Finally, substituting Eq. 4.76 into Eq. 4.78, the elasto-plastic constitutive matrix is given by:

$$[D_{ep}] = [D] - \frac{[D] \left\{ \frac{\partial Q}{\partial \sigma} \right\} \left\{ \frac{\partial F}{\partial \sigma} \right\}^T [D]}{\left\{ \frac{\partial F}{\partial \sigma} \right\}^T [D] \left\{ \frac{\partial Q}{\partial \sigma} \right\} - c \left\{ \frac{\partial F}{\partial \sigma^b} \right\}^T \left\{ \frac{\partial Q}{\partial \sigma} \right\} - \frac{\partial F}{\partial \kappa} \{\sigma\}^T \left\{ \frac{\partial Q}{\partial \sigma} \right\}} \quad (4.80)$$

Matrix $[D_{ep}]$ is symmetric if $F = Q$.

4.2.4 Isotropic visco-plastic model

In visco-plasticity, plastic strains in the material (called visco-plastic strains) are developed with time (as opposed to instantaneously as it is the case in classical plasticity.) Figure 4-5 illustrates a rheological analogue of elasto-visco-plastic materials. It consists of a spring that is in series with a dashpot and a slider system in parallel. The slider represents yielding and permanent straining; however, the latter is not instantaneous since the viscous dashpot needs time to strain. Thus, it is assumed that instantaneously the material behaves elastically, with all the stresses being taken by the spring.

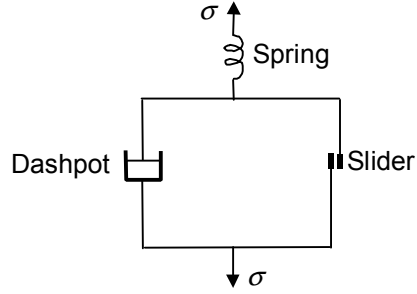


Figure 4-5: Rheological analogue of elasto-visco-plastic model.

Similar to rate-independent plasticity, here the total strain ε is separated into elastic ε_e and visco-plastic ε_{vp} components, so that the total strain rate can be expressed as:

$$\dot{\varepsilon} = \dot{\varepsilon}_e + \dot{\varepsilon}_{vp} \quad (4.81)$$

The onset of visco-plastic behaviour occurs when $F - F_o > 0$, where F is a scalar yield function and F_o is the uni-axial yield stress. Unlike the theory of rate-independent plasticity, here it is postulated that stress trajectories can cross the yield surface, giving rise to visco-plastic strains. A steady-state is reached when the stress is on the yield surface, i.e., there is not a further increase in visco-plastic strains. This situation leads to the same results given by rate-independent plasticity.

For associated visco-plasticity, the visco-plastic strain rate $\dot{\varepsilon}_{vp}$ is given by [28]:

$$\dot{\varepsilon}_{vp} = \gamma \langle \Phi(F) \rangle \frac{\partial F}{\partial \sigma} \quad (4.82)$$

where γ (s^{-1}) is a fluidity parameter controlling the plastic flow rate ($\gamma = 1/\mu$, where μ is the viscosity), and $\Phi(x)$ is a positive monotonic increasing function for $x > 0$ ($\Phi(x) = 0$ for $x \leq 0$).

The flow function $\Phi(x)$ in program UMAR can take any of the following forms:

$$\Phi(F) = F \quad (4.83)$$

$$\Phi(F) = \left(\frac{F - F_o}{F_o} \right)^m \quad (4.84)$$

$$\Phi(F) = e^{n \left(\frac{F - F_o}{F_o} \right)} - 1 \quad (4.85)$$

The visco-plastic strain increment $\Delta \varepsilon_{vp}^n$ occurring in a time interval $\Delta t_n = t_{n+1} - t_n$ is calculated from:

$$\Delta \varepsilon_{vp}^n = \dot{\varepsilon}_{vp}^n \Delta t_n + C^n \Delta \sigma^n \quad (4.86)$$

with

$$C^n = \theta \Delta t_n H^n \text{ and } H^n = \left(\frac{\partial \dot{\epsilon}_{vp}}{\partial \sigma} \right)^n \quad (4.87)$$

Parameter θ is a weighting factor ranging from 0 to 1 ($\theta = 0$ corresponds to the forward difference time integration scheme; $\theta = 0.5$ corresponds to the Crank-Nicolson time integration scheme; and, $\theta = 1$ corresponds to the backward difference time integration scheme.) Although the time integration scheme is unconditionally stable for $\theta \geq 0.5$ regardless of the value of the time step Δt_n , the accuracy of the solution is not guaranteed, and thus limits for Δt_n need to be imposed. Matrix H^n must be explicitly determined for the yield criterion assumed for material behaviour. For the Von-Mises yield criterion, matrix $[H]$ is given by:

$$H = p_1 M_1 + p_2 M_2, \quad p_1 = \gamma \left\langle \frac{\sqrt{3}}{2(J_2')^{1/2}} \cdot \Phi \right\rangle, \quad p_2 = \gamma \left\langle \frac{3}{4J_2'} \frac{d\Phi}{dF} - \frac{(\sqrt{3})\Phi}{4(J_2')^{3/2}} \right\rangle \quad (4.88)$$

$$M_1 = \begin{bmatrix} 2/3 & -1/3 & -1/3 & 0 & 0 & 0 \\ & 2/3 & -1/3 & 0 & 0 & 0 \\ & & 2/3 & 0 & 0 & 0 \\ & \text{Symm.} & & 2 & 0 & 0 \\ & & & & 2 & 0 \\ & & & & & 2 \end{bmatrix}$$

$$M_2 = \begin{bmatrix} s_x^2 & s_x s_y & s_x s_z & 2s_x \tau_{yz} & 2s_x \tau_{zx} & 2s_x \tau_{xy} \\ & s_y^2 & s_y s_z & 2s_y \tau_{yz} & 2s_y \tau_{zx} & 2s_y \tau_{xy} \\ & & s_z^2 & 2s_z \tau_{yz} & 2s_z \tau_{zx} & 2s_z \tau_{xy} \\ & \text{Symm.} & & 4\tau_{yz}^2 & 4\tau_{yz} \tau_{zx} & 4\tau_{yz} \tau_{xy} \\ & & & & 4\tau_{zx}^2 & 4\tau_{zx} \tau_{xy} \\ & & & & & 4\tau_{xy}^2 \end{bmatrix} \quad (4.89)$$

The stress change $\Delta \sigma^p$ occurring in the time interval Δt_n is obtained from:

$$\Delta \sigma^n = D(\Delta \epsilon^n - \Delta \epsilon_{vp}^n) \quad (4.90)$$

By substituting Eq. 4.86 into Eq. 4.90, $\Delta \sigma^p$ is then calculated as:

$$\Delta \sigma^n = \hat{D}^n (\Delta \epsilon^n - \dot{\epsilon}_{vp}^n \Delta t_n) \text{ with } \hat{D}^n = (D^{-1} + C^n)^{-1} \quad (4.91)$$

Time step length

The time step can be either constant or allowed to vary at each time interval. If it varies, its value is limited by a factor τ which limits the maximum effective viscoplastic strain increment $\Delta\bar{\epsilon}_{vp}^n$ as a fraction of the total effective strain $\bar{\epsilon}^n$, i.e.,

$$\Delta\bar{\epsilon}_{vp}^n = \left(\sqrt{\frac{2}{3}} \left\| \left(\dot{\epsilon}_{ij}^n \right)_{vp} \right\| \right)^{1/2} \Delta t_n \leq \tau \bar{\epsilon}^n \quad (4.92)$$

The time step Δt_n needs to be calculated at each integration point according to Eq. 4.92, and the least value taken for analysis. Parameter τ gives accurate results in the range $0.01 < \tau < 0.15$ for $\theta = 0$ and $\tau < 10$ for $\theta \geq 0.5$ [28]. The change in the time step length between any two intervals is limited according to $\Delta t_{n+1} \leq k \Delta t_n$, where k is a constant (a value of 1.5 is suggested by [28].)

Theoretical restrictions have been provided by [2] for associated viscoplasticity, $\Phi(F) = F$, and $\theta = 0$ for the following yield criteria:

$$\begin{aligned} \Delta t &\leq \frac{(1+\nu)F_o}{\gamma E} && \text{Tresca} \\ \Delta t &\leq \frac{4(1+\nu)F_o}{3\gamma E} && \text{Von Mises} \\ \Delta t &\leq \frac{4(1+\nu)(1-2\nu)F_o}{\gamma(1-2\nu+\sin^2\phi)E} && \text{Mohr - Coulomb} \end{aligned} \quad (4.93)$$

4.3 Theory of continuum damage mechanics

Load-induced damage of brittle materials can be assessed by solving the equations of mechanics at the meso-scale [28], since the mechanisms that consume most of the applied energy are only activated at this level. However, it is at the macro-scale level where the collective effect of mechanisms acting at the microstructure level of the material are manifested. To evaluate the global mechanical response at the macro-scale level (i.e., laboratory specimens, real structures, etc.), a mapping of the field variables (e.g., cracks, shear bands, flaws, etc.) can be used between the two levels [20]. Such a mapping requires adopting a proper homogenisation procedure. To employ the principles of mechanics in deriving the required model within a minimum representative volume element (RVE), the governing variables can be assumed to be smooth and continuous up to their second derivatives with respect to their positions in the material space [26]. This means that the elasticity and plasticity theories can be used at this scale to find the mechanical response of a material due to the existence of a single crack or an ensemble of cracks [43].

In developing the following set of unified elasto-visco-plastic damage-based constitutive equations, the material is assumed to be isothermal and free of body forces. The total strain tensor

is decomposed into three components: an elastic strain, \mathbf{e}_{ij}^e , a damage strain, \mathbf{e}_{ij}^{cr} , and a visco-plastic strain, \mathbf{e}_{ij}^{vp} , i.e.

$$\boldsymbol{\varepsilon}_{ij} = \boldsymbol{\varepsilon}_{ij}^e + \boldsymbol{\varepsilon}_{ij}^{cr} + \boldsymbol{\varepsilon}_{ij}^{vp} = \boldsymbol{\varepsilon}_{ij}^t + \boldsymbol{\varepsilon}_{ij}^{vp} \quad (4.94)$$

The visco-plastic and part of the damage strains are permanent in nature and irreversible. The stress-strain relationship of the cracked material can be written as:

$$\mathbf{e}_{ij}^t = \bar{C}_{ijmn} \mathbf{s}_{mn} \quad (4.95)$$

where \bar{C}_{ijmn} is the effective elastic compliance and \mathbf{e}_{ij}^t is the sum of elastic strain, \mathbf{e}_{ij}^e , and damage strain, $\mathbf{e}_{ij}^d = \mathbf{e}_{ij}^{cr}$. The increment of the total strain can therefore be written as:

$$d\mathbf{e}_{ij} = d\mathbf{e}_{ij}^t + d\mathbf{e}_{ij}^{vp} \quad (4.96)$$

By substituting Eq. 4.95 in Eq. 4.96, the material constitutive relationship is written as:

$$d\mathbf{s}_{ij} = \bar{D}_{ijmn} (d\mathbf{e}_{mn} - d\mathbf{e}_{mn}^{vp}) \quad (4.97)$$

where \bar{D}_{ijmn} is the effective material stiffness that reflects the impact of a crack and the heterogeneity of the quasi-brittle solid on its mechanical properties.

Inclusions presence at the micro-level of the material, such as cracks, introduces disturbances into the elastic stress and strain fields of the material. These disturbances are influenced by the geometry and mechanical properties of the inclusion [7]. These strains must satisfy the general statement of equilibrium, i.e.,

$$\begin{aligned} \sigma_{ij}^s &= \frac{1}{V} \int_{V^s} \sigma_{ij} dV \\ \varepsilon_{ij}^s &= \frac{1}{V} \int_{V^s} \varepsilon_{ij} dV \end{aligned} \quad (4.98)$$

where superscript s takes the symbol e or cr for the matrix and the inclusion (crack), respectively, and V is the total volume of the RVE. The strains, ε_{ij} , in the right-hand side of Eq. 4.98 must satisfy the general requirement of equilibrium, i.e.,

$$\varepsilon_{ij} = \frac{1}{2} (u_{i,j} + u_{j,i}) \quad (4.99)$$

Substituting Eq. 4.99 into Eq. 4.98, and making use of the divergence theorem [16] yields:

$$\varepsilon_{ij}^{cr} = \frac{1}{V} \int_{V^{cr}} \frac{1}{2} (u_{i,j} + u_{j,i}) dV = \frac{1}{V} \int_{S^{cr}} \frac{1}{2} (u_i \cdot n_j + u_j \cdot n_i) dS^{cr} \quad (4.100)$$

where S^{cr} is the surface of the crack. Equation 4.100 can be written in terms of applied stresses as:

$$\boldsymbol{\varepsilon}_{ij}^{cr} = C_{ijmn}^{cr} \boldsymbol{\sigma}_{mn} \quad (4.101)$$

By substituting Eq. 4.101 into Eq. 4.95, the following expression results:

$$\mathbf{e}_{ij}^t = \bar{C}_{ijmn} \mathbf{s}_{mn} = \left(C_{ijmn}^e + C_{ijmn}^{cr} \right) \mathbf{s}_{mn} \quad (4.102)$$

Equation 4.102 can be written in incremental form as:

$$d\mathbf{e}_{ij}^t = \bar{C}_{ijmn} d\mathbf{s}_{mn} + dC_{ijmn}^{cr} \mathbf{s}_{mn} = \frac{\partial \bar{C}_{ijmn}}{\partial \mathbf{s}_{mn}} d\mathbf{s}_{mn} + \frac{\partial C_{ijmn}^{cr}}{\partial \mathbf{s}_{mn}} \mathbf{s}_{mn} d\mathbf{s}_{mn} \quad (4.103)$$

The overall effective elastic moduli can be obtained from Eq. 4.103 as:

$$\bar{D}_{ijmn} = \frac{\partial \bar{C}_{ijmn}}{\partial \mathbf{s}_{mn}} + \frac{\partial C_{ijmn}^{cr}}{\partial \mathbf{s}_{mn}} \mathbf{s}_{mn} \quad (4.104)$$

It can be shown that the overall effective elastic moduli given in Eq. 4.104 can be written in terms of the virgin material elastic moduli as:

$$\bar{D}_{ijmn} = \left(I - \omega_{ijkl} \right) D_{klmn}^e \quad (4.105)$$

where ω_{ijkl} is the damage parameter due to cracking, I is the unity tensor, and D_{klmn}^e is the fourth-order elastic material tensor. The damage parameter in Eq. 4.105 is calculated based on the evolution of the micro-cracks at the micro-level. A description on the method used to calculate the crack compliance for a given applied state of stresses follows.

4.3.1 Crack compliance

The compliance of a given single crack can be determined from the relationships between the crack displacements and stresses, depending on whether the crack is open or closed. Here, the crack compliance is calculated at the end of the application of a given load increment. This means that the damage model implemented in the program is applied when the cracks reach their expected final sizes, and their diameters remain unchanged for the current loading increment. Equation 4.103 is general in nature so that it can be used to obtain the constitutive relationships for either 2-D or 3-D applications. For the sake of brevity, the calculation of the crack compliance is only described here when the material is subjected to plane stress conditions. An element of material, as illustrated in Figure 4-6(a) and (b), is replaced by an equivalent solid containing a single elliptical crack of length, $2a$, Figure 4-6(c), with the axis of the ellipse being x' and y' . The crack position and orientation is defined in the space of the material by the angle, θ , of the axis, x' , with respect to the major axes of applied principal stress, X . If the element in Figure

4-6(c) is subjected to stresses, $\{\sigma\}$, the elastic and damage strain, $\{\epsilon'\}$, can be calculated using Eq. 4.102.

According to Lekhnitskii [22], for an open crack of length, $2a$, in an anisotropic, homogeneous, and linearly-elastic solid, the displacement discontinuities, $u_{x'}$, and $u_{y'}$, across the crack faces are given by:

$$\begin{aligned} \begin{Bmatrix} u_{x'} \\ u_{y'} \end{Bmatrix} = 2\sqrt{a-x} \begin{Bmatrix} \bar{C}_{11} \bar{\epsilon}_{11} (a_1 b_2 + a_2 b_1) s_{y\phi} + (b_1 + b_2) t_{x\phi} \\ \bar{C}_{22} \bar{\epsilon}_{22} \frac{b_1}{a_1^2 + b_1^2} + \frac{b_2}{a_2^2 + b_2^2} s_{y\phi} + \frac{a_1 b_2 + a_2 b_1}{(a_1^2 + b_1^2)(a_2^2 + b_2^2)} t_{x\phi} \end{Bmatrix} \end{aligned} \quad (4.106)$$

where α and β are the real and imaginary parts of the roots $\lambda_r = \alpha_r \pm i\beta_r$ of the characteristic equation of the governing strain compatibility equation of an anisotropic body, i.e.,

$$\bar{C}_{11} \lambda^4 - (\bar{C}_{12} + \bar{C}_{21}) \lambda^3 + (\bar{C}_{12} + \bar{C}_{21} + \bar{C}_{33}) \lambda^2 - (\bar{C}_{22} + \bar{C}_{32}) \lambda + \bar{C}_{22} = 0 \quad (4.107)$$

where $(r=1,2)$ and $i=\sqrt{-1}$, with $\beta_1, \beta_2 > 0; \beta_1 \neq \beta_2$. The characteristic equation is written in terms of the overall effective inelastic compliance in the primed (crack) co-ordinate system. This means that the solutions of these equations are required for each crack orientation. Fortunately, the latter solutions can be obtained by solving for their roots, λ_r , for each trial compliance, $[\bar{C}]^n$, at the orientation plane $\theta_{a_k} = 0$ only. For other orientations, (i.e. $\theta_{a_k} \neq 0$) according to Lekhnitskii [22], the local roots, λ'_r , can be expressed in terms of the roots λ_r at $\theta_{a_k} = 0 = 0$ as follows:

$$\lambda'_r = \frac{\lambda_r \cos \theta - \sin \theta}{\cos \theta + \lambda_r \sin \theta}; \quad \bar{\lambda}'_r = \frac{\bar{\lambda}_r \cos \theta - \sin \theta}{\cos \theta + \bar{\lambda}_r \sin \theta} \quad (4.108)$$

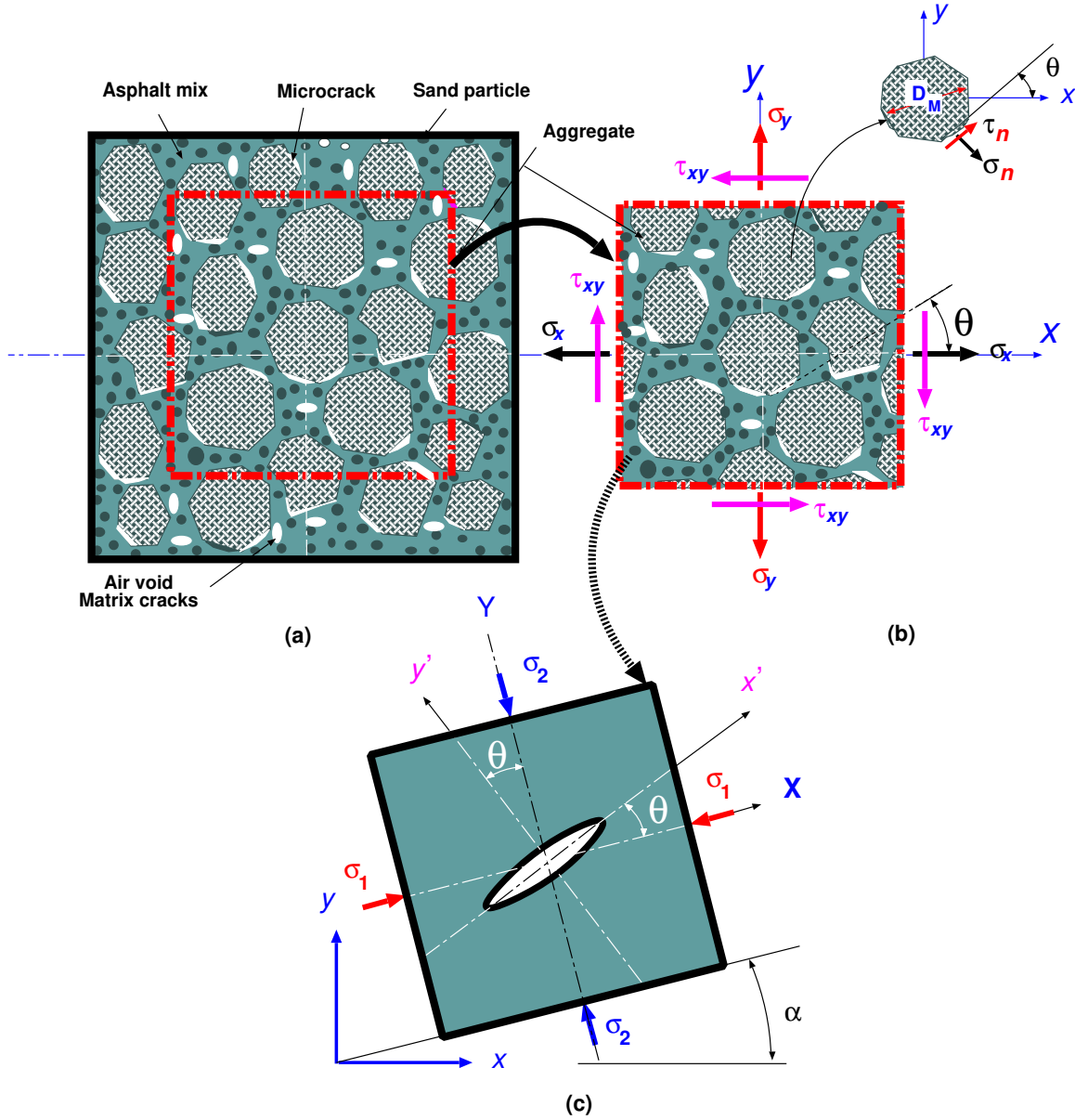


Figure 4-6: Typical section subjected to general state of stresses.

The crack strains, $\{\varepsilon'\}^{cr}$, can now be obtained according to:

$$A_c \begin{Bmatrix} \varepsilon_{x'x'} \\ \varepsilon_{y'y'} \\ \gamma_{x'y'} \end{Bmatrix} = \int_{-a}^a \begin{Bmatrix} [u_{x'}]n'_1 \\ [u_{y'}]n'_2 \\ \frac{1}{2}([u_{x'}]n'_2 + [u_{y'}]n'_1) \end{Bmatrix} dS \quad (4.109)$$

where A_c is the representative-surface area (RSA), the square brackets $[]$ indicates the jump of the displacement functions inside them, and n'_1 and n'_2 are the direction cosines of the normal to

the crack surface, S . Note that for a slit (line crack), $n'_1 = 0$, $n'_2 = 1$. Substituting for $u_{x'}$ and $u_{y'}$ from Eq. 4.106 into Eq. 4.109, Eq. 4.109 can be rewritten as:

$$\begin{Bmatrix} \varepsilon_{x'x'} \\ \varepsilon_{y'y'} \\ \gamma_{x'y'} \end{Bmatrix} = \frac{\pi a^2}{A_c} \begin{bmatrix} 0 & 0 & 0 \\ 0 & G_{11} & G_{12} \\ 0 & G_{21} & G_{22} \end{bmatrix} \begin{Bmatrix} \sigma_{x'x'} \\ \sigma_{y'y'} \\ \tau_{x'y'} \end{Bmatrix} \quad (4.110)$$

Determination of the coefficients in Eq. 4.110 depends on the type of crack openings. A discussion illustrating the calculation of the compliance for open, closed, and kinked cracks follows.

Open crack compliance

For open cracks, the elements of the G_{ij} in Eq. 4.110 are given by:

$$[G]^o = \begin{bmatrix} \frac{b_1}{a_1^2 + b_1^2} + \frac{b_2}{a_2^2 + b_2^2} & \frac{a_1 b_2 + a_2 b_1}{(a_1^2 + b_1^2)(a_2^2 + b_2^2)} \\ \frac{a_1 b_2 + a_2 b_1}{(a_1^2 + b_1^2)(a_2^2 + b_2^2)} & \frac{b_1 + b_2}{(a_1^2 + b_1^2) + (a_2^2 + b_2^2)} \end{bmatrix} \quad (4.111)$$

Closed crack compliance

In the case of a closed crack, $u_{y'} = 0$, the crack is able to transmit both compression and shear. However, if the shear, $\tau_{x'y'}$, across the crack surfaces is less than the frictional shear resistance, $\mu \sigma_{y'y'}$, where μ is the coefficient of dry friction and $\sigma_{y'y'}$ is the normal compression on the crack, then no crack displacements can occur. This means that:

$$[C\mathcal{Q}]^{cr} = 0 \quad (4.112)$$

which according to Eq. 4.104 clearly indicates that under these cases of overall compression the inelastic damage strains, $\{\varepsilon'\}^{cr}$, become zero. However, experiments on Portland cement concrete [45] and rock materials [16] show non-linear responses for these cases of loading, which contradicts the above conclusion. This paradox has puzzled many investigators, but the experimental work of Zaitsev [45] and Horii and Nemat-Nasser [16] has indicated that heterogeneous brittle materials under these loading conditions ignore the existing cracks and deform in a ductile manner. Therefore, the proposed model calculates the inelastic strain using the theory of plasticity, assuming that the non-linearity beyond this point is solely ascribed to plastic flow and yield-like deformations. The above stress distribution on the crack will occur when the applied principal external stress ratio, $s_r = \sigma_1/\sigma_2$, exceeds a certain critical value. This value is

known as the ductility parameter, Δ_c , which separates brittle behaviour from ductile one [28]. The heterogeneous materials behaviour is load dependent.

On the other hand, if $\tau_{x'y'}$ is greater than $\mu\sigma_{y'y'}$, then the crack will slide. The non-vanishing displacements and normal stress, respectively, can be written as [15]:

$$u_{x\phi} = 2\sqrt{a^2 - x\phi} \bar{C} \frac{\dot{\epsilon}}{c} (a_1 b_2 + a_2 b_1) (s_{y\phi\phi} - s_{y\phi\phi}^c) + (b_1 + b_2) (t_{x\phi\phi} + m \operatorname{sgn}(t_{x\phi\phi}) s_{y\phi\phi}^c) \dot{u} \quad (4.113)$$

with

$$s_{y\phi\phi}^c = \frac{\frac{\dot{\epsilon}}{c} b_1 (a_2^2 + b_2^2) + b_2 (a_1^2 + b_1^2) \dot{u} s_{y\phi\phi} + (a_1 b_2 + a_2 b_1) t_{x\phi\phi}}{b_1 (a_2^2 + b_2^2) + b_2 (a_1^2 + b_1^2) - m \operatorname{sgn}(t_{x\phi\phi}) (a_1 b_2 + a_2 b_1)} < 0 \quad (4.114)$$

where the symbol sgn can be 1, 0, or -1, depending on whether its argument is positive, zero, or negative. This leads to the elements G_{ij} in Eq. 4.110:

$$[G]^c = \begin{bmatrix} \dot{\epsilon} & 0 & 0 & \dot{u} \\ \bar{C} \frac{\dot{\epsilon}}{c} (a_1 b_2 + a_2 b_1) \dot{u} - R_1 & \bar{C} \frac{\dot{\epsilon}}{c} (b_1 + b_2) \dot{u} - R_2 & \dot{u} & \dot{u} \end{bmatrix} \quad (4.115)$$

with the quantities, R_1 and R_2 , given by:

$$\begin{bmatrix} R_1 \\ R_2 \end{bmatrix} = a_c \begin{bmatrix} \frac{\dot{\epsilon}}{c} b_1 (a_2^2 + b_2^2) + b_2 (a_1^2 + b_1^2) \dot{u} \\ (a_1 b_2 + a_2 b_1) \dot{u} \end{bmatrix} \quad (4.116)$$

where the coefficient, a_c , is:

$$a_c = \frac{(a_1 b_2 + a_2 b_1) - m \operatorname{sgn}(t_{x\phi\phi}) (a_1 b_2 + a_2 b_1)}{b_1 (a_2^2 + b_2^2) + b_2 (a_1^2 + b_1^2) - m \operatorname{sgn}(t_{x\phi\phi}) (a_1 b_2 + a_2 b_1)} \quad (4.117)$$

Kinked crack compliance

Experimentally, it has been observed that a closed crack may branch in the matrix due to increased applied compressive load [45]. The crack shows first curving for a finite length (referred to henceforth as the opening wing) and then propagates (snaps) in a straight-line fashion (referred to as the sliding wing) until it gets arrested by the energy barrier of the matrix.

Nofal [28] made use of the kinked crack displacement function proposed by Horii and Nemat-Nasser [16] to develop the kinked crack strain. Following the same procedure given by Eqs. 4.109 and 4.110, the kinked crack strain is the sum of the strain of the open wing, i.e.,

$$\begin{Bmatrix} \epsilon_{x'x'} \\ \epsilon_{y'y'} \\ \gamma_{x'y'} \end{Bmatrix} = \beta_k \begin{bmatrix} 0 & \mu \sin 2\theta & -\sin 2\theta \\ 0 & -\mu \sin 2\theta & \sin 2\theta \\ 0 & -2\mu \cos 2\theta & 2 \cos 2\theta \end{bmatrix} \begin{Bmatrix} \sigma_{x'x'} \\ \sigma_{y'y'} \\ \tau_{x'y'} \end{Bmatrix} \quad (4.118)$$

and the strain of the sliding wing, i.e.,

$$\begin{Bmatrix} \varepsilon_{x'x'} \\ \varepsilon_{y'y'} \\ \gamma_{x'y'} \end{Bmatrix} = 2\beta_k \begin{bmatrix} 0 & 0 & 0 \\ 0 & \mu & -1 \\ 0 & -\mu \tan \theta & \tan \theta \end{bmatrix} \begin{Bmatrix} \sigma_{x'x'} \\ \sigma_{y'y'} \\ \tau_{x'y'} \end{Bmatrix} \quad (4.119)$$

where

$$\beta_k = \frac{9.6(1-\nu^2)}{\pi EA_c} \left[l_k + \frac{\bar{d}}{2} \right] F_1(D_M, \theta, l_k) \quad (4.120)$$

E being the Young's modulus, ν the Poisson's ratio, and A_c its surface area. The function, $F_1(D_M, \theta, l_k)$ is defined as:

$$F_1(D_M, \theta, l_k) = \frac{D_M \cos \theta}{\bar{d}} \left\{ \sqrt{l_k (\bar{d} + l_k)} \left[\sin^{-1} \left(\frac{\bar{d}}{\bar{d} + 2l_k} \right) + \frac{\bar{d}}{2} \ln \left(\frac{\bar{d} + 2l_k}{\bar{d}} \right) \right] \right\} \quad (4.121)$$

in which D_M is the maximum crack diameter, \ln denotes natural logarithm, and the distance is calculated from $\bar{d} \approx \alpha_k D_M \sin \theta$. The coefficient α_k can be chosen such that the results of this proposed approximate solution fits the exact numerical solution given by Horii and Nemat-Nasser [16] over the entire spectrum of the inclination angle, θ , for a given kink length, l_k . Fenalla [8] has found out that a value of $\alpha_k = 0.25$ will yield results close to these numerical solutions. The same value has been used in the pavement mechanistic model. The kink length l_k is calculated according to Nofal [28] as:

$$l_k = \frac{1}{\pi} \begin{cases} \frac{1}{4} \left[\frac{K_{IC}^m}{\sigma_x} \sqrt{\left(\frac{K_{IC}^m}{\sigma_x} \right)^2 + \frac{4}{s_r} DG(s_r, \theta) \cos \theta} \right]; & |s_r| > 0 \\ \left[\frac{\sigma_y}{K_{IC}^m} DG(s_r = 0, \theta) \cos \theta \right]^2; & |s_r| = 0 \end{cases} \quad (4.122)$$

where the ratio, $s_r = \sigma_x / \sigma_y$, signifies the degree of confinement provided by the applied stresses, in which σ_x and σ_y are the minor and major applied principal stresses, respectively. Variable D , on the other hand, is the parent crack (without kink) diameter, K_{IC}^m is the mode-I crack intensity factor of the matrix, and the stress transformation function, $G(s_r, \theta)$, is obtained by combining two other stress transformation functions, $N(s_r, \theta)$ and $S(s_r, \theta)$, as:

$$G(s_r, \theta) = S(s_r, \theta) - \mu N(s_r, \theta) \quad (4.123)$$

where $N(s_r, \theta)$ and $S(s_r, \theta)$ are given by:

$$\begin{cases} N(s_r, \theta) \\ S(s_r, \theta) \end{cases} = \begin{cases} \cos^2 \theta + s_r \sin^2 \theta \\ (1 - s_r) \sin \theta \cos \theta \end{cases} \quad (4.124)$$

Compliance of an element with an array of cracks

For an element with N_c cracks, each with orientation θ_k and initial diameter $2a_k$, the crack ensemble compliance, is written as:

$$[C]^{cr} = \sum_{k=1}^{N_c} [T]_k^T [C]_k^{cr} [T]_k \quad (4.125)$$

where $[T]_k$ is the appropriate transformation matrix. Earlier discussion on the calculation of the crack compliance showed that $[C]^{cr}$ is both an explicit and implicit function of the as yet unknown overall compliance $[\bar{C}]$. The solution can be obtained by utilising the self-consistent model [13]. In this model, the iterative process outlined by Horii and Nemat-Nasser [15] is adopted. Subsequently, the overall non-linear damage compliance for the $(n+1)^{th}$ iteration can be written as:

$$[\bar{C}]^{n+1} = [C] + \sum_{k=1}^{N_c} [T]_k^T \left[C'([\bar{C}]^n) \right]_k^{cr} [T]_k \quad (4.126)$$

where $[\bar{C}]^n$ is the desired overall compliance which corresponds to the n^{th} iteration. The process is terminated if the following convergence criteria are met:

$$\frac{|\bar{C}^{(n)} - \bar{C}^{(n+1)}|_2}{|\bar{C}^{(n+1)}|_\infty} \leq \text{tolerance}; \quad \frac{|\bar{C}^{(n)} - \bar{C}^{(n+1)}|_\infty}{|\bar{C}^{(n+1)}|_\infty} \leq \text{tolerance} \quad (4.127)$$

which are based on L_2 , L_∞ norms [2]. The tolerance value assumed in the program is 10^{-6} .

Equation 4.125 is not, however, directly useful in numerical implementation, because the number of cracks is a non-deterministic quantity. To overcome this limitation, the summation in Eq. 4.125 is replaced by an integral relation, i.e.,

$$[C]^{cr} = \int \int p(\theta, a) [T]^T [C']^{cr} [T] da d\theta \quad (4.128)$$

where $p(\theta, a)$ is the joint probability density function of the crack size and orientation. Assuming that the sizes of the existing cracks are independent of their orientations, the latter function can be decomposed into a product of two separate functions, i.e.,

$$p(\theta, a) = p(\theta) p(a) = \frac{2}{\pi} p(a) \quad (4.129)$$

where the joint probability density function of the micro-crack orientation angle, $(0 \leq \theta \leq \pi/2)$, is assumed to be Gaussian (normal), $p(\theta) = 2/\pi$, while different forms for the function that describes the crack diameter variable are used.

In carrying out the integration of Eq. 4.128, two types of cracks need to be differentiated: stable cracks and propagating cracks. Thus, Eq. 4.125 can be written as:

$$[C]^{cr} = [C]_g^{cr} + [C]_a^{cr} \quad (4.130)$$

where $[C]_g^{cr}$ and $[C]_a^{cr}$ are the compliance contributions from the growing and arrested micro-cracks, respectively. Stable and propagating cracks can be identified by the critical crack orientation angle, θ_k , the magnitude of the applied stress ratio, s_r , and the mode-I and II fracture parameters. To evaluate the critical angles, θ_k , the following kinetic algorithm and associated damage evolution law are utilised.

4.3.2 Crack evolution criteria

It is sufficient to assume that failure of brittle materials is of a “Cleavage 1” or “Cleavage 2” deformation type, and, therefore, linear fracture mechanics laws can be applied [1]. It is likely that an open crack will experience mode-I type deformation, a closed crack will display mode-II deformation, while an open/closed crack will undergo mixed mode-I/II deformation. For mixed mode-I/II, the strain-energy release rate governs the crack movements. The strain-energy release rate, G' , along the weak plane for the mixed mode-I/II should include the contribution G'_1 of mode-I and G'_2 of mode-II [35], i.e.,

$$G' = G'_1 + G'_2 = \frac{1}{2} [G'_{11}K_I'^2 + (G'_{12} + G'_{21})K_I'K_{II}' + G'_{22}K_{II}'^2] \quad (4.131)$$

where K_I' and K_{II}' are respectively the mode-I and mode-II stress intensity factors, at a given orientation, θ_k . The coefficients G'_{ij} , ($i = j = 1, 2$) are given by Eqs. 4.111 and 4.115 for open and closed cracks, respectively. The calculated value of G' should be calibrated against a given critical strain energy release rate G_c to determine whether a micro-crack is experiencing propagation or it has been arrested. The micro-crack kinetic algorithm need be considered for (i) tension-tension (mode-I); (ii) compression-compression (mode-II); and, finally, (iii) tension-compression (mixed mode-I/II) stress regimes.

Uniaxial and biaxial tension (Mode-I)

According to the fracture criterion utilised, the stress intensity factors, K_I and K_{II} , can be written as a function of the applied stress, σ_Y , a given crack size, $2a$, and the crack orientation angle, θ , as:

$$\begin{Bmatrix} K_I \\ K_{II} \end{Bmatrix} = \sigma_Y \sqrt{\pi a} \begin{Bmatrix} N(s_r, \theta) \\ S(s_r, \theta) \end{Bmatrix} \quad (4.132)$$

where the two stress transformation functions, $N(s_r, \theta)$ and $S(s_r, \theta)$, are given by Eq. 4.124.

The determination of the effective stiffness of the cracked material can be achieved by employing Eq. 4.126, which requires the calculation of the cracks' compliance. In order to carry out the computation of the integrals in Eq. 4.126, the exact amount of arrested, η_a , and propagating, η_g , cracks, their sizes, D 's, as well as their orientation, θ , must be evaluated a priori. Making use of the first equation from Eq. 4.132, propagating cracks are differentiated from arrested ones as:

$$\theta_i = \tan^{-1} \sqrt{\frac{\sigma_Y - f_t^r}{f_t^r - s_r \sigma_Y}} \quad (4.133)$$

where the threshold stress, f_t^r , to initiate crack evolution is estimated as:

$$f_t^r = \frac{K_{IC}^{ef}}{\rho} \sqrt{\frac{2}{\pi D_M}} \quad (4.134)$$

where $\rho = \sqrt{2a_0/D_M}$ is a scalar (less than one) that designates the fraction of the initially de-bonded interfaces. The magnitude of ρ depends on the mix of the material, the compaction method, and the curing procedure of the material, and it can be obtained via micro-graphic analysis of a typical specimen [9] or via microscopic observation [36]. It can also be measured using radioactive techniques such as gamma or x-ray radiography, or the method of acoustic emission [10].

It is assumed here that the expected crack diameter varies from $2a_i = D_{\min}$ to only $2a_f = D_M$. Thus, the crack diameter, $D(\theta)$, at any orientation angle, θ , may be obtained by considering Eqs. 4.132 and 4.134, i.e.,

$$D(\theta) = \left[\frac{\rho f_t^r}{\sigma_Y N(s_r, \theta)} \right]^2 D_M \quad (4.135)$$

Using Eqs. 4.133 and 4.135 in Eq. 4.125, and carrying out the necessary integration over the domains defined above, the propagating unstable cracks compliance is given by:

$$[C]_g^{cr} = \int_{\pm\theta_1^c}^{\pm\theta_1^p} p_g^t(s_r, a) [T]^T \left[C^{(k)'}([\bar{C}], \lambda_r, \theta) \right]_o^{cr} [T] d\theta \quad (4.136)$$

and the arrested stable cracks compliance is:

$$[C]_a^{cr} = \int_{\pm\theta_1^p}^{\pm\frac{\pi}{2}} p_a^t(s_r, a) [T]^T \left[C^{(k)'}([\bar{C}], \lambda_r, \theta) \right]_o^{cr} [T] d\theta \quad (4.137)$$

where the functions, $p_g^t(s_r, a)$ and $p_a^t(s_r, a)$, can be determined, respectively, according to:

$$\begin{Bmatrix} p_g^t(s_r, a) \\ p_a^t(s_r, a) \end{Bmatrix} = \frac{\pi N_c}{A_c} \begin{Bmatrix} \frac{2\eta_g^t}{\pi} \int_{a(\theta)}^{a_M} a^2 p(a) da \\ \frac{2(1-\eta_g^t - \gamma_t)}{\pi} \int_{a_{\min}}^{a_M} a^2 p(a) da \end{Bmatrix} \quad (4.138)$$

in which $\gamma_t = \frac{D_{\min}}{D_M}$ and the current propagating crack portion, η_g^t , can be calculated as [27]:

$$\eta_g^t|_c = \frac{2}{\pi} \left[\theta_{t_1} - \left(\frac{\rho f_t^r}{\sigma_Y} \right)^2 \int_0^{\theta_{t_1}} \frac{d\theta}{N^2(s_r, \theta)} \right] \quad (4.139)$$

Uniaxial and biaxial compression (Mode-II)

Under uniaxial and biaxial compressive stresses, pre-existing cracks are mainly closed and may grow in a mode-II manner. Strictly speaking, the fracture criterion of Eq. 4.131 should be employed; however, since the cracks will not grow in mode-I fashion, it is sufficient to employ mode-II fracture criterion only [18]. The effective shear stresses acting on the crack faces can be obtained from:

$$\tau_s = \sigma_Y G(s_r, \theta) \quad (4.140)$$

Assuming Coulomb's type friction, micro-cracks surfaces will slide relative to each other if the normal stress, $\sigma_n = \sigma_{y'} < 0$ and the absolute net shear stresses $|\tau_s| \geq 0$. Hence, Eq. 4.123 can be solved for the upper and lower bounds $[\pm\theta_{s_2}, \pm\theta_{s_1}]$ of micro-crack orientation for the given stress combination:

$$\theta_{s_1, s_2} = \pm \tan^{-1} \left[\frac{1 \pm \sqrt{-4C_s(C_s + \mu)}}{2C_s} \right] \quad (4.141)$$

where $C_s = \frac{\mu\sigma_X}{(\sigma_Y - \sigma_X)} = \frac{\mu s_r}{(1 - s_r)}$. It should be realised that cracks oriented at the critical angle given by Eq. 4.141 are the only ones that will slide. The minimum required value of θ_0 for sliding to occur is:

$$\theta_0 = \tan^{-1} \left[\mu + \sqrt{\mu^2 + 1} \right] \quad 4.142$$

In a similar fashion to the previous loading case, the crack orientation and diameters need to be calculated to compute their compliance. In this loading case, in addition to the sliding cracks, there is a need to define propagating, kinked, and arrested cracks.

For propagating closed cracks, the orientation angle can be calculated according to:

$$\theta_{f_1, f_2} = \pm \tan^{-1} \left[\frac{1 \pm \sqrt{-4C_f(C_f + \mu)}}{2C_f} \right] \quad 4.143$$

where $C_f = \frac{1}{(1 - s_r)} \left[\mu s_r + \left(\frac{\rho f_c^r}{\sigma_Y} \right) G(s_{r_0}, \theta_0) \right]$, with the threshold stress,

$f_c^r = \frac{K_{IIC}^{if}}{\rho G(s_{r_0}, \theta_0)} \sqrt{\frac{2}{\pi D_M}}$. The corresponding crack diameter is obtained from:

$$D(\theta_f) = \left[\frac{\rho f_c^r G(s_{r_0}, \theta_0)}{\sigma_Y G(s_r, \theta)} \right]^2 D_M \quad 4.144$$

The kinked crack is defined by:

$$\theta_{k_1, k_2} = \pm \tan^{-1} \left[\frac{1 \pm \sqrt{-4C_k(C_k + \mu)}}{2C_k} \right] \quad 4.145$$

where $C_k = \frac{1}{(1 - s_r)} \left[\mu s_r + \left(\frac{\sqrt{3} \rho K_{IC}^m f_c^r}{2 K_{IIC}^{if} \sigma_Y} \right) G(s_{r_0}, \theta_0) \right]$, while its diameter is calculated using:

$$D(\theta_k) = \left[\frac{\left(\frac{\sqrt{3} \rho K_{IC}^m}{2 K_{IIC}^{if}} \right) f_c^r G(s_{r_0}, \theta_0)}{\sigma_Y G(s_r, \theta)} \right]^2 D_M \quad (4.146)$$

Note that these cracks will begin to grow beyond the stress level, $f_c^k = \frac{K_{IC}^m}{2 G(s_{r_0}, \theta_0)} \sqrt{\frac{6}{\pi D_M}}$.

Following a similar procedure for the tensile loading case, the propagating crack compliance is calculated according to:

$$[C]_g^{cr} = \int_{\pm\theta_{f_1}^c}^{\pm\theta_{f_2}^c} p_g^c(s_r, a) [T]^T \left[C^{(k)'}([\bar{C}], \lambda_r, \theta) \right]_c^{cr} [T] d\theta \quad (4.147)$$

and the arrested stable crack compliance is:

$$\begin{aligned} [C]_a^{cr} &= \int_{\pm\theta_{s_1}^c}^{\pm\theta_{f_2}^p} p_a^c(s_r, a) [T]^T \left[C^{(k)'}([\bar{C}], \lambda_r, \theta) \right]_c^{cr} [T] d\theta \\ &+ \int_{\pm\theta_{f_1}^p}^{\pm\theta_{s_2}^c} p_a^c(s_r, a) [T]^T \left[C^{(k)'}([\bar{C}], \lambda_r, \theta) \right]_c^{cr} [T] d\theta \end{aligned} \quad (4.148)$$

The kinked crack contribution is calculated from:

$$[C]_k^{cr} = \int_{\pm\theta_{k_1}^c}^{\pm\theta_{k_2}^c} p_k^c(s_r, l_k) [T]^T \left(\left[C^{(k)'}(\theta, l_k) \right]_{k_o}^{cr} + \left[C^{(k)'}(\theta, l_k) \right]_{k_c}^{cr} \right) [T] d\theta \quad (4.149)$$

where the functions, $p_g^c(s_r, a)$, $p_a^c(s_r, a)$, and $p_k^c(s_r, l_k)$, can be determined from:

$$\begin{Bmatrix} p_g^c(s_r, a) \\ p_a^c(s_r, a) \\ p_k^c(s_r, l_k) \end{Bmatrix} = \frac{\pi N_c}{A_C} \begin{Bmatrix} \frac{2\eta_g^c}{\pi} \int_{a(\theta_f)}^{a_M} a^2 p(a) da \\ \frac{2(1-\eta_g^c - \eta_k^c - \gamma_t)}{\pi} \int_{a_{\min}}^{a_M} a^2 p(a) da \\ \frac{9.6(1-\nu^2)\eta_k^c}{\pi^2 E} \int_{a(\theta_k)}^{a_M} \left(l_k + \frac{\bar{d}}{2} \right) F_1(D_M, \theta, l_k) p(a) da \end{Bmatrix} \quad (4.150)$$

The crack amount, η_k^c , for kinked cracks is calculated as:

$$\eta_k^c = \frac{1}{(\theta_{s_2} - \theta_{s_1})} \left[(\theta_{k_2} - \theta_{k_1}) - \left(\frac{\sqrt{3}\rho K_{IC}^m f_c^r}{2K_{IIC}^{if} \sigma_Y} \right)^2 G^2(s_{\theta_0}, \theta_0) \int_{\theta_{k_1}}^{\theta_{k_2}} \frac{d\theta}{G^2(s_r, \theta)} \right] \quad (4.151)$$

whereas the crack amount, η_g^c , for the growing cracks portion is obtained from:

$$\eta_g^c = -\eta_k^c + \frac{1}{(\theta_{s_2} - \theta_{s_1})} \left[(\theta_{f_2} - \theta_{f_1}) - \left(\frac{\rho f_c^r}{\sigma_Y} \right)^2 G^2(s_{\theta_0}, \theta_0) \int_{\theta_{f_1}}^{\theta_{f_2}} \frac{d\theta}{G^2(s_r, \theta)} \right] \quad (4.152)$$

Biaxial compression-tension (Mixed Mode-I/II)

In the tension-compression stress regime, two possibilities of crack growth exist. Some cracks may open while others may close under this loading condition. Furthermore, open cracks may close, or closed cracks may open during the loading process. Open cracks grow in a mixed mode-

I/II fashion, while closed cracks grow in mode-II. To identify the domain of open cracks from the closed cracks, the normal stress at the crack site is equated to zero, i.e.,

$$\sigma_n = \sigma_{y'} = \sigma_Y N(s_r, \theta) \quad (4.153)$$

the solution of which indicates that the limit angle, θ_l , is:

$$\theta_l = \tan^{-1} \sqrt{\frac{1}{|s_r|}} \quad (4.154)$$

Thus, for a given load combination, mode-II fracture takes place for the cracks oriented at $\theta < \theta_l$, while cracks oriented at $\theta > \theta_l$ experience mixed mode-I/II. The upper and lower bounds for open cracks are $\frac{\pi}{2}$ and θ_l , respectively.

Closed crack kinematics

For closed cracks (i.e., $\sigma_n < 0$), the shear stress, τ_s , is evaluated in a similar fashion as for the biaxial compression case, bearing in mind that the biaxial stress ratio, s_r , is negative. Hence, the bound of the sliding angle θ_s can also be evaluated now as:

$$\theta_s = \tan^{-1} \left[\frac{1 \pm \sqrt{-4C_s(C_s + \mu)}}{2C_s} \right] \quad C_s < 0 \quad (4.155)$$

The threshold angle, θ_{0II} , at which cracks deform in mode-II fashion can also be obtained from Eq. 4.142. The domain $[\theta_{f1} - \theta_{f2}]$ of unstable cracks can also be found in a similar fashion from Eq. 4.143. The latter equation is applicable if $\mu\sigma_X < 2K_{IIC}^{if}/\pi D_{\min}$, which is nearly always the case. However, when $\mu\sigma_X > 2K_{IIC}^{if}/\pi D_{\min}$, which is unlikely to occur, it has again only one root, i.e.,

$$\theta_f = \tan^{-1} \left[\frac{1 \pm \sqrt{-4C_f(C_f + \mu)}}{2C_f} \right] \quad (4.156)$$

Open crack kinematics

Unlike the biaxial tension case, an open crack subjected to the current loading condition will be subjected to normal tensile stresses and significant shear stresses. This implies that the crack is experiencing both opening and sliding modes. Therefore, the mixed mode fracture criterion

specified by Eq. 4.131 must be applied in order to determine the micro-cracks stability. The governing fracture criterion can be written as:

$$\zeta^2 K_I'^2 + K_{II}'^2 = K_{IIC}^{if^2} \quad (4.157)$$

where $\zeta^2 = \frac{K_{II}'^2}{K_{IIC}^{if^2}} > 1.0$. Solution of Eq. 4.156 requires the introduction of the transformation

matrix, $M(s_r, \theta, \zeta)$, which can be calculated according to Nofal [28] as:

$$M(s_r, \theta, \zeta) = \zeta^2 [\cos^2 \theta + s_r \sin^2 \theta]^2 + [(1 - s_r) \sin \theta \cos \theta]^2 \quad (4.158)$$

The threshold angle, θ , for the open crack domain can be obtained by maximising the function $M(s_r, \theta, \zeta)$ with respect to θ , i.e.,

$$\theta = \begin{cases} \frac{\pi}{2} \\ \frac{1}{2} \cos^{-1} \frac{\zeta^2 (1 + s_r)}{(1 - s_r)(1 - \zeta^2)} \end{cases} \quad (4.159)$$

The critical crack diameter of the tensile cracks in the open domain is calculated from:

$$D(\theta_i) = \left[\left(\frac{\rho f_m^r}{\sigma_Y} \right)^2 \frac{M(s_{r_0}, \theta_0, \zeta_0)}{M(s_r, \theta, \zeta)} \right] D_M \quad (4.160)$$

with the threshold stress, $f_m^r = \frac{K_{IIC}^{if}}{\rho} \sqrt{\frac{2}{\pi D_M M(s_{r_0}, \theta_0, \zeta_0)}}$. The orientation is obtained as:

$$\theta_{i_1, i_2} = \tan^{-1} \sqrt{\frac{-c_2 + \sqrt{c_2^2 - 4c_1 c_3}}{2c_1}} \quad (4.161)$$

where the constants, $c_i, (i = 1, 2, 3)$ are given by:

$$\begin{Bmatrix} c_1 \\ c_2 \\ c_3 \end{Bmatrix} = \begin{Bmatrix} \zeta^2 s_r^2 - \left(\frac{\rho f_m^r}{\sigma_Y} \right)^2 M(s_{r_0}, \theta_0, \zeta_0) \\ 2\zeta^2 s_r + (1 - s_r)^2 - 2 \left(\frac{\rho f_m^r}{\sigma_Y} \right)^2 M(s_{r_0}, \theta_0, \zeta_0) \\ \zeta^2 - \left(\frac{\rho f_m^r}{\sigma_Y} \right)^2 M(s_{r_0}, \theta_0, \zeta_0) \end{Bmatrix} \quad (4.162)$$

Finally, the compliance for the cracks that lie in the closed crack domain are:

the sliding (propagating) closed cracks

$$[C]_g^{cr} = \int_{\pm\theta_{f1}^p}^{\pm\theta_{f2}^p} p_g^c(s_r, a) [T]^T \left[C^{(k)'}([\bar{C}], \lambda_r, \theta) \right]_c^{cr} [T] d\theta \quad (4.163)$$

the arrested (stable) closed cracks

$$\begin{aligned} [C]_a^{cr} &= \int_{\pm\theta_s^c}^{\pm\theta_{f1}^p} p_a^c(s_r, a) [T]^T \left[C^{(k)'}([\bar{C}], \lambda_r, \theta) \right]_c^{cr} [T] d\theta \\ &+ \int_{\pm\theta_{f2}^p}^{\pm\theta_f^c} p_a^c(s_r, a) [T]^T \left[C^{(k)'}([\bar{C}], \lambda_r, \theta) \right]_c^{cr} [T] d\theta \end{aligned} \quad (4.164)$$

the kinked closed cracks

$$[C]_k^{cr} = \int_{\pm\theta_{k1}^c}^{\pm\theta_{k2}^c} p_k^c(s_r, l_k) [T]^T \left(\left[C^{(k)'}(\theta, l_k) \right]_{k_o}^{cr} + \left[C^{(k)'}(\theta, l_k) \right]_{k_c}^{cr} \right) [T] d\theta \quad (4.165)$$

where the functions, $p_g^c(s_r, a)$, $p_a^c(s_r, a)$, and $p_k^c(s_r, l_k)$, are given by Eq. 4.150. The amount of kinked cracks, η_k^c , is obtained from:

$$\eta_k^c = \frac{1}{\left(\frac{\pi}{2} - \theta_s\right)} \left[\theta_k - \left(\frac{\sqrt{3}\rho K_{IC}^m f_c^r}{2K_{IIC}^{if} \sigma_Y} \right)^2 G^2(s_0, \theta_0) \int_0^{\theta_k} \frac{d\theta}{G^2(s_r, \theta)} \right] \quad (4.166)$$

and the amount of cracks growing because of sliding is calculated as:

$$\eta_g^c = -\eta_k^c + \frac{1}{\left(\frac{\pi}{2} - \theta_s\right)} \left[\theta_f - \left(\frac{\rho f_c^r}{\sigma_Y} \right)^2 G^2(s_0, \theta_0) \int_0^{\theta_f} \frac{d\theta}{G^2(s_r, \theta)} \right] \quad (4.167)$$

In this case, some cracks lie in the open domain. The amount of these cracks is computed using:

$$\eta_g' = \frac{1}{\left(\frac{\pi}{2} - \theta_s\right)} \left[(\theta_{t2} - \theta_{t1}) - \left(\frac{\rho f_m^r}{\sigma_Y} \right)^2 M(s_0, \theta_0, \zeta_0) \int_{\theta_{t1}}^{\theta_{t2}} \frac{d\theta}{M(s_r, \theta, \zeta)} \right] \quad (4.168)$$

At the same time, open cracks will contribute the following growing and arrested compliance to the overall effective material compliance:

the growing (propagating) open cracks

$$[C]_g^{cr} = \int_{\pm\theta_{12}^p}^{\pm\theta_{11}^p} p_g^t(s_r, a) [T]^T \left[C^{(k)'}([\bar{C}], \lambda_r, \theta) \right]_o^{cr} [T] d\theta \quad (4.169)$$

the arrested (stable) open cracks

$$\begin{aligned} [C]_a^{cr} = & \int_{\pm\theta_{12}^c}^{\pm\theta_{11}^p} p_a^t(s_r, a) [T]^T \left[C^{(k)'}([\bar{C}], \lambda_r, \theta) \right]_o^{cr} [T] d\theta \\ & + \int_{\pm\theta_{12}^p}^{\pm\frac{\pi}{2}} p_a^t(s_r, a) [T]^T \left[C^{(k)'}([\bar{C}], \lambda_r, \theta) \right]_o^{cr} [T] d\theta \end{aligned} \quad (4.170)$$

where the functions, $p_g^t(s_r, a)$ and $p_a^t(s_r, a)$, can be calculated using Eq. 4.138. The amount of evolving and arrested cracks can be computed using Eq. 4.139.

The proposed damage-based model can be used to predict the behaviour of brittle and cracked materials as well as composites subjected to various types of loading. The model application is limited to small deformation and static or cyclic non-proportional loading. The basic steps for implementing the proposed micro-mechanical damage-based model in the finite element method are illustrated in Figure 4-7. The code implementation of the damage-based model can be found in the module <damage_library> in file damage.f90.

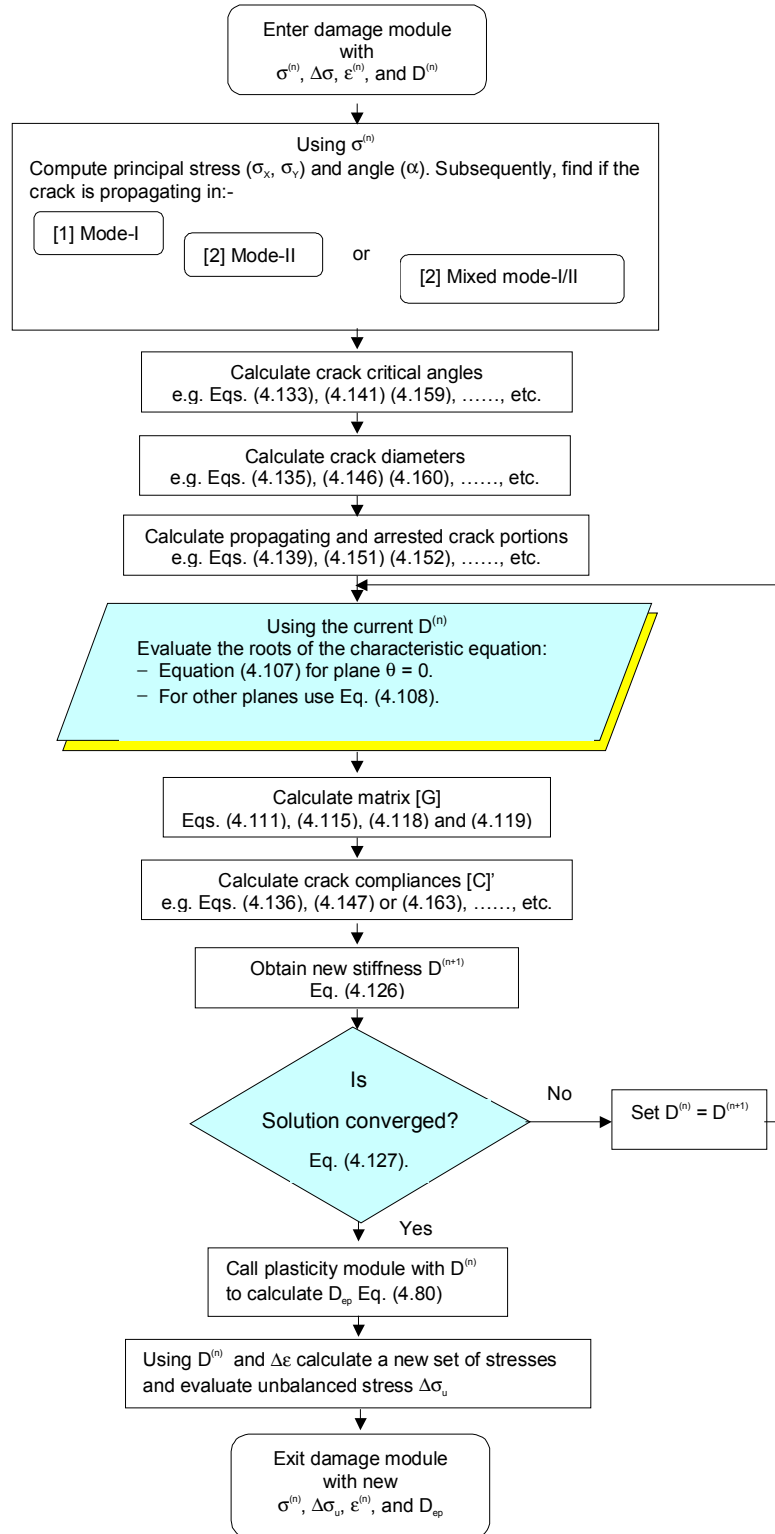


Figure 4-7: Flowchart to implement micro-mechanical damage-based model [27].

5 Structural analysis

Structural mechanics problems are solved with the computer program UMAR by minimising the total potential energy, resulting in the following equation of equilibrium:

$$[K]\{d\} = \{R\} + \{F\}_b + \{F\}_s + \{F\}_{\bar{\epsilon}} + \{F\}_{\bar{\sigma}} \quad (5.1)$$

where $[K]$ is the structural stiffness matrix, $\{d\}$ is the vector of nodal displacements, $\{R\}$ is the vector of applied nodal forces, $\{F\}_b$ is the vector of nodal forces due to body forces, $\{F\}_s$ is the vector of nodal forces due to surface tractions, $\{F\}_{\bar{\epsilon}}$ is the vector of nodal forces due to initial strains, and $\{F\}_{\bar{\sigma}}$ is the vector of nodal forces due to initial stresses. The displacement field $\{\delta\}$ inside an element can be related to the nodal displacements $\{d\}^e$ as:

$$\{\delta\} = [N]\{d\}^e \quad (5.2)$$

where $[N]$ is the shape functions vector (superscript e is used to denote quantities at the element level.) The strains $\{\epsilon\}$ and nodal displacements $\{d\}^e$ are related by the strain-displacement matrix $[B]$ as:

$$\{\epsilon\} = [B]\{d\}^e \quad (5.3)$$

Using the constitutive matrix $[D]$, the element stresses are computed from the element strains as follows:

$$\{\sigma\} = [D](\{\epsilon\} - \{\bar{\epsilon}\}) + \{\bar{\sigma}\} \quad (5.4)$$

where $\{\bar{\epsilon}\}$ is the vector of initial strains and $\{\bar{\sigma}\}$ is the vector of initial stresses.

By using Eqs. 5.2 to 5.4, elements of Eq. 5.1 can now be written in more detail as:

$$[K] = \sum_e [k]^e \quad \text{with} \quad [k]^e = \int [B]^T [D] [B] dV^e \quad (5.5)$$

$$\{F\}_b = \sum_e \int [N]^T \{g\} dV^e \quad (5.6)$$

$$\{F\}_s = \sum_e \int [N]^T \{p\} dS^e \quad (5.7)$$

$$\{F\}_{\bar{\epsilon}} = \sum_e \int [B]^T [D] \{\bar{\epsilon}\} dV^e \quad (5.8)$$

$$\{F\}_{\bar{\sigma}} = \sum_e \int [B]^T \{\bar{\sigma}\} dV^e \quad (5.9)$$

where $\{g\}$ and $\{p\}$ are respectively the vectors of body forces and surface tractions.

5.1 Boundary conditions

Matrix $[K]$ in Eq. 5.1 is singular, and hence its inverse does not exist. This means that no unique solution for $\{d\}$ is possible if the structure is unsupported. The physical significance of this is that the loaded structure is free to undergo unlimited rigid body motion unless some support constraints are imposed to keep the structure in equilibrium under the applied loads. Thus some boundary conditions need to be applied to Eq. 5.1 before solving for the vector of displacements $\{d\}$.

There are two types of boundary conditions: essential and natural. In structural mechanics problems, only the essential boundary conditions need to be specified, i.e., those values of the entries in the displacement vector $\{d\}$ that are known.

5.2 Solution procedure

An incremental-iterative procedure is applied to solve the system of non-linear equations resulting from Eq. 5.1 [26]. This non-linearity can result from either of two sources:

- Material non-linearity, in which the nature of the stress-strain relationship of a particular material is non-linear, making the constitutive matrix $[D]$ a function of the stress level, i.e., $[D] = f(\sigma)$.
- Geometric non-linearity, resulting from ‘large strain’ or ‘large displacement’ analysis.

5.2.1 Material non-linearity

In the case of material non-linearity, since stresses are dependent on the calculated nodal displacements, the stiffness matrix $[K]$ (Eq. 5.5) is also a function of the nodal displacements, making Eq. 5.1 non-linear. Equation 5.1 can be simplified as:

$$[K]\{d\} = \{F\} \quad (5.10)$$

where $\{F\}$ is the total nodal force vector. In order to solve Eq. 5.10, the applied load is divided into a number of increments. For a load increment i , the tangent stiffness evaluated at the end of the preceding load increment, $[K]_{i-1}$, is used to evaluate the incremental displacements of the current increment, i.e.,

$$[K]_{i-1}\{\Delta d\}_i = \{\Delta F\}_i \quad (5.11)$$

where $\{\Delta F\}_i$ is the vector of incremental load corresponding to increment i . Using $\{\Delta d\}_i$, the incremental strains $\{\Delta \epsilon\}_i$ are calculated from Eq. 5.3. The resulting incremental strains are added to the previous total strains to obtain the new total strains. These total strains are then used in conjunction with the available stress-strain relations to obtain the new total stresses. The internal nodal forces corresponding to the total stresses are next evaluated, and then equilibrium is checked between the internal and external forces. If there are any residual forces, these are

reversed in direction and applied as new nodal forces. This procedure is repeated until equilibrium is satisfied within prescribed limits. A flowchart of the just described algorithm is illustrated in Figure 5-1. More details of non-linear finite element analysis are given by [1] and [45]. The code implementation of UMAR can be found in the module <structral_analysis_library> (file structural_analysis.f90).

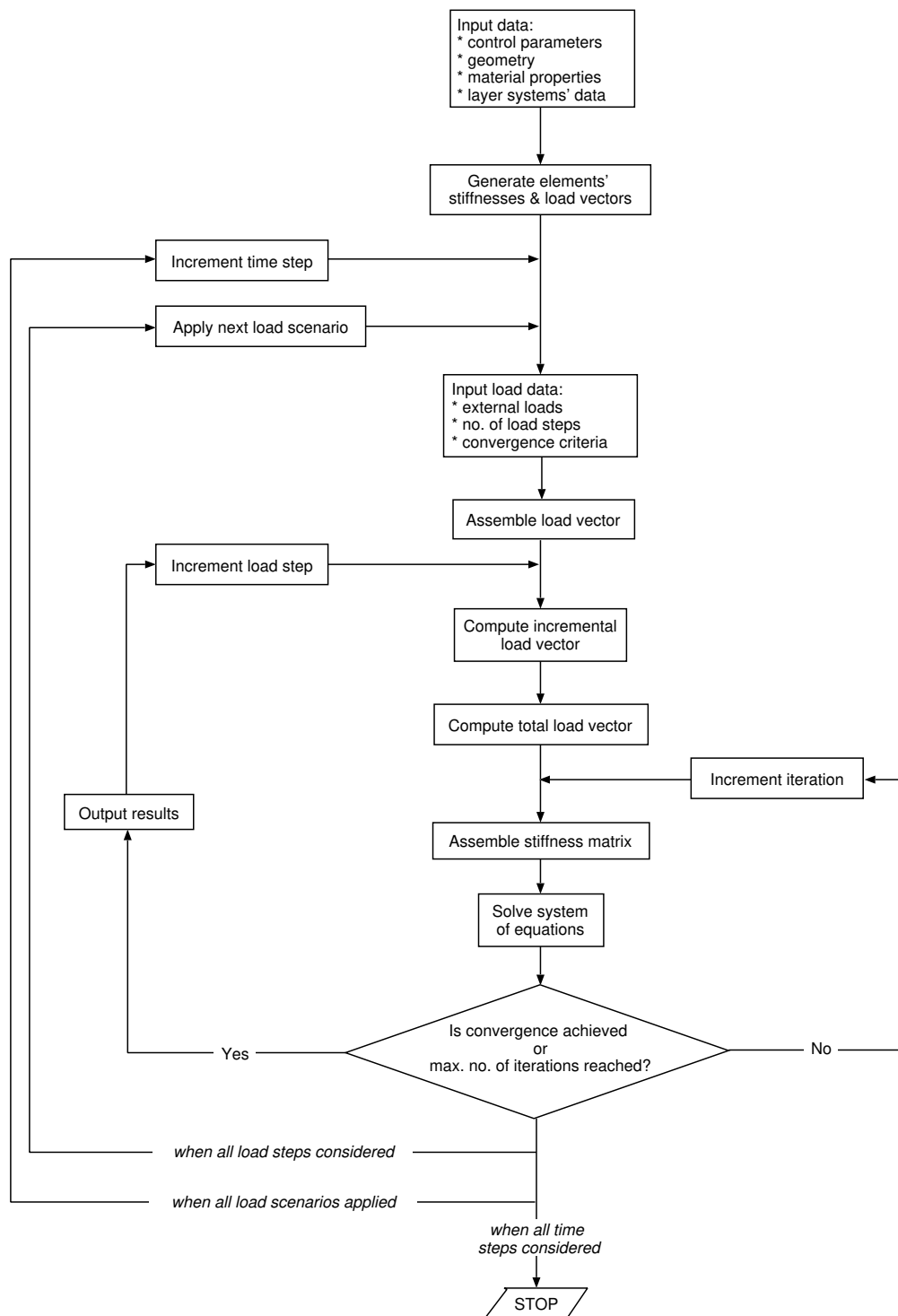


Figure 5-1: Algorithm implemented in UMAR for non-linear analysis.

5.3 Convergence criteria

The efficiency and reliability of the incremental/iterative procedure are dependent on the convergence criteria used in terminating the iteration process when the desired degree of accuracy

is achieved. At the end of each iteration, accuracy of the solution is checked, and if it falls in the specified tolerance limits, the iterations are stopped and the solution procedure is continued with the next load increment. The tolerance limits that are usually set by the user play an important role in achieving the desired accuracy. In the case of a too large convergence tolerance, the iterations are terminated prematurely leading to inaccurate solution. When the convergence tolerance is too severe, the increase in computational effort may not be justified by the gains in the accuracy of the solution. Similarly, an ineffective divergence check may stop the iterations prematurely indicating divergence when in fact the solution is slowly converging. In conclusion, the choice of the convergence criteria may influence the quality of the results significantly. For practical purposes, the user should check the response using different convergence criteria for the same problem in order to get more confidence in the solution accuracy.

There are three convergence criteria used in program UMAR:

1. Displacement norm

$$\frac{\sum_{i=1}^N \Delta d_i^2}{\sum_{i=1}^N d_i^2} \leq \varepsilon \quad (5.12)$$

2. Force norm

$$\frac{\sum_{i=1}^N \Delta F_i^2}{\sum_{i=1}^N F_i^2} \leq \varepsilon \quad (5.13)$$

3. Energy norm

$$\frac{\Delta d \cdot \Delta F}{d \cdot F} \leq \varepsilon \quad (5.14)$$

Convergence is achieved in Eqs. 5.12, 5.13, and 5.14 when the specified norm becomes smaller than the specified tolerance ε .

6 Construction analysis

Equation Section (Next)Program UMAR is capable of simulating a construction process by means of two modules: one simulating the removal of material or structural members from the initial structure, and another simulating restoration or inclusion of new members.

6.1 Removal analysis

When certain number of elements are removed from a structure, the remaining structure needs to experience a degree of stress-relief so that the surface corresponding to the removed material is free from any stresses (see Figure 6-1). To simulate this process, UMAR applies removal forces along this boundary. These forces depend on the state of stress (σ) and the self-weight (γ) of the removed elements, i.e.,

$$F_{\text{removal}} = \int_V B^T \sigma dV + \int_V N^T \gamma dV \quad (6.1)$$

where B is the strain-displacement matrix, σ is the tensor of stresses in the removed elements prior to removal, V is the volume of removed elements, N is the vector of shape functions (dependent on the type of finite element used in the analysis), and γ is the unit weight of the removed material [39].

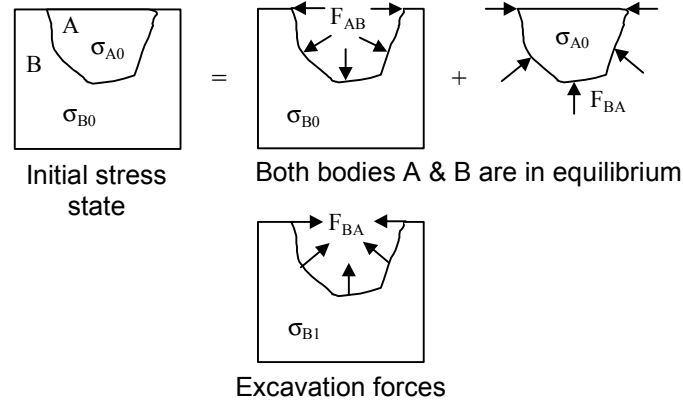


Figure 6-1: Removal forces (adapted from [38]).

The code implementation of the removal analysis in UMAR can be found in the module <removal_analysis_library> (file removal_analysis.f90).

6.2 Restoration analysis

Restoration analysis is currently under development.

7 Transient analysis

Equation Section (Next)Program UMAR is capable of solving problems related to physical phenomena that are described by parabolic partial differential equations.

7.1 Governing equation

The equation governing transient analysis in program UMAR is that of unsteady, three-dimensional diffusive processes, i.e.,

$$\kappa \frac{\partial \phi}{\partial t} + \frac{\partial J_x}{\partial x} + \frac{\partial J_y}{\partial y} + \frac{\partial J_z}{\partial z} = 0 \quad (7.1)$$

where ϕ is the field variable under consideration, κ is a coefficient, t denotes time, and J_x , J_y , and J_z are respectively the diffusive fluxes along the x -, y -, and z -directions. Table 7-1 shows the correspondence between Eq. 7.1 and the different field equations implemented in UMAR.

Table 7-1: Correspondence between Eq. 7.1 and the governing differential equations.

Physical problem	ϕ	κ	J_x	J_y	J_z
Heat transfer	T	ρc_q	$-\lambda_x \frac{\partial T}{\partial x}$	$-\lambda_y \frac{\partial T}{\partial y}$	$-\lambda_z \frac{\partial T}{\partial z}$
Moisture diffusion	h	$\frac{\partial w}{\partial h}$	$-D_{hx} \frac{\partial h}{\partial x}$	$-D_{hy} \frac{\partial h}{\partial y}$	$-D_{hz} \frac{\partial h}{\partial z}$
Chloride diffusion	C	1	$-D_{cx} \frac{\partial C}{\partial x}$	$-D_{cy} \frac{\partial C}{\partial y}$	$-D_{cz} \frac{\partial C}{\partial z}$

In the above table, T denotes temperature, ρ is the density, c_q is the specific heat capacity, λ_x , λ_y , and λ_z are respectively the thermal conductivities in the x -, y -, and z -directions, h is humidity, $\partial w / \partial h$ is the moisture capacity (slope of the equilibrium adsorption isotherm), D_{hx} , D_{hy} , and D_{hz} are respectively the humidity diffusion coefficients in the x -, y -, and z -directions, C is the chloride concentration, and D_{cx} , D_{cy} , and D_{cz} are respectively the chloride diffusion coefficients in the x -, y -, and z -directions.

7.2 Boundary conditions

To obtain a solution for Eq. 7.1, the initial conditions of the problem as well as the conditions existing at the boundaries of the domain need to be defined. Boundary conditions are enforced by specifying either the value of ϕ at the boundary or the flux across it. When fluxes across the boundary are specified, the boundary condition takes the following form:

$$-D \frac{\partial \phi}{\partial n} = L\phi_b - M \quad (7.2)$$

where $\partial\phi/\partial n$ is the normal flux across the boundary surface, ϕ_b represents the value of ϕ at the boundary (unknown quantity), and L and M are two constants. Table 7-2 shows the correspondence between L and M and the different field problems implemented in UMAR. Equation 7.2 assumes the boundary flux going into the body.

Table 7-2: Correspondence between Eq. 7.2 and the imposed boundary conditions.

Physical problem	ϕ_b	L	M
Heat transfer	T	B_T	$B_T \cdot T_{en}$
Moisture diffusion	h	B_h	$B_h \cdot h_{en}$
Chloride diffusion	C	B_c	$B_c \cdot C_{en}$

In the above table, B_T , B_h , and B_c denote the convection heat transfer coefficient, the surface moisture transfer coefficient, and the surface chloride transfer coefficient, respectively, and T_{en} , h_{en} , and C_{en} are respectively the temperature, humidity and chloride concentration of the surrounding environment.

7.3 Finite element formulation

Equation 7.1 is solved numerically in space as a boundary-value problem using the finite element technique and in time as an initial-value problem using a finite-difference scheme. The Galerkin weighted residual method is implemented in UMAR to solve Eq. 7.1, which in expanded form takes the form of:

$$\kappa \frac{\partial \phi}{\partial t} = \frac{\partial}{\partial x} \left(D_x \frac{\partial \phi}{\partial x} \right) + \frac{\partial}{\partial y} \left(D_y \frac{\partial \phi}{\partial y} \right) + \frac{\partial}{\partial z} \left(D_z \frac{\partial \phi}{\partial z} \right) \quad (7.3)$$

Applying the consistent formulation, where both ϕ and $\dot{\phi}$ use the same spatial approximation, the following expression results at the element level:

$$[c^{(e)}] \{\dot{\Phi}^{(e)}\} + [k^{(e)}] \{\Phi^{(e)}\} = \{f^{(e)}\} \quad (7.4)$$

where

$$[c^{(e)}] = \int_V \kappa_1 [N]^T [N] dV \quad \text{capacitance matrix} \quad (7.5)$$

$$[k^{(e)}] = \underbrace{\int_V [B]^T [D] [B] dV}_{[k_1^{(e)}]} + \underbrace{\int_\gamma L [N]^T [N] ds}_{[k_2^{(e)}]} \quad \text{characteristic matrix} \quad (7.6)$$

with

$$[B]^T = \begin{bmatrix} \frac{\partial [N]^T}{\partial x} & \frac{\partial [N]^T}{\partial y} & \frac{\partial [N]^T}{\partial z} \end{bmatrix} \quad (7.7)$$

and

$$\{f^{(e)}\} = \oint_s M[N]^T ds \quad \text{load vector} \quad (7.8)$$

The integrals in Eqs. 7.5, 7.6, and 7.8 are evaluated numerically using Gauss quadrature.

When all the element contributions are added, a system of linear first-order differential equations in the time domain results. By applying a finite-difference approximation, the following expression is obtained:

$$([C] + \theta \Delta t [K])\{\Phi\}^{t+\Delta t} = ([C] - (1 - \theta)\Delta t [K])\{\Phi\}^t + \Delta t((1 - \theta)\{F\}^t + \theta\{F\}^{t+\Delta t}) \quad (7.9)$$

where θ is a weighting factor that ranges from 0 to 1 and Δt is the time step. Equation 7.9 evaluates physical quantities at time $t + \Delta t$, i.e., $\{\Phi\}^{t+\Delta t}$, as a function of quantities at the previous time step, i.e., $\{\Phi\}^t$.

The gradient vector is obtained from:

$$\{g_v\} = \begin{Bmatrix} \frac{\partial \phi}{\partial x} \\ \frac{\partial \phi}{\partial y} \\ \frac{\partial \phi}{\partial z} \end{Bmatrix} = \begin{Bmatrix} \frac{\partial [N]}{\partial x} \\ \frac{\partial [N]}{\partial y} \\ \frac{\partial [N]}{\partial z} \end{Bmatrix} \{\Phi^{(e)}\} = [B]\{\Phi^{(e)}\} \quad (7.10)$$

Since the shape functions are written in terms of natural co-ordinates ξ, η, ζ , matrix $[B]$ must also be written in terms of ξ, η, ζ . Thus,

$$\begin{Bmatrix} \frac{\partial [N]}{\partial x}(\xi, \eta, \zeta) \\ \frac{\partial [N]}{\partial y}(\xi, \eta, \zeta) \\ \frac{\partial [N]}{\partial z}(\xi, \eta, \zeta) \end{Bmatrix} = [J(\xi, \eta, \zeta)]^{-1} \begin{Bmatrix} \frac{\partial [N]}{\partial \xi}(\xi, \eta, \zeta) \\ \frac{\partial [N]}{\partial \eta}(\xi, \eta, \zeta) \\ \frac{\partial [N]}{\partial \zeta}(\xi, \eta, \zeta) \end{Bmatrix} \quad (7.11)$$

where $[J]$ is the Jacobian matrix given by:

$$[J] = \begin{bmatrix} \frac{\partial x}{\partial \xi} & \frac{\partial y}{\partial \xi} & \frac{\partial z}{\partial \xi} \\ \frac{\partial x}{\partial \eta} & \frac{\partial y}{\partial \eta} & \frac{\partial z}{\partial \eta} \\ \frac{\partial x}{\partial \zeta} & \frac{\partial y}{\partial \zeta} & \frac{\partial z}{\partial \zeta} \end{bmatrix} \quad (7.12)$$

The implementation of transient analysis UMAR can be found in the module <transient_analysis_library> (file transient_analysis.f90).

7.4 Transient elements

Since the integrals expressed in Eqs. 7.5, 7.6, and 7.8 only require first-spatial derivatives of the element shape functions, the formulation used in the finite elements can be simplified to that of a linear distribution of the field variable ϕ with respect to x , y , and z . The two elements implemented in UMAR for these types of problems are the bilinear rectangular element and the 8-node brick element. Elements of higher order can be used; however, they add to computational expense and do not provide higher accuracy for problems described by Eq. 7.1 [23].

Transient elements are implemented in the module `<formulate_transient_elements_library>`, which can be found in the file `formulate_transient_elements.f90`.

7.5 Numerical solution

Solutions to Eq. 7.9 obtained for $\theta \geq 0.5$ are known to be unconditionally stable for any time step Δt [4]. In these cases, the choice of time step is based on accuracy and computing efficiency considerations only. The Crank-Nicolson method in which $\theta = 0.5$ is usually preferred in numerical applications since its asymptotic rate of convergence is Δt^2 . However, its implementation is frequently characterised by oscillations around the correct solution. The user should carry a preliminary parametric analysis to determine what values of θ and Δt best suit the particular application at hand [24].

8 Types of solvers

Equation Section (Next) In solving the system of linear algebraic equations that results during the incremental solution of the non-linear problem (Eqs. 5.11 and 7.9), program UMAR can employ several solvers. The type of solver used to solve Eqs. 5.11 and 7.9 is a major factor influencing the computational efficiency of the finite element program. Several options are open to the user of program UMAR ranging from iterative methods such as the Gauss-Seidel technique to the direct Gaussian elimination algorithms. The code implementation of all the solvers that can be used with UMAR can be found in the module <system_of_equations_library> in the file solvers.f90.

8.1 LU decomposition method

The LU decomposition method is a direct solution algorithm based on Gaussian elimination in which the coefficient matrix $[A]$ is decomposed into an upper triangular matrix $[U]$ and a lower triangular matrix $[L]$, i.e.,

$$[A] = [L] \cdot [U] \quad (8.1)$$

By using the decomposition of Eq. 8.1, a system of N linear equations such as

$$[A]\{X\} = ([L] \cdot [U])\{X\} = [L] \cdot ([U]\{X\}) = \{B\} \quad (8.2)$$

can be solved by first solving for the vector $\{Y\}$ such that

$$[L]\{Y\} = \{B\} \quad (8.3)$$

and then solving

$$[U]\{X\} = \{Y\} \quad (8.4)$$

The advantage of using the LU method is that the solution of a triangular set of equations is straight forward. Equation 8.3 can be solved by forward substitution as follows:

$$y_i = \frac{1}{l_{ii}} \left[b_i - \sum_{j=1}^{i-1} l_{ij} y_j \right] \quad i = 2, 3, \dots, N \quad (8.5)$$

while Eq. 8.4 can then be solved by back substitution as:

$$x_i = \frac{1}{u_{ii}} \left[y_i - \sum_{j=i+1}^N u_{ij} x_j \right] \quad i = N-1, N-2, \dots, 1 \quad (8.6)$$

More details on how to perform LU decomposition can be found in [31].

8.2 Frontal solver

The frontal equation solution technique, originated by Irons [17], is a direct solution algorithm. It can be considered a particular technique for first assembling finite element characteristic matrices

and nodal forces into a global characteristic matrix and load vector, and then solving for the unknowns by means of Gaussian elimination and back substitution process. It is designed to minimise core storage requirements and the number of arithmetic operations. Among all the direct algorithms, the frontal solution technique results in the most efficient from a computational point of view for large problems.

The main idea of the frontal solver solution is to assemble the equations and eliminate the variables at the same time. As soon as the coefficients of an equation are completely assembled from the contributions of all relevant elements, the corresponding variable is eliminated. Therefore, the complete characteristic matrix is never formed as such, since after elimination the reduced equation is immediately transferred to back-up disc storage.

The core contains, at any given instant, the upper triangular part of a square symmetric matrix containing the equations which are being formed at that particular time. These equations, their corresponding nodes and degrees of freedom are termed the *front*. The number of unknowns in the front is the *frontwidth*; this length generally changes continually during the assembly/reduction process. There is not an upper limit for the frontwidth in UMAR, and the program automatically calculates the maximum possible frontwidth for the problem at hand. The equations, nodes, and degrees of freedom belonging to the front are termed *active*; those which are yet to be considered are *inactive*; and those which have passed through the front and have been eliminated are said to be *deactivated*.

During the assembly/elimination process the elements are considered each in turn according to a prescribed order. Thus, the element numbering adopted is critical for the efficiency of the frontal solution technique. Whenever a new element is called in, its characteristic coefficients are read from a file and summed either into existing equations, if the degrees of freedom are already active, or into new equations which have to be included in the front if the degrees of freedom are being activated for the first time. If some degrees of freedom are appearing for the last time, the corresponding equations can be eliminated, stored away in a file, and deactivated. In doing so, they free space in the front, which can then be employed during assembly of the next element. Further details of this method can be found in [14].

8.3 Gauss-Seidel method

The Gauss-Seidel method is an iterative solution algorithm. Iterative methods start with an assumed solution and iterate to the desired solution of the system of equations within a specified convergence criterion. These methods are best suited for the solution of large systems of equations, and they are more computationally efficient than direct methods for these large systems.

Given a set of N linear equations such as $[A]\{X\}=\{B\}$, the Gauss-Seidel method computes the $(l+1)^{\text{th}}$ iteration for x_i as:

$$x_i^{(l+1)} = \frac{b_i - \sum_{j=1}^{i-1} a_{ij}x_j^{(l+1)} - \sum_{j=i+1}^N a_{ij}x_j^{(l)}}{a_{ii}} \quad \text{for } i=1, 2, \dots, N \quad (8.7)$$

According to Eq. 8.7, each iterative computation of the unknown employs the most recent values of the other unknowns, replacing the values from the previous iteration by new ones and thus requiring only one computer storage space for each unknown. The iterative computation of the unknowns is terminated when a specified convergence criterion is satisfied. In UMAR, convergence is assumed to have been achieved if the change in the value of each unknown from one iteration to the next is less than 10^{-12} , i.e.,

$$\left| x_i^{(l+1)} - x_i^{(l)} \right| \leq 10^{-12} \quad \text{for } i=1, 2, \dots, N \quad (8.8)$$

or if 500 iterations or more have taken place. The Gauss-Seidel method has good convergence characteristics for diagonally dominant systems, that is, for systems in which each diagonal element a_{ii} is larger in absolute value than the sum of the magnitudes of the other elements in the

row (i.e., $|a_{ii}| > \sum_{j=1, j \neq i}^N |a_{ij}|$.)

8.4 Domain decomposition method

The domain decomposition method consists of partitioning the initial problem domain into sub-domains, which can be partially assembled and solved before the entire system. Thus, the domain decomposition method involves solving the initial problem on each sub-domain, solving the problem at the interfaces of the sub-domains, and back-substituting the solution on the sub-domains. For each sub-domain, the unknown variables are divided into internal degrees of freedom (d.o.f.), designated by the subscript i , and interface d.o.f., designated by the subscript b , as illustrated in Figure 8-1. The division of the initial domain into sub-domains can be used to reduce the global system of equations to a much smaller system of equations involving only the interface d.o.f.

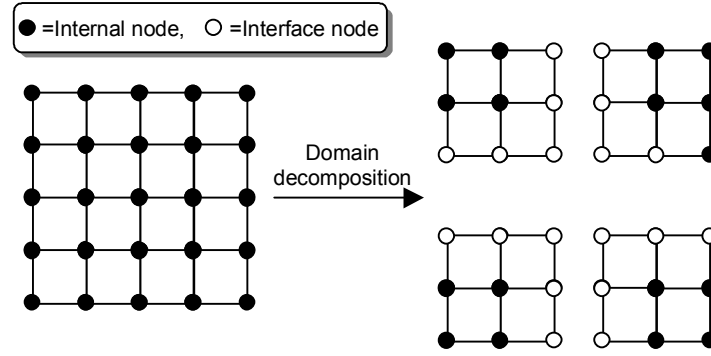


Figure 8-1: Finite element mesh partitioned into sub-domains.

The algorithm for the domain decomposition method is as follows:

Divide the initial finite element mesh into sub-domains

1. Evaluate $[k]$ and $\{f\}$ for each sub-domain, where $[k]$ and $\{f\}$ refer to all d.o.f. of the sub-domain, and the vector of d.o.f. $\{d\}$ is partitioned into $\{d\} = [d_b \ d_i]^T$, $\{d_b\}$ being the interface d.o.f. of the sub-domain and $\{d_i\}$ being the internal d.o.f.

$$[k]\{d\} = \{f\} \Rightarrow \begin{bmatrix} k_{bb} & k_{bi} \\ k_{ib} & k_{ii} \end{bmatrix} \begin{Bmatrix} d_b \\ d_i \end{Bmatrix} = \begin{Bmatrix} f_b \\ f_i \end{Bmatrix} \quad (8.9)$$

2. Eliminate internal d.o.f. by condensation, by solving the lower partition of Eq. 8.9:

$$\{d_i\} = -[k_{ii}]^{-1} ([k_{ib}]\{d_b\} - \{f_i\}) \quad (8.10)$$

and by substituting Eq. 8.10 into the upper partition of Eq. 8.9:

$$\underbrace{\left([k_{bb}] - [k_{bi}][k_{ii}]^{-1}[k_{ib}] \right)}_{\text{condensed } [k]} \{d_b\} = \underbrace{\left(\{f_b\} - [k_{bi}][k_{ii}]^{-1}\{f_i\} \right)}_{\text{condensed } \{f\}} \quad (8.11)$$

The condensed $[k]$ and $\{f\}$ pertain only to the interface d.o.f. $\{d_b\}$.

3. Assemble the sub-domains by connecting the interface nodes, i.e., those nodes shared by the sub-domains. The resulting system of equations is $[K]\{d\} = \{F\}$, in which $\{d\}$ contains all the interface d.o.f. of all the sub-domains.
4. Solve for $\{d\}$.
5. For each sub-domain, extract from $\{d\}$ the interface d.o.f. $\{d_b\}$ of that sub-domain. Use Eq. 8.10 to compute the internal d.o.f. $\{d_i\}$.

8.5 Biconjugate gradient method

Given a set of N linear equations such as $[A]\{X\}=\{B\}$, the biconjugate gradient approach, an iterative method, computes the $(l+1)^{\text{th}}$ iteration for x_i as:

$$x_i^{(l+1)} = x_i^{(l)} + \alpha^{(l)} p_i^{(l)} \quad (8.12)$$

The biconjugate gradient method constructs four sequences of vectors: $\{r\}^{(l)}$, $\{\bar{r}\}^{(l)}$, $\{p\}^{(l)}$, and $\{\bar{p}\}^{(l)}$, where r_i denotes the residual $b_i - a_{ij}x_j$ and l is the iteration number. Vectors These vectors satisfy respectively the *biorthogonality* and *biconjugacy* conditions, i.e.,

$$\{\bar{r}\}^{(i)} \cdot \{r\}^{(j)} = \{r\}^{(i)} \cdot \{\bar{r}\}^{(j)} = 0, \quad j < i \quad (8.13)$$

$$\{\bar{p}\}^{(i)} \cdot [A] \cdot \{p\}^{(j)} = \{p\}^{(i)} \cdot [A]^T \cdot \{\bar{p}\}^{(j)} = 0, \quad j < i \quad (8.14)$$

and they are also mutually orthogonal:

$$\{\bar{r}\}^{(i)} \cdot \{p\}^{(j)} = \{r\}^{(i)} \cdot \{\bar{p}\}^{(j)} = 0, \quad j < i \quad (8.15)$$

By specifying the initial residual vector $\{r\}^{(1)}$ and setting $\{\bar{r}\}^{(1)} = \{r\}^{(1)}$, $\{p\}^{(1)} = \{r\}^{(1)}$, $\{\bar{p}\}^{(1)} = \{\bar{r}\}^{(1)}$, the following recurrence is carried out [31]:

$$\begin{aligned} \alpha^{(l)} &= \frac{\{\bar{r}\}^{(l)} \cdot \{r\}^{(l)}}{\{\bar{p}\}^{(l)} \cdot [A] \cdot \{p\}^{(l)}} \\ \{r\}^{(l+1)} &= \{r\}^{(l)} - \alpha^{(l)} [A] \cdot \{p\}^{(l)} \\ \{\bar{r}\}^{(l+1)} &= \{\bar{r}\}^{(l)} - \alpha^{(l)} [A]^T \cdot \{\bar{p}\}^{(l)} \\ \beta^{(l)} &= \frac{\{\bar{r}\}^{(l+1)} \cdot \{r\}^{(l+1)}}{\{\bar{r}\}^{(l)} \cdot \{r\}^{(l)}} \\ \{p\}^{(l+1)} &= \{r\}^{(l+1)} + \beta^{(l)} \{p\}^{(l)} \\ \{\bar{p}\}^{(l+1)} &= \{\bar{r}\}^{(l+1)} + \beta^{(l)} \{\bar{p}\}^{(l)} \end{aligned} \quad (8.16)$$

As long as the recurrence in Eq. 8.16 does not break down because one of the denominators is zero, it terminates after $m \leq N$ iterations, with $\{r\}^{(m+1)} = \{\bar{r}\}^{(m+1)} = 0$. To use the algorithm of Eq. 8.16, an initial guess for $\{x\}^{(1)}$ needs to be made to calculate the residual $\{r\}^{(1)}$. Since $\{r\}^{(m+1)} = 0$, $\{x\}^{(m+1)}$ is the solution to the system of equations $[A]\{X\}=\{B\}$.

The rate of convergence of this algorithm can be increased by *preconditioning* the system of equations $[A]\{X\}=\{B\}$, i.e.,

$$[\tilde{A}]^{-1}[A]\{X\}=[\tilde{A}]^{-1}\{B\} \quad (8.17)$$

where $[\tilde{A}]$ is the *preconditioner* and is selected so that $[\tilde{A}]^{-1} \cdot [A] \approx 1$. This scheme is known as the preconditioned biconjugate gradient method or PBCG, and it requires an additional set of vectors $\{z\}^{(l)}$ and $\{\bar{z}\}^{(l)}$ defined as:

$$[\tilde{A}] \cdot \{z\}^{(l)} = \{r\}^{(l)} \quad \text{and} \quad [\tilde{A}]^T \cdot \{\bar{z}\}^{(l)} = \{\bar{r}\}^{(l)} \quad (8.18)$$

The recurrence in Eq. 8.16 is therefore modified by [31]:

$$\begin{aligned} \alpha^{(l)} &= \frac{\{\bar{r}\}^{(l)} \cdot \{z\}^{(l)}}{\{\bar{p}\}^{(l)} \cdot [A] \cdot \{p\}^{(l)}} \\ \beta^{(l)} &= \frac{\{\bar{r}\}^{(l+1)} \cdot \{z\}^{(l+1)}}{\{\bar{r}\}^{(l)} \cdot \{z\}^{(l)}} \\ \{p\}^{(l+1)} &= \{z\}^{(l+1)} + \beta^{(l)} \{p\}^{(l)} \\ \{\bar{p}\}^{(l+1)} &= \{\bar{z}\}^{(l+1)} + \beta^{(l)} \{\bar{p}\}^{(l)} \end{aligned} \quad (8.19)$$

8.5.1 Convergence criteria

The algorithm outlined by Eqs. 8.16 and 8.19 is iterative in nature, and it is stopped when some appropriate error criterion is met. UMAR provides four options to test for convergence of the biconjugate gradient algorithm. These convergence criteria are application dependent, and the user should test all of them to find out which one suits best the problem at hand. The convergence criteria implemented are:

1. Test 1

$$\frac{|[A] \cdot \{X\} - \{B\}|}{|\{B\}|} < \varepsilon \quad (8.20)$$

where ε is the specified tolerance.

2. Test 2

$$\frac{|[\tilde{A}]^{-1} \cdot ([A] \cdot \{X\} - \{B\})|}{|[\tilde{A}]^{-1} \cdot \{B\}|} < \varepsilon \quad (8.21)$$

3. Test 3 uses the L_2 norm.
4. Test 4 uses the L_∞ norm.

9 References

- [1] Ashby, M. F., (1979) "Micromechanisms of fracture in static and cyclic failure," In *Fracture Mechanics, current status, future, prospects*, Smith, R. A., (Eds.) Pergamon, Oxford, 1, 1-27.
- [2] Bathe, R.J. (1982) *Finite Element Procedures in Engineering Analysis*, Prentice-Hall, New Jersey.
- [3] Cormeau, I. (1975) "Numerical stability in quasistatic elasto-visco-plasticity," *Int. J. Num. Meth. Engng.*, **9**, 109-127.
- [4] Cook, R.D., Malkus, D.S., and Plesha, M.E. (1989) *Concepts and Applications of Finite Element Analysis*, John Wiley & Sons, 630 pp.
- [5] Darwin, D., and Pecknold, D.A. (1977) "Non-linear biaxial stress-strain law for concrete," *Journal of the Engineering Mechanics Division*, **103**(2), 229-241.
- [6] Elwi, A.A., and Murray, D.W. (1979) "A 3D hypoelastic concrete constitutive relationship," *Journal of the Engineering Mechanics Division*, **105**(4), 623-641.
- [7] Eshelby, J.D. (1957) "The determination of the elastic field on an ellipsoidal inclusion, and related problems," *Proc. Roy. Soc. London*, **A241**, 376-396.
- [8] Fenalla, D., (1986) *A micromechanical continuous damage model for plain concrete*, Ph. D. thesis, University of Illinois at Chicago, Chicago.
- [9] Fenalla, D. (1990) "Fracture and failure of concrete in uniaxial and biaxial loading," *J. Engrg. Mech.*, ASCE, **116**(11), 2341-2362.
- [10] Fernando, V. M., (1987) *A continuum damage theory for cyclic loading of concrete*, Ph. D. thesis, University of Miami, Coral Gables.
- [11] Ghoneim, G.A.M (1978) *Nonlinear Analysis of Concrete Structures*, Ph.D. Thesis, Department of Civil Engineering, University of Calgary, Calgary, Canada.
- [12] Harichandran, R.S., Yeh, M.S., and Baladi, G. (1990) "MICH-PAVE: A nonlinear finite element program for analysis of flexible pavements," *Transportation Research Record*, **1286**, 123-131.
- [13] Hershey, A.V. (1954) The elasticity of an isotropic aggregate of anisotropic cubic crystals, *J. Appl. Mech.*, ASME, **21**(2), 236-241.
- [14] Hinton, E., and Owen, D. (1977) *Finite Element Programming*. Academic Press, 305 pp.
- [15] Horii, H., and Nemat-Nasser, S. (1983) "Overall moduli of solids with microcracks: load induced anisotropy," *J. of Mech. of Phys. and solids*, **31**(2), 155-171.

- [16] Horii, H., and Nemat-Nasser, S. (1985) "Compression induced growth in brittle solids: Axial splitting and shear faulting," *J. Geophys. Res.*, **90**(10), 3105-3121.
- [17] Irons, B.M. (1970) "A frontal solution program for finite element analysis," *International Journal for Numerical Methods in Engineering*, **2**, 5-32.
- [18] Ju, J. W., (1991) "On two-dimensional self-consistent micromechanical damage models for brittle solids," *Int. J. of Solids and Struct.*, **27**(2), 227-258.
- [19] Khogali, W.E.I. (1995) *Assessing Seasonal Variations in Cohesive Subgrade Soils*, Ph.D. Thesis, University of Alberta, Edmonton, Canada, 474 pp.
- [20] Kunin, I.A. (1983) "Elastic media with microstructure II, three dimensional models," Springer series in *Solid-State Sciences*, **44**, Springer, Berlin.
- [21] Kupfer H.B., and Gerstle, K.H. (1973) "Behavior of concrete under biaxial stresses," *Journal of the Engineering Mechanics Division*, **99**(4), 853-866.
- [22] Lekhnitskii, S.G. (1963) *Theory of Elasticity of An Anisotropic Elastic Body*, Holden-Day, San Francisco.
- [23] Martín-Pérez, Beatriz (1999) *Service Life Modelling of R.C. Highway Structures Exposed to Chlorides*, Ph.D. Thesis, University of Toronto, Toronto, Canada, 168 pp.
- [24] Martín-Pérez, B., Pantazopoulou, S.J., and Thomas, M.D.A.. (2001) "Numerical solution of mass transport equations in concrete structures," *Computers & Structures*, **79**(13), 1251-1264.
- [25] Melan, E. (1938) *Ing. Arch.*, **9**(116).
- [26] Muskhelishvili, N.I. (1953) *Some Basic Problems of the Theory of Elasticity*, Noordhoff, Groningen (translated from Russian by J.R.M. Radok.)
- [27] Nofal, Mostafa (1988) *Inelastic Load Distribution of Slab-on-Steel Girder Bridges: An Analytical and Experimental Study*, M.Eng. Thesis, Carleton University, Ottawa, Canada.
- [28] Nofal, Mostafa (1997) *Continuum Damage Mechanics for Plain, Fibre-Reinforced, and Reinforced Concrete Materials and Structures*, Ph.D. Thesis, Carleton University, Ottawa, Canada.
- [29] Owen, D.R.J., and Hinton, E. (1980) *Finite Elements in Plasticity: Theory and Practice*, Pineridge Press Ltd., Swansea, U.K., 594 pp.
- [30] Pezo, R.F. (1993) "A general method of reporting resilient modulus tests of soils – a pavement engineer's point of view," in 72nd Annual Meeting of the Transportation Research Board, National Research Council, Washington, D.C.

- [31] Press, W.H., Teukolsky, S.A., Vetterling, W.T, and Flannery, B.P. (1992) *Numerical Recipes in Fortran 77: The Art of Scientific Computing*, 2nd ed., Cambridge University Press.
- [32] Razaqpur, A.G., and Nofal, M.E. (1987) "Performance of a new quadrilateral finite element with rotational degrees of freedom," *Proceedings of the 5th World Congress*, J. Robinson (ed.), 121-130.
- [33] Saenz, L.P. (1964) Discussion of "Equation for the stress-strain curve of concrete," by Desayi and Krishnan, *ACI Journal*, **61**(9), 1229-1235.
- [34] Shayanfar, M.A. (1995) *Nonlinear Finite Element Analysis of Normal and High Strength Concrete Structures*, Ph.D. Thesis, Department of Civil Engineering and Applied Mechanics, McGill University, Montreal.
- [35] Sih, G. C., Paris, P. C., Irwin, G. R. (1965) "On cracks in rectilinearly anisotropic bodies," *International J. Fract. Mech.*, **1**(2), 189-203.
- [36] Slate, F.O. (1983) Microscopic observation of cracks in concrete with emphasis on techniques developed and used at Cornell University, *Fracture Mechanics of Concrete*, Wittmann, H. (ed.), Elsevier Applied Science, Amsterdam.
- [37] Smith, G.H., and Young, L.E. (1955) "Ultimate theory in flexure by exponential function," *ACI Journal*, **52**(3).
- [38] Smith, I.M., and Griffiths, D.V. (1998) *Programming the Finite Element Method*, 3rd ed., John Wiley & Sons, 534 pp.
- [39] Smith, I.M., and Ho, D.K.H. (1992) "Influence of construction technique on the performance of a braced excavation in marine clay," *International Journal for Numerical and Analytical Methods in Geomechanics*, **16**, 845-867.
- [40] Uzan, J. (1985) "Characterization of granular materials," *Transportation Research Record*, **1022**, 52-59.
- [41] Vasilescu, A. (2000) *Analysis of Geometrically Nonlinear and Softening Response of Thin Structures by A New Facet Shell Element*, M.Eng. Thesis, Dept. of Civil Engineering, Carleton University, Ottawa, Canada.
- [42] Viggiani, G., and Tamagnini, C. (2000) "Ground movements around excavations in granular soils: a few remarks on the influence of the constitutive assumptions on FE predictions," *Mechanics of Cohesive-Frictional Materials*, **5**, 399-423.
- [43] Wu, C.H. (1985) "Tension-compression test of a concrete specimen via damage theory," in *Damage Mechanics and Continuum Modeling*, ASCE, New York.

- [44] Yam, L.C.P., and Chapman, J.C. (1968) “The inelastic behavior of simply supported composite beams of steel and concrete,” *Proceeding of Civil Engineer*, 651-683.
- [45] Zaitsev Y., (1983). Crack propagation in a composite material. In *Fracture Mechanics of Concrete*, Wittmann, H., (Eds.) Elsevier Applied Science, Amsterdam.
- [46] Zienkiewicz, O.C. (1976) *The Finite Element Method*, 3rd edition, McGraw-Hill Book Co., Bewrkshire.
- [47] Zienkiewicz, O.C., and Chung, Y.K. (1964) “The finite element method for analysis of elastic and orthotropic slabs,” *Proceedings of Institution of Civil Engineers*, **28**, 471-488.

Appendix A: Using the program

A.1 Entering required input

The program reads the required input data from an existing input file. This file is in ASCII format and can be readily modified by any text editor. The program prompts for the name of the file and automatically appends the extension '.inp'. As long as consistency is maintained, units employed can be in either the S.I. or the Imperial systems, i.e., N/mm and lb/in, respectively. For convenience, the data contained in the input file is divided into different records. A record can contain one single line or may have several lines. The following is a description of the different records found in the input file.

Heading information, as required in Table A-1, is enclosed by commands:

***HEADINGS ... *END HEADINGS**

Table A-1: Heading information.

Record No.	Input data
*HEADINGS	
1	Title of the problem (up to a maximum of 128 characters can be entered)
*END HEADINGS	

Control data, as required in Table A-2, is enclosed by commands:

***CONTROL DATA ... *END CONTROL DATA**

Table A-2: Control data (refer to Table A-3.)

Record No.	Input data
*CONTROL DATA	
2	Units system
3	Type of solver to be used
4	Gravity direction (=1 for <i>x</i> -direction, 2 for <i>y</i> -direction, and 3 for <i>z</i> -direction)
5	Type of structural construction, type of structural analysis indicator, large deformation analysis indicator, creep analysis indicator, shrinkage analysis indicator, hygroscopic analysis indicator, thermal analysis indicator, chloride analysis indicator
*END CONTROL DATA	

Table A-3: Input indicators for control data.

Indicators	0	1	2	3	4	5	6
System of units	---	S.I. system	Imperial system	---	---	---	---
Type of solver	---	LU for banded matrices	LU for full matrices	Frontal	Iterative Gauss-Seidel	Sky Line decomposition	Domain decomposition with LU for full matrices
Construction analysis	New construction	Segmental construction	Removal only	Addition only	Removal & addition	---	---
Structural analysis	Not required	Static analysis	Dynamic analysis	---	---	---	---
Large deformation analysis	Not required	Required	---	---	---	---	---
Creep analysis	Not required	Required	---	---	---	---	---
Shrinkage analysis	Not required	Required	---	---	---	---	---
Hygroscopic analysis	Not required	Stress analysis for user defined hygroscopic load	Hygroscopic analysis only	Uncoupled hygroscopic -stress analysis	Coupled hygroscopic -stress analysis	---	---
Thermal analysis	Not required	Stress analysis for user defined thermal load	Thermal analysis only	Uncoupled thermal-stress analysis	Coupled thermal-stress analysis	---	---
Chloride analysis	Not required	Required [†]	---	---	---	---	---

[†] For chloride analysis, it is required to run both hygroscopic and thermal analysis.

Data specifying the output options, as required in Table A-4, is enclosed by commands:

***OUTPUT OPTIONS ... *END OUTPUT OPTIONS**

Table A-4: User output options.

Record No.	Input data
*OUTPUT OPTIONS	
6	Time step interval, load repetition interval, load scenario interval, and load step interval at which output is required
7	Scaling factor to output deflections
*END OUTPUT OPTIONS	

Nodal data, as required in Table A-5, is enclosed by commands:

***NODES ... *END NODES**

Table A-5: Nodal point data.

Record No.	Input data
*NODES	
8	Number of total nodes, problem dimension
9	Node number, indicator of whether node generation is required or not [†] , x-, y-, and z-coordinate of the node (depending on the problem dimension)
*END NODES	

[†] For node generation, enter either 0 if not required, or *number* if required, “*number*” being indicative of the increment in node number when generating nodes.

Material data, as required in Table A-6, is enclosed by commands:

***MATERIALS ... END MATERIALS**

Table A-6: Material data.

Record No.	Input data
*MATERIALS	
<i>For each material type:</i>	
10	Material name (up to a maximum of 40 characters can be entered)
11	Number of constituents of the composite material (1 for one-phase materials)
Physical properties	
For one-phase materials or the matrix of multi-phase materials:	
12	Material type (=1 for asphalt-based material, 2 for cementitious-based material, 3 for metallic-based material, 4 for wood-based material, 5 for ceramic-based material, 6 for rubber-based material, 7 for rock-based material, 8 for clay and silt material, 9 for granular material), degree of homogeneity (=0 for homogeneous, 1 for heterogeneous), degree of anisotropy
13	Density ρ , coefficient of friction μ , cohesion c , angle of internal friction ϕ (in degrees)
14	Volume fraction v_f (=1 for one-phase materials), crystals shape (=1 for cubic crystals, 2 for hexagonal crystals, 3 for rod or needle-shaped crystals), aspect ratio of crystals
15	If thermal analysis needed, coefficient of thermal expansion
16	If hygroscopic analysis needed, coefficient of thermal expansion
If hygroscopic analysis needed and cementitious-based material:	
17	Input parameters option (=1 for user defined values, 2 for default values)
18	If user defined values, curing, age at loading, slump, cement content, water cement ratio, fine aggregate ratio, air ratio, volume surface ratio, maximum aggregate size, shrinkage strain
19	If soil-based material, moisture content (%)
For multi-phase materials:	
20	Number of embedded inclusions
21	For each inclusion, input records 12 to 19
Thermal properties (if thermal analysis required)	
For each degree of isotropy:	
22	Thermal conductivity, heat capacity
23	Convection transfer coefficient
Hygroscopic properties (if hygroscopic analysis required)	
For each degree of isotropy:	
24	Diffusivity
25	Surface transfer coefficient

Mechanical properties (if stress analysis required)	
26	Mechanical properties input option (=0 read in user defined values, 1 employ program database empirical equations), mechanical model (=1 for theory of elasticity, 2 for theory of plasticity, 3 for theory of continuum damage mechanics, 4 for theory of coupled elastic damage-based plasticity, 5 for theory of fracture mechanics, 6 for theory of coupled Mr-based plasticity)
27	Constitutive model to be used (refer to numbers in bold in Table A-7)
28	For plastic materials, yield criterion, hardening function to be used, and flow rule (refer to numbers in bold in Table A-8)
29	For micro-mechanics-based models, fracture mechanics model to be used (according to Table A-7)
For one-phase materials or the matrix of multi-phase materials:	
For each degree of anisotropy	30 Tensile and compressive properties data indicator (=1 for similar tensile and compressive properties, 2 for distinct tensile and compressive properties)
	31 Young's modulus E , Poisson's ratio ν , shear modulus G (this latter value is only entered if the degree of anisotropy > 1). If the tensile and compressive properties data indicator is 2, then the two values of E , ν , and G corresponding to tension and compression, respectively, have to be entered. For 2-D problems, only plane-stress conditions are implemented in the program. For linear elastic materials, plane-stress can be related to plane-strain through the elastic parameters. By denoting the elastic constants corresponding to plane stress and plane strain as E, ν and $\bar{E}, \bar{\nu}$, respectively, plane strain values can be obtained from: $\bar{\nu} = \frac{\nu}{1 + \nu}, \quad \bar{E} = E \cdot (1 - \bar{\nu}^2)$ To simulate plane-strain conditions, the user needs then to modify Young's modulus and Poisson's ratio according to the above expression.
	For the resilient modulus constitutive model:
	32 Model to be used (refer to Eqs. 4.42 to 4.45)
	33 Resilient modulus coefficients
	For plastic materials:
	34 Yield stress σ_y . For the Mohr-Coulomb and Drucker-Prager yield criteria, the equivalent yield stress is given by Table A-9
	35 For isotropic hardening: strain hardening modulus E^*
	For mixed hardening: isotropic hardening parameters (a_I, b_I) and kinematic hardening parameters (a_K, b_K)
	For visco-plastic materials:
	36 Viscosity
	37 Flow type indicator
	38 Flow type coefficient (if any)
	39 Effective strain factor
	40 Initial time step
	41 Time step factor
	42 Weighting factor
	For micro-mechanics based or fracture mechanics models:
	43 Fracture toughness mode I K_I , fracture toughness mode II K_{II} , fracture toughness mode III K_{III}
	44 If the material is heterogeneous, enter: interface fracture toughness mode I K^{if}_I , interface fracture toughness mode II K^{if}_{II} , interface fracture toughness mode III K^{if}_{III}
	45 Stress-strain curve option (=0 use program database linear model, 1 use program database non-linear models, 2 use actual values obtained from experiments, 3 user defined equations to describe ascending and descending branches)
	46 For the stress-strain curve options 2 and 3, enter: number of points on the stress-strain curve
	47 Stresses σ on stress-strain curve
	48 Strains ε on stress-strain curve
	Repeat records 47 and 48 if the tensile properties differ from the compressive ones.

For multi-phase materials, input records 26 to 48 for each of the inclusions.	
For micro-mechanics based models:	
49	Minimum crack diameter $2a_o$, maximum crack diameter D_{max} , crack probability function (=1 for homogeneous distribution, 2 for triangular distribution)
50	Initial damage ω_o , final damage ω_f
*END MATERIALS	

Table A-7: Constitutive models implemented in program UMAR.

Constitutive models	1	2	3	4	5
Elasticity	Linear elasticity	Non-linear hyper-elasticity	Non-linear hypo-elasticity	Compression field theory	Resilient modulus (soils)
Plasticity	Plasticity	Visco-plasticity	---	---	---
Continuum damage mechanics	Phenomenological models	Micro-mechanics-based models	---	---	---
Fracture mechanics	Linear fracture mechanics	Non-linear fracture mechanics	---	---	---

Table A-8: Yield criteria and hardening functions implemented in program UMAR.

	Yield criteria	Hardening functions	Flow rule
1	Isotropic Tresca	Isotropic hardening	Associated
2	Isotropic Von-Mises	Linear kinematic hardening	Non-associated
3	Isotropic Mohr-Coulomb	Mixed hardening	---
4	Isotropic Drucker-Prager	Non-linear kinematic hardening	---
5-9	Anisotropic $F_{ij} \cdot s_i \cdot s_j = 1$	---	---
10-14	Anisotropic $F_i \cdot s_i + F_{ij} \cdot s_i \cdot s_j = 1$	---	---
15	Anisotropic $F_i \cdot s_i + \sqrt{F_{ij} \cdot s_i \cdot s_j} = 1$	---	---

Table A-9: Equivalent yield stress.

Yield criteria	σ_y
Mohr-Coulomb	$c \cos \phi$
Drucker-Prager	$\frac{6c \cos \phi}{\sqrt{3}(3 - \sin \phi)}$

c and ϕ are the cohesion and the angle of internal friction of the material, respectively. It is assumed in the above that the Drucker-Prager yield surface coincides with the outer apices of the Mohr-Coulomb yield surface.

Layering systems data (Table A-10), if required, is enclosed by commands:

***LAYERS ... *END LAYERS**

Table A-10: Layering systems data.

Record No.	Input data
*LAYERS	
For each layer system:	
51	Number of layers
52	z-co-ordinates
53	Material number
54	Orientation
*END LAYERS	

Cross-section data (Table A-11), if required, is enclosed by commands:

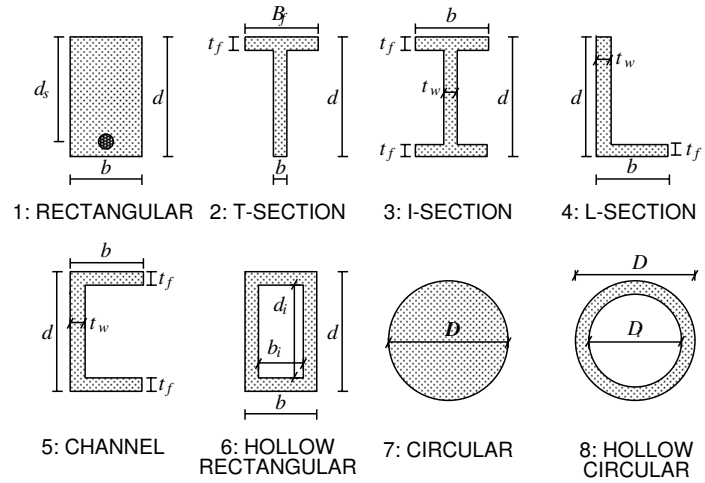
***SECTIONS ... *END SECTIONS**

Table A-11: Cross-section data (refer to Table A-12.)

Record No.	Input data
*SECTIONS	
For each cross-section system:	
55	Cross section shape, material number, number of reinforced materials, section orientation with respect to the x -axis
56	For shapes 1-6: b, d For shapes 7-8: D
57	For shape 2: B_f, t_f For shapes 3-5: t_f, t_w For shape 6: b_i, d_l For shape 8: D_l
58	If there are reinforcing materials, for each of them enter: material number, cross-sectional area A_s , distance to the top fibers d_s
*END SECTIONS	

Table A-12: Input indicators for cross sections data.

Indicators	Shape
1	Rectangular
2	T-section
3	I-section
4	L-section
5	Channel
6	Hollow rectangular
7	Circular
8	Hollow circular



Element data, as required by records number 56- in Table A-13, is enclosed by commands:

***ELEMENTS ... *END ELEMENTS**

Table A-13: Element data.

Record No.	Input data
*ELEMENTS	
59	*SPRnxyz, *TRUnxyz, ... (refer to Table A-14)
For each element type	60 Number of first element, number of last element [†] , element number increment, element nodes increment, element material layer or cross-section system number, number of embedded bars, element loading (0 do not specify loads, 1 specify loads), element nodes
	61 <i>If there are embedded bars, for each bar enter:</i> identification number of the bar, cross-sectional area, material number, bar loading (0 do not specify loads, 1 specify loads), ends natural co-ordinates ($\xi_1, \xi_2, \eta_1, \eta_2, \zeta_1, \zeta_2$)
	62 <i>If there are embedded bars with initial loading, for each bar enter:</i> initial strain ϵ_o , initial stress σ_o
	63 <i>If need to specify element loads:</i> element normal load, element global loads
*END SPRnxyz, *END TRUnxyz, ...	
*END ELEMENTS	

[†]The number of the last element needs to be greater or equal than the first element in the series.

Table A-14: Line commands for different element types.

Line command	Element type
*SPRnxyz	Spring element
*TRUnxyz	2-D or 3-D truss element
*BEAnxyz, *FRAnxyz	2-D or 3-D frame or beam element
*FACnxyz	Facet shell element
*SHEnxyz	General shell element
*BRInxyz, *SOLnxyz	Solid 3-D element

“n” refers to the number of nodes in the element, “i” refers to the formulation used to calculate the elements (0 for isoparametric –QBE- and 1 for special formulation –IDKQ-; for the brick element, 0 refers to no layering and 1, 2, or 3 refer to the local layering direction if layered element is to be used), and “xyz” refers to the order of numerical integration to be used in the element direction (depending on the element simulation type). Thus, *FAC4133 refers to the facet shell element with special formulation and 3x3 order of numerical integration, and *BRI82333 refers to the solid element with layering in the local y-direction and 3x3x3 order of numerical integration.

Table A-15: Deformation boundary conditions data (if stress analysis required.)

Record No.	Input data
*DEFORMATIONS, *DISPLACEMENTS	
64	Number of degrees of freedom per node
65	Node number, indicator of whether node generation is required or not (=0 for node generation not required, =number for node generation required, “number” being indicative of the increment in node number when generating nodes), nodal boundary conditions for each degree of freedom x, y, z, xx, yy, zz (=F for unrestrained, x for restrained, number, “number” being the specified value)
*END DEFORMATIONS, *END DISPLACEMENTS	

Data required for the analysis of field problems, as listed in Table A-16, is enclosed by the following commands depending on the type of problem being solved:

*THERMAL ... *END THERMAL for thermal analysis
 *HYGROSCOPIC ... *END HYGROSCOPIC for hygroscopic analysis
 *CHLORIDE ... *END CHLORIDE for chloride analysis

Table A-16: Analysis data for field problems (if thermal or/and hygroscopic or/and chloride analysis required.)

Record No.	Input data
*THERMAL, *HYGROSCOPIC, *CHLORIDE	
<i>Initial conditions data</i>	
66	Initial condition
<i>Boundary conditions data</i>	
67	Number of prescribed nodes
68	For each prescribed node, enter: node number, prescribed value
69	Number of element faces on which prescribed flux boundary conditions are imposed
70	For each prescribed flux, enter: element number, side number, environmental value
*END THERMAL, *END HYGROSCOPIC, *END CHLORIDE	

Numerical data, as required in Table A-17, is enclosed by commands:

***NUMERICAL DATA ... *END NUMERICAL DATA**

Table A-17: Numerical data.

Record No.	Input data
*NUMERICAL DATA	
71	Time step, weighting factor
*END NUMERICAL DATA	

The remaining of the data is enclosed by the following commands:

***STEP ... *END STEP**

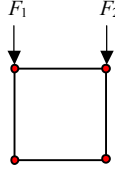
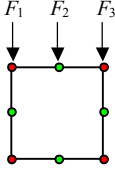
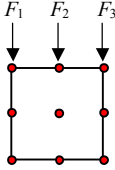
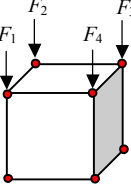
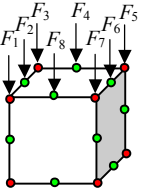
Table A-18: Load data for each time step if stress, removal or restoration analysis required.

Record No.	Input data
Mechanical load data	
*DYNAMIC	
72	Number of load repetitions, number of load scenarios applications
For each load scenario:	73 Number of load steps, maximum number of iterations permitted, tolerance to check convergence, convergence criterion (refer to Table A-19)
	74 Load types applied: uniform load, concentrated load, excavation or removal load, hygrothermal load (0 = ignore load type, 1 = include load type)
	75 If concentrated load type = 1, total number of loaded nodes
	76 If concentrated load type = 1, node #, P_x , P_y , P_z , M_x , M_y , M_z (depending on degrees of freedom)
	77 For each of the load steps, load fraction
Removal data (if removal analysis required for this time step)	
*REMOVE	
78	Elements to be removed
*END REMOVE	
79	Repeat 72-77 as required
Restoration data (if restoration analysis required for this time step)	
*ADD	
80	Elements to be added
*END ADD	
81	Repeat 72-77 as required

Table A-19: Input indicators for load data.

Indicators	1	2	3
Convergence criterion	Displacement norm	Force norm	Energy norm

Table A-20: Consistent nodal loads.

Element type	Nodal forces
Four-node quadrilateral	$F_1 = F_2 = \frac{1}{2}$ 
Eight-node quadrilateral	$F_1 = F_3 = \frac{1}{6}$ $F_2 = \frac{2}{3}$ 
Nine-node quadrilateral	$F_1 = F_3 = \frac{1}{6}$ $F_2 = \frac{2}{3}$ 
Eight-node cube	$F_1 = F_2 = F_3 = F_4 = \frac{1}{4}$ 
Twenty-node cube	$F_1 = F_3 = F_5 = F_7 = -\frac{1}{12}$ $F_2 = F_4 = F_6 = F_8 = \frac{1}{3}$ 

It is assumed in the above that the applied stress is one unit, the element width is one unit for 2-D elements, and the loaded area is one unit for 3-D elements.

A.2 Reading program output

Upon completion of execution, UMAR creates the following output files depending on the type of application run:

1. *filename.dat* echoes the input data,
2. *filename_mesh.dat* contains the finite element mesh (and changes in geometry for structural problems) in a format to be read by program Techplot 8.0,
3. *filename_cpu.txt* displays the cpu times required for the different sequences in the computer run,
4. *filename.out* contains the nodal results for structural problems,
5. *filename_field.plt* contains the nodal results for field problems in a format to be read by program Techplot 8.0, and
6. *filename.plt* contains the element results for structural problems in a format to be read by program Techplot 8.0.

A.3 Problem reporting

To report any problem with UMAR, contact Mostafa Nofal at Mostafa.Nofal@nrc.ca or (613) 993-9672.